2021

Climate resilience: Examination of revised heat transfer models in the enhanced integrated climatic model for pavement temperature prediction

Austin Michael Jarrell

CLIMATE RESILIENCE: EXAMINATION OF REVISED HEAT TRANSFER MODELS IN THE ENHANCED INTEGRATED CLIMATIC MODEL FOR PAVEMENT TEMPERATURE PREDICTION

A thesis submitted to
the Graduate College of
Marshall University
In partial fulfillment of
the requirements for the degree of
Master of Science in Engineering
In
Civil and Environmental Engineering
by
Austin Michael Jarrell
Approved by
Dr. James Bryce, Committee Chairperson
Dr. Arka Chattopadhyay
Dr. Gregory Michaelson

Marshall University
May 2021

APPROVAL OF THESIS

We, the faculty supervising the work of Austin Michael Jarrell, affirm that the thesis, *Climate Resilience: Examination of Revised Heat Transfer Models in the Enhanced Integrated Climatic Model for Pavement Temperature Prediction*, meets the high academic standards for original scholarship and creative work established by the Master of Science in Engineering and the Department of Civil Engineering. This work also conforms to the editorial standards of our discipline and the Graduate College of Marshall University. With our signatures, we approve the manuscript for publication.

Dr. James Bryce, Department of Civil Engineering — Committee Chairperson — 21-Apr-2021 Date

Dr. Arka Chattopadhyay, Department of Civil Engineering — 21-April-2021 Date

Dr. Gregory Michaelson, Department of Civil Engineering — 21-Apr-2021 Date

ACKNOWLEDGMENTS

Thank you to my mother, father, and brother for supporting me throughout the completion of this thesis, and my graduate studies. The support that you all offered is priceless, and this thesis would not have been possible without it.

Thank you to Dr. James Bryce, for assisting with the implementation of the updated heat transfer models for temperature prediction, providing guidance for navigating MEPDG documentation, aiding with MATLAB coding, and assisting with analysis and results compilation. Furthermore, thank you for providing the revised EICM for use in analysis.

Dr. Arka Chattopadhyay – For assisting with the formulation and troubleshooting of MATLAB coding, and the interpretation of total strain results.

Thank you to the following members of the Federal Highway Administration (FHWA) Office of Infrastructure Pavement Design and Performance Team: Dr. Heather Dylla, Dr. Milena Rangelov, and LaToya Johnson – for assisting with a literature review in pavement resiliency, and ultimately preparing me for this thesis topic. Also, thank you to the FHWA HIF Resiliency Group for providing valuable information that contributed to the literature review.

TABLE OF CONTENTS

LIST OF TABLES

LIST OF FIGURES

ABSTRACT

The Mechanistic Empirical Pavement Design Guide (MEPDG) is commonly referenced as the state-of-the-practice for the analysis and design of new and rehabilitated pavement assets. The Enhanced Integrated Climatic Model (EICM) incorporated within the MEPDG is a well-recognized and standardized method for estimating temperature profiles in pavements; temperature is a portion of the climate inputs in the MEPDG. Many have already begun to convert atmospheric temperature predictions from externally based climate models into the MEPDG to create robust designs for climate change. As pavement designers and researchers seek robust solutions while formulating resilient pavement designs, it is likely that the EICM will be used to import predicted pavement temperature profiles. Previous research by Bryce & Ihnat (2020) has shown that the heat transfer models within the EICM are fundamentally flawed in a way that permits over-predicted temperatures within pavement profiles. This could possibly have tremendous negative social, environmental, and economic repercussions if the models are not corrected. Increased temperatures in flexible pavements have already been shown to contribute to a variety of deformations and increases in total strain. Total strain has an elastic and plastic component; accounting for total strain in a flexible pavement design are a universal step, regardless of pavement design methodology. After research was concluded, we examined total strain results and temperature distribution results and found evidence that increased temperatures cause measured decreases in pavement layer dynamic moduli. Correspondingly, we found corresponding increases in compressive total strain. Directly proportional to the changes in dynamic moduli and total strains are demonstrated shifting in temperature distributions that show shifting towards higher temperatures over time.

CHAPTER 1: INTRODUCTION

Recently, major environmental events such as powerful storms, hurricanes, and increased flooding have raised concerns for the safety, security, and economic viability of American infrastructure. Major environmental concerns due to climate change are formally acknowledged as climate stressors; the climate stressor of increased temperature could have significant negative effects for flexible pavement assets. Many researchers and engineers have begun studying the implementation of resilient designs and frameworks to adapt infrastructure assets for climate change. One fundamental input of flexible pavement design is climate, which includes air temperature as a variable; if the assumption of static climate is false due to climate change, we could see a wide-spread increase of flexible pavement degradation.

As pavement designers complete more-robust pavement designs that are resilient to climate change, said designers are undoubtedly going to be using the EICM to project future climate. The EICM is a long-standing climatic model that is currently integrated within the MEPDG to account for the climate inputs in pavement design. There is a multitude of literature where researchers attempt to capture the effects of climate change for pavement degradation using the MEPDG and an EICM with updated parameters, with varying methods and results (Meagher et al., 2012; Shafiee et al., 2019; Stoner et al., 2019; Qiao et al., 2020). While the purpose of updating parameters for the EICM and performing pavement designs with the MEPDG is to quantify changes to pavement degradation and long-term performance, research has yielded that rutting in flexible pavement increases as increased temperatures from climate change are considered as EICM inputs (Bryce & Ihnat, 2020; Qiao et al., 2020). The primary output of most concern is the ability to predict pavement temperatures at specified depths given

the consideration of future climate, with temperature prediction at specified depths being an input into the MEPDG itself (Schwartz et al., 2011).

While the EICM serves the purpose of being the standardized model for use in estimating temperatures at depth within the MEPDG and expanded research into temperature prediction, little research has been done to assess the validity of the fundamental energy balance and heat transfer models of the EICM (Bryce & Ihnat, 2020). Bryce & Ihnat (2020) note that there have been multiple efforts to validate the EICM, however aforementioned models are essentially the same as they were in 1970, when Dempsey's work was published, forming the basis of the EICM (Dempsey & Thompson, 1970). Research was recently completed that proposed updates to the fundamental heat transfer and energy balance models contained within the EICM (Bryce & Ihnat, 2020). Their work showed that the EICM consistently over-predicted pavement profile temperatures when predicted pavement surface temperatures were at high ranges, and in windless conditions (Bryce & Ihnat, 2020). Consequently, a revised EICM was proposed, and a demonstration proving an improvement over the original Dempsey model was completed that shows an improvement for pavement profile temperature prediction (Bryce & Ihnat, 2020).

While use of the revised EICM provided by Bryce & Ihnat (2020) serve as a fundamental resource of this thesis, also the effect of increased temperatures due to adiabatic climate change are captured. While it is important to use the most-correct version of the EICM for pavement temperature prediction, researchers should also be considering the methods in which climate data are being applied to the EICM, and the robustness of background data sources. All these factors combined influence the computation of total strain at depths in pavement layers, with the changes in said strains across different versions of the EICM and assumptions for future climate being the primary deliverable of this thesis.

CHAPTER 2: SUMMARY OF PREVIOUS STUDIES

Background

The Transportation Research Board (TRB) Critical Issues in Transportation 2019 publication documented changes approaching our transportation infrastructure. The publication listed 12 critical issues grouped by inter-related topics; the fourth critical issue, resilience and security, presents a significant threat to American transportation infrastructure due to climate change. Recently, major environmental events such as powerful storms, hurricanes, and increased flooding have raised concerns about the safety, security, and economic viability of American infrastructure (National Academies of Sciences, Engineering, and Medicine, 2019). Major environmental concerns due to climate change listed in the TRB publication are formally acknowledged as climate stressors. The list of climate stressors that affect infrastructure is extensive and contain complex effects and relationships. Literature has previously indicated that the climate stressor of increased temperature could have significant negative effects on flexible pavement assets (Qiao et al., 2020). One fundamental input of flexible pavement design is climate, which includes air temperature as a variable; if the assumption of static climate becomes false due to climate change, we could see a wide-spread increase of flexible pavement degradation, increases in maintenance, agency, and user costs, as well as a significant increase in raw material usage.

Climate Change Risk, Impacts, and Key Drivers

Anthropogenic climate change is the concept that the climate is changing, and human activities contribute to said changes; greenhouse gas (GHG) emissions from anthropogenic sources were the highest in recorded history in 2014 (IPCC, 2014). The continuation of GHG emissions in the future will cause further aggravation of climate stressors, including increased

temperatures with a strong probability of irreversible impacts in the future that will impact global citizens. Emission of GHGs, particularly CO_2 emissions, will largely determine the severity of climate stressors by 2100, and beyond. The projection of GHG emissions, particularly those the emission scenarios and representative concentration pathways, are set forth by the Intergovernmental Panel on Climate Change (IPCC), are influenced by a multitude of factors, including economic policy, technology development, and sustainable practices to mitigate emissions (IPCC, 2000; IPCC, 2014).

Climate Stressors Affecting Flexible Pavement Infrastructure

There are a wide variety of climate stressors that affect flexible pavement infrastructure assets, each of which are related with varying levels of complexity. Common climate stressors of concern for flexible pavements are increased temperature, increased precipitation, and seasonal temperature shifting (and variation in duration) that functions as a combination of the previous two stressors (Meagher et al., 2012). Sometimes it can be confusing to understand the function, effects, and implications of individual climate stressors; it is useful to examine climate stressors from the scope of flexible pavement degradation.

Thermal (Transverse) Cracking

Thermal cracking is an environmental deformation that results in decreased structural load-carrying capacity (Mills, et al., 2007). There are two main types of thermal cracking: low-temperature cracking, and thermal fatigue cracking because of age-hardening, thermal loading cycles, and residual stresses. Mills et al. (2007) found that freeze seasons in southern Canada could shorten due to climate change, resulting in less transverse cracking. While this is a probable outcome, transverse cracking can still occur because of increased temperatures as a function of thermal fatigue cracking. Typical triggers for thermal fatigue cracking are thermal

load cycles and extreme minimum temperatures, however previous research has contented high extreme temperature values may prematurely intensify age-hardening and therefore increase the brittleness of a pavement. As a pavement's brittleness increases, the probability for low-temperature transverse cracking increases. Therefore, increasing temperatures, particularly in extreme thresholds, could influence transverse cracking.

Frost Heave, Freeze Thawing Cycles, and Thaw Weakening

Qiao et al. (2020) designates the "freeze-thaw" phenomenon as being mainly influenced by moisture and temperature in regions with lower temperatures. The main concern with the freeze-thaw phenomenon is moisture content in the unbound layers that can cause reductions in layer strength (Meagher et al., 2012). Meagher et al. (2012) indicates that increased precipitation is also a driver of moisture content changes within unbound layers. During freezing seasons, water is drawn into pavement layers from soil below which forms ice lenses. Between the formation of ice lenses and the freezing of pore water in pavement layers, the phenomenon of frost heave can occur; a deformation that causes a rise in a pavement surface. Frost Heave occurs in regions with regular freeze-thaw cycles, and high precipitation; primary and secondary roads that are poorly constructed and contain fine-grained subgrades are the most susceptible.

Qiao et al. (2020) contends increased amounts of moisture in pavement layers from ice lenses can be present during thawing periods, which decreases resilient modulus and increases the probability of rutting to occur. Climate change could have many effects on freeze-thaw cycles, namely being prolonged thaw periods increasing the periods of time that pavements contain moisture and extended spring traffic loading restrictions, and delays to the beginning of seasonal frost periods leading to additional freeze-thaw cycles (Qiao et al., 2020). The argument can be made that because winters in certain areas could become milder because of climate

change, pavement degradation due to spring thawing periods could decrease. Qiao et al. (2020) contended that agencies in northern areas would still need to consider placing load restrictions on pavement roadways where businesses rely on increased pavement strength during freezing months if the freezing of layers in those areas becomes variable or decreases.

Rutting

Rutting is a type of flexible pavement deformation that occurs in the wheel paths of asphalt concrete (AC) pavements, which, relative to the level of a pavement surface, is described as a depression depth for deterioration models (Mills, et al., 2007). Mills et al. (2007) also dictates that rutting as a pavement deformation can fundamentally be described by densification of pavement materials in the wheel path from traffic loading, subsequent displacement of other pavement materials as an effect of the densification process, and a decrease in "functional" performance. Rutting is a distress that is used as an indicator of overall structural pavement performance where traffic loading, temperature, and moisture all contribute to the distress. Furthermore, rutting is further influenced by characteristics of a flexible pavement, such as performance binder grade. Mills et al. (2007) argues that an effective Performance Grade Asphalt Concrete (PGAC) should minimize thermal cracking in low temperature conditions, and additionally minimize rutting that is a result of traffic loading. PGACs are also affected by temperature, as two thresholds for selection are extreme minimum pavement temperature (°C) and 7-day maximum pavement temperature (°C) usually at a 20mm depth from the pavement surface. Moisture content in unbound layers directly influences rutting, especially during freeze-thaw cycles. The timing and sequence of all factors, environmental and otherwise, could affect the intensity of rutting for a pavement over a long period of time. Mills et al. (2007) concluded that for the effect of temperature on AC resilient moduli values specifically, effects that are

hysteric in nature can be observed depending on whether the pavement surface is cooling or heating. For cooling surfaces, the unbound layers would be relatively soft, and for a heating surface the unbound layers would be relatively stiff.

Temperature

It has already been discussed what types of pavement deformations could be seen from climate stressors due to climate change. For the purposes of this thesis, the effects of increased temperature and its subsequent effect on rutting was of major interest due to temperature being cited as the most influential climate stressor for flexible pavements (Qiao et al., 2020). Temperature has a unique effect on flexible pavements; asphalt concrete is very sensitive to temperature increases, which can reduce stiffness, limit stress-strain response, and limit the ability of asphalt concrete (AC) layers in the pavement structure to spread loads effectively. Pavement-related deterioration from stiffness decreases usually are not significant over the short term; changes in limitations to the stress strain response and load-spreading effectiveness of AC layers is a long-term process. Furthermore, brittleness from faster aging of AC materials could result from temperature increases.

The most serious impact of increased temperatures is the effect on resilient modulus values of individual pavement layers. In empirical pavement design, subgrade resilient modulus values are determined from repeated laboratory loading tests, or from computing seasonal moduli values from correlations between temperature and soil moisture conditions (Huang, 2003). While resilient modulus is used by many practitioners and researchers for calculation of stresses and strains, dynamic modulus is used in the MEPDG, for calculation of stresses and strains at specified depths (Stempihar et al., 2015). In the MEPDG, dynamic modulus values are calculated within a sublayer dependent upon average temperature values within each respective

quintile value for each month of an analysis period (AASHTO, 2020). Resilient and dynamic modulus are not equivalent, and it is mathematically difficult to convert directly from resilient modulus to dynamic modulus (Stempihar et al., 2015). However, fundamentally it is true that both properties relate a strain response of a specified magnitude to an applied stress. Additionally, through mathematical manipulation of stress-strain relationships in linear viscoelastic analysis, research has also confirmed that it is possible to compute resilient modulus values based on dynamic modulus values at specified temperatures and frequencies.

A previous study performed captured the changes in duration, average temperature, and temperature-dependent resilient modulus for seasons due to temperature increases at a coastal site in New Hampshire (Knott et al., 2019). The results yielded in this study were interesting for projected seasonal changes; the fall season is expected to lengthen initially with the winter season simultaneously decreasing in length with temperature rise. Furthermore, when temperatures surpassed 2°C and then 2.5°C, the winter season is projected to cease to exist followed by an extended fall season, then a lengthening summer season. Seasonal average temperatures were projected to change with increased temperature rise, with average temperature increases projected for every season besides fall. Eventually, average fall season temperatures were projected to rise once an increase in 2°C occurs in the analysis area. Knott et al. (2019) examined the effect of seasonal changes on resilient modulus for this study, which has a strong correlation between temperature and rutting. Knott et al. (2019) concluded that 90% of pavement deformation is seen during the late spring and summer seasons at the coastal site in analysis. Rutting damage is anticipated to become more prevalent because of shifting seasonal durations and temperature increases; as the fall season for the site lengthens and the winter subsequently decreases, there is a projected increase in rutting. At a temperature increase of 4.5°C at the site,

early spring contributions to rutting are expected, as well as an overall even damage spread throughout the duration of the rest of the year. One caveat is that this is one analysis, for one specific area in the country. Depending on methodology, location, and analysis techniques the effects of rutting will be different for each location in America, but common effects for similar areas should be noted and summarized. One likely outcome of increased temperatures is that there could be a strong effect on stiffness, modulus values, and an increase in rutting in varying degrees of magnitude across the United States.

Heat Waves

Heat Waves are best described as extreme weather events where extended periods of time, or high numbers of cumulative days exhibit extreme temperature thresholds (99^{th} percentile of all temperatures) (ICF International, 2006). Extreme temperatures, like the general category of increased temperatures, have significant effects for rutting (ARA, Inc., ERES Consultants Division, 2004). It is important to account for extreme temperatures in pavement design, which is not possible if practitioners use average monthly temperatures. The EICM temperature model built into the MEPDG utilizes a frequency distribution for pavement temperature as a function of time and depth within a pavement profile. Temperatures for a given month in an analysis period are divided into five different sub-seasons, with each sub-season containing 20% of the frequency distribution for each sub-layer temperature. Sub-layers are divided AC layers that account for variations in AC depths for temperature and frequency. In summary, mechanisms in the EICM were designed to account for extreme temperatures.

Implications of Climate Change

The prospect of a changing climate carries implications for infrastructure asset management, pavement design, and economic cost increases. Qiao et al. (2020) contends that, for

new and rehabilitated pavement projects in high-impact areas for climate change, alternate designs may need to be proposed to prevent significant damages and decreases in reliability for road networks. Previous work examined estimates for the financial impacts for infrastructure due to climate change (Stoner et al., 2019). These estimates indicated that the highest cost increases seen in maintaining infrastructure will result from increased temperatures. Under a net cost per year estimate, by 2050 the net increase in keeping infrastructure maintained could be $2.8 billion dollars with analysis under a higher emissions scenario. An additional net cost per year estimate completed using higher emissions scenarios for analysis concluded that costs could increase to $35.8 billion dollars if the current state of pavement design practice is maintained by the end of the century.

Qiao et al. (2020) indicates that asset management plans could need updates for critical transportation infrastructure within road networks to offset the effects of climate change. In this instance, stakeholders should be aware that this could mean maintenance, rehabilitation, and activity timelines could have to be moved up, which means maintenance budgets could have to arrive earlier than expected to match demand (Qiao et al., 2020). Many practitioners have already considered trying to prepare flexible pavement assets for increased temperatures, and to maintain asset reliability levels. Previous studies have suggested increasing pavement binder grade to prepare for temperature increases (Stoner et al., 2019), and increasing pavement layer thicknesses to maintain reliability levels (Knott et al., 2019). While both practices may certainly yield effective solutions for preparing flexible pavement assets for temperature increases, the effectiveness of binder upgrades and layer thickness increases still require economic research and additional studies to ensure robust solutions (Qiao et al., 2020). Additionally, viewed from the scope of balancing the triple bottom line, all solutions for climate preparedness, robust or

otherwise, need to minimize negative effects for environmental, economic, and social categories, therefore maximizing positive benefits.

Transportation Emissions

One of the chief contributions of the transportation sector to climate change is emissions, which originate from a variety of sources. According to a statistic cited by Van Dam et al. (2015), transportation contributed to 27.3% of U.S. GHG emissions in 2013, with subsequent breakdowns by transportation type (Cars: 62.2%, Medium/Heavy Trucks: 21.9%, Aircraft: 8.2%, and Other: 7.8%). An important caveat to note is that the transportation sector emissions cited by Van Dam et al. (2015) is just focused on vehicle operations emissions. While vehicle operation emissions in the transportation sector do produce substantial GHG emissions, there are also embodied emissions associated with materials and pavement construction, as well as maintenance. Pavements, as well as construction and maintenance activities therein, are their own transportation system. The key here is this: transportation GHG emissions are either attributed to operational activities, or embodied activities (construction, maintenance, etc.) that are represented elsewhere in statistics. According to the same statistic cited by Van Dam et al. (2015), embodied GHG emissions from transportation construction make up a portion of the Industry sector, which accounted for 19.9% of U.S. GHG emissions in 2013. Therefore, a portion of industry GHG emissions are directly attributable to pavement construction, rehabilitation, and maintenance activities. It is important to emphasize that GHG emissions occur throughout a pavement's lifecycle, and therefore are not attributable to any one construction activity, but the collective (Qiao et al., 2020).

Climate Mitigation

There are two primary schools of thought used to address adiabatic climate change: mitigation and adaptation. While there are fundamentally different outcomes that arise from mitigation and adaptation strategies, both mitigation and adaptation strategies are needed to combat/prepare for climate change. Fundamentally, mitigation arises from the understanding that pavements contribute to climate change, in addition to being affected by it (Qiao et al., 2020). Therefore, mitigation strategies fundamentally focus on preventing and reducing GHG emissions to alleviate climate change.

Climate Adaptation and Incorporating Resiliency

Traditionally, many practitioners have attempted to capture the risk of climate change with many different approaches, all differing in complexity and creativity. These approaches can be divided into two separate categories: bottom-up and top-down approaches (Knott et al., 2019). Bottom-up approaches focus on changes in incremental temperature and its effect on pavement life. Similarly, Knott et al. (2019) states that top-down approaches are those that utilize projections from climate models and apply the results to model pavement life prediction. Bottom-up approaches may result in a better examination of pavement deformation due to temperature. Top-down approaches are criticized for lack of ability to predict seasonal, or otherwise short-term pavement response characteristics. These approaches are best described as climate adaptation strategies.

Climate adaptation is a set of strategies to adapt to climate change (Choate, et al., 2017). Climate adaptation differs from mitigation, as adaptation (or resilience) is focused on adapting to climate change as it currently exists and could exist in the future. Community resilience is an important piece of climate adaptation, which is the ability of a community to anticipate, react to,

and recover from extreme weather events and damaging climate stressors. Community resilience thinking can also be applied generally to flexible pavement assets at the strategic, network, and project level. Similarly, my definition of pavement resiliency is preparing an asset for damaging climate stressors and extreme weather events, ensuring resistance to accelerated pavement deformation, and retaining the reliability level that it was designed for. This definition focuses on preparedness for daily climate stressor damage that will ultimately accumulate into long term pavement deformation for pavements. Yet another definition from the Presidential Policy Directive (PPD-8: National Preparedness) is also helpful for understanding resilience: "the term resilience refers to the ability to adapt to changing conditions and withstand and rapidly recover from disruption due to emergencies" (Obama, 2011). Ideally, resilience for flexible pavement assets would consist of preparing assets for daily climate stressor damage via updated engineering design and climate adaptation strategies, as well as maintaining the balance of the triple bottom line to maximize positive benefits by minimizing negative outcomes.

The Federal Highway Administration Sustainable Pavements Program gives helpful guidance and insight for how sustainability should be ensured for pavements; from Van Dam et al. (2015), the triple bottom line of sustainability is made up of three components (economic, environment, and social). Although guidance from other sources recommends balancing the triple bottom line (the definition of sustainability in engineering), said guidance usually does not expand upon how these components should be prioritized and consequently optimized (Van Dam, et al., 2015). Directly from the Sustainable Pavements Program reference document, sustainable pavements should "achieve the engineering goals for which they were constructed, preserve and (ideally) restore surrounding ecosystems, use financial, human, and environmental resources economically, and meet human needs such as health, safety, equity, employment,

comfort, and happiness". In the presence of adiabatic climate change and potential acceleration of pavement degradation, resilient design practices and upgrades for existing infrastructure are a way of ensuring fulfillment of what sustainable pavements should provide.

One helpful resource for understanding climate adaptation for infrastructure assets in the Synthesis of Approaches for Addressing Resilience in Project Development under the Transportation Engineering Approaches to Climate Resiliency (TEACR) Study (FHWA-HEP-17-082) from the Federal Highway Administration Office of Planning, Environment, and Realty (Choate, et al., 2017). This document provides adaptation options and summaries of adaptation studies that are engineering informed. These adaptation strategies/options fundamentally address that infrastructure assets are vulnerable and likely to be affected by climate change. Step 1 is integrating climate considerations, which consists of understanding the climate stressors that will affect an infrastructure asset in the early stages of the project development process (the planning, scoping, and preliminary design/engineering phases). Step 2 is using climate information, which primarily consists of deviating from assumptions of static climate to complete climate projections to ensure robust climate inputs. Choate et al. (2017) provide guidance for the selection and interpretation of climate emission scenarios, models, and future projections. Step 3 is the completion of engineering assessments and design, of which the report from Choate et al. (2017) provides adaptation options for the four following engineering areas: coastal hydraulics, riverine flooding, pavement and soils, and mechanical and electrical systems. Step 4 is conducting an economic analysis for decision support for the selection of a robust adaptation scenario which includes design and management. Step 5 includes evaluating additional considerations, which means layering additional factors outside of strategic-level planning into adaptation options and ultimately decision support. These considerations are considered outside

of strategic-level planning to prevent "adaptation islands," where, for example, a road is designed to be resilient toward increased temperatures only but ignores other climate stressor risks, such as sea level rise (SLR) and inundation. Step 6 is the final step in the process and is monitoring and revisiting a course of action as needed. Due to the uncertainty of climate change, all adaptation strategies should have adaptive management plans that ensure project resiliency, and performance targets are being fulfilled.

Flexible Pavement Resilient Adaptation Framework

Resilient adaptation strategies share common goals and characteristics, however generally understanding the process can be aided by the following strategic level framework in Figure 1. The importance of this framework lies in the focus on resilient adaptation, as well as an overarching theme of sustainability. Figure 1 was adapted from multiple frameworks from Li et al., 2011, Gudipudi et al., 2017, Qiao, Y., 2015, and Qiao et al., 2020 addressing resilience and mitigation.

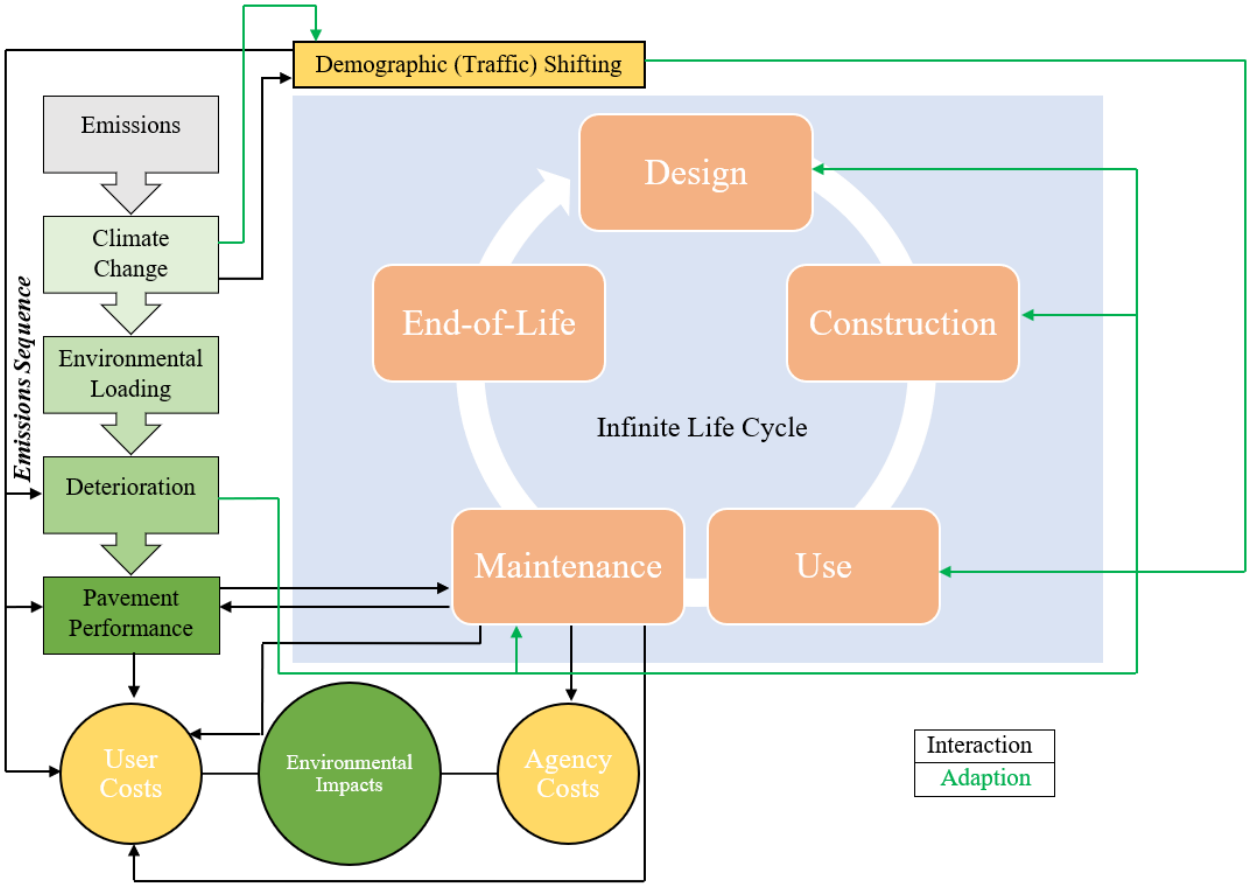

Figure 1: Pavement Resiliency Adaptation Framework; Adapted from (Gudipudi et al., 2017; Li et al., 2011; Qiao, Y., 2015; Qiao et al., 2020)

This framework begins with the emissions sequence, which directly leads to climate change, and henceforth additional environmental loading (Qiao et al., 2020). Environmental loading has a direct effect on pavement deterioration, and it has been well-established that pavement deterioration and pavement performance are directly correlated. Climate change serves only to increase environmental loading that already occurs naturally. One major portion of this framework is the infinite life cycle. In this case, the infinite life cycle considers sustainability from the scope of resiliency and adaptation. Although individual pavement projects have a finite service life and use, the environmental and social impacts of pavement infrastructure at the

strategic level never end. For example, pavement aggregates have a potential environmental impact depending on whether they are recycled or disposed of in landfills. If these materials are recycled, they fit within the infinite life cycle. Furthermore, opportunities for adaptation should also be continuous for networks with high levels of need for resiliency. This framework outlines opportunities for the mitigation of GHG emissions in the design, construction, use, and maintenance phases of a flexible pavement asset.

Additionally, the framework outlines a need for adaptation in multiple areas. First and foremost, pavement deterioration could provide a need for resilient adaptation in the maintenance, construction, and design phase of a flexible pavement asset. Finally, climate change could provide a serious need for adaptation strategies to account for demographic (traffic) shifting. Demographic shifting serves as the last main portion of this framework and is characterized by indirect impacts that could affect pavement systems (Qiao et al., 2020).

Chiefly, demographic shifting could have significant effects during the use phase of a pavement (Qiao et al., 2020). This phenomenon was listed as an indirect impact because it would be pavement deterioration occurring due to people responding to climate change, and not necessarily climate change being the primary cause of the deterioration. For example, if a coastal highway system became permanently inundated due to SLR at a coastal town, daily travel, public transportation, and shipping would all change due to the loss of the highway. As demographic shifting occurs in that scenario, alternate routes needed for transportation would have an increase in pavement degradation. The effects and severity of demographic shifting on pavement degradation could be difficult to quantify, especially if we assume that climate change does not slow, and climate stressors become more intense.

Discussion

To study the effects of climate change on flexible pavement infrastructure, we needed to define the types of pavement deformation most likely to be affected by climate change, as well as the climate stressors driving those changes. Previous research reviewed in this chapter contain outcomes clearly relating increased temperatures to potential increases in transverse cracking, freeze/thaw activity, and rutting. Particularly, the review of rutting caused by climate change was necessary, as total strain calculated in this research is made up elastic and plastic components.

The implications of climate change were also examined in this chapter, with a discussion of the effect of transportation emissions on anthropogenic climate change, and the need for climate mitigation and resiliency. Climate mitigation is the reduction of GHG emissions to limit anthropogenic climate change, while climate adaptation is the practice of building resiliency for infrastructure assets to prepare for increases in future climate stressors. The research in this study examines increases in total strain given increased temperatures; analyses such as these quantify the opportunity to build resiliency for an infrastructure asset.

Resilient adaptation for an infrastructure asset is fundamentally controlled by location, and climate stressor type. Furthermore, guidance should be followed to optimize all resilient design activities. The information in this chapter regarding resilient adaption, as well as the resilient adaption framework serve as general steps for how the outcomes of this research could be used to build resiliency of pavement infrastructure to increased temperatures.

CHAPTER 3: RESILIENT STRAIN MODEL SELECTION

Introduction

Chapters 1 and 2 serve as the foundational literature review that partially determined the direction and scope of this thesis. This chapter details the research conducted to ensure that the total strain calculation procedures for this thesis analysis match those found in the MEPDG. The following sections detail the steps taken to prepare our analysis to follow the MEPDG for strain calculation.

Sublayering in the MEPDG

Sublayering is a sub-process of the pavement deformation prediction procedure outlined in the MEPDG (ARA Inc, ERES Division (2), 2004). The permanent pavement deformation procedure outline in Appendix GG can be seen in Figure 2.

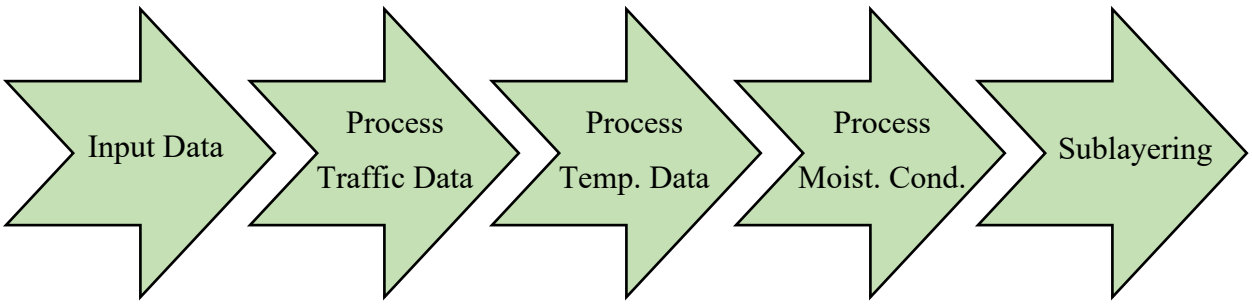

Figure 2: Pavement Deformation Prediction Procedure Adapted from (ARA Inc, ERES Division (2), 2004)

This thesis focuses on the prediction of total strain at critical depths and does not predict permanent deformation. However, total strain is made up of plastic and elastic components, which both contribute to the prediction of pavement deformation. Many of the processes needed for the computation of permanent plastic strains are also necessary for the computation of total strain in the MEPDG, which is seen in Figure 2. As a matter of fact, all steps but step 4 are

completed in this thesis research, where assumptions for moisture, or moisture condition data otherwise were not needed for the computation of total strain in AC layers.

Step 5, or the sublayering of pavement structures became vital to the success of the overall analysis and was the one step that was considered throughout multiple phases of the analysis calculation for total strain. Sublayering is the process of subdividing pavement layers into small sublayers to account changes in temperature frequency for AC layers and moisture content in unbound layers (ARA Inc, ERES Division (2), 2004). The method outline in Appendix GG for sublayering consists of the following:

1. Divide the first inch of the AC layer into two half-inch sublayers.
2. Divide the same AC layer into one-inch sublayers until a depth of four inches is achieved.
3. At that point if the thickness of the AC layer greater than four inches then a four-inch layer is added.
4. Whatever AC thickness remains is created into a new sublayer.
5. Divide the base/subbase, and subgrade layers in accordance with Figure 3.

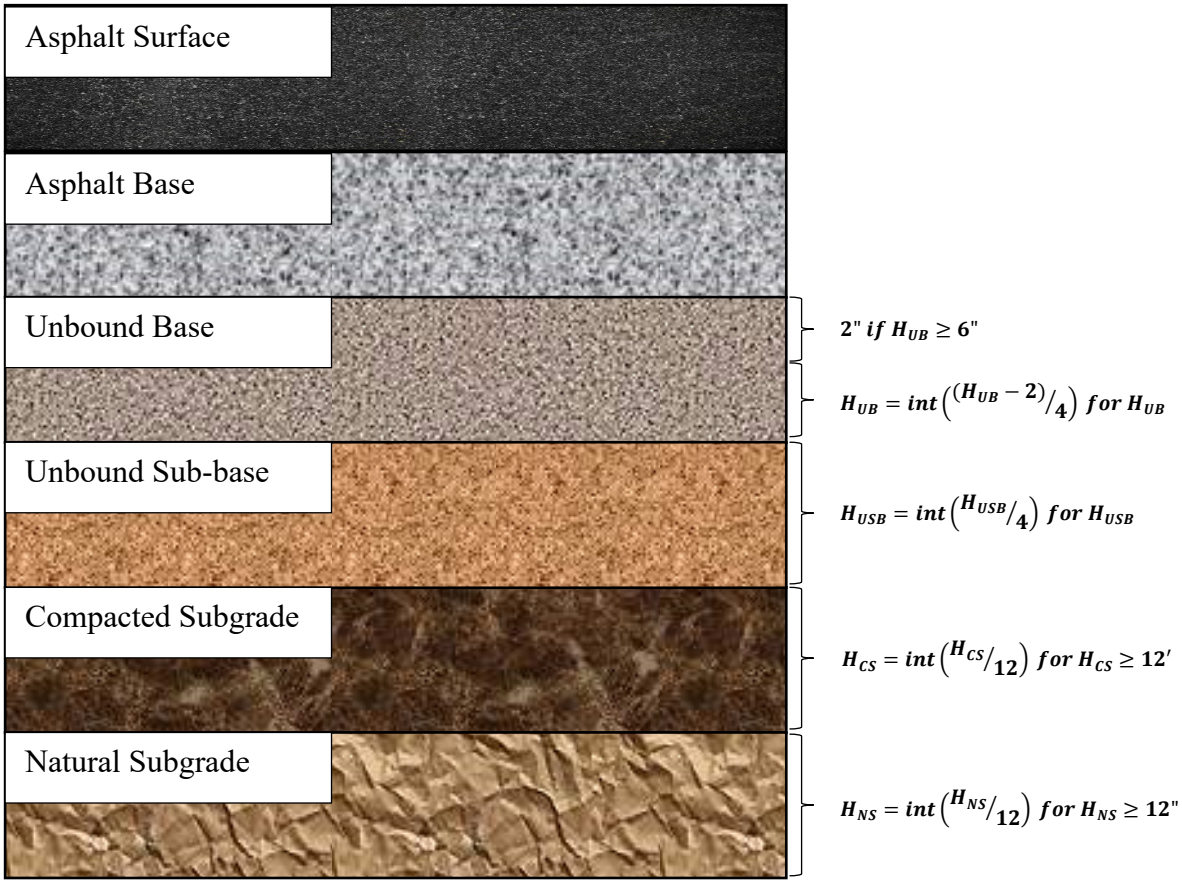

Figure 3: Sublayering Schematic Adapted from ARA Inc, ERES Division (2004)

After sublayering is completed for all pavement layers, vertical elastic and plastic strains can be calculated based on the satisfaction of the steps in Figure 2. The sublayering routine was completed for our analysis LTPP Section 51-0113 for use with temperature data obtained from the current climate and future climate models (with extra computational points for temperature processing), which is detailed in Chapter 5. The sublayering schematic was then used to determine thicknesses and analysis locations within the ALVA function, as detailed in Chapter 3. Sublayering is a critical step to the correct calculation of strains.

Total Strain

Heavy traffic loads on pavement sections cause the slow accumulation of stresses and strains throughout a pavement's structure (Papagiannakis & Masad, 2017). Overtime, stresses, and strains that occur throughout pavement structures result in pavement deformation, which ranges in severity. Calculating strains for a pavement section is quite challenging because there are many complex inputs and outputs. The numerical analysis section of this report details the extensive modification of inputs required before the strain calculations take place. During the strain calculation step (6) of the permanent deformation prediction procedure (ARA Inc, ERES Division (2), 2004), it becomes important to compute the locations in the pavement structure where loading will cause what are referred to as critical response values. The MEPDG makes use of JULEA, a layered elastic analysis software. We used the ALVA MATLAB Software package for total strain computation. Both software's have the same fundamental function: determining super positioning between axle load groups to better estimate critical response. For reference, MEPDG Appendix GG contains a very useful guide for visualizing the critical response location computation process (ARA Inc, ERES Division (2), 2004). In the case of Appendix GG, however, the documentation includes steps (for clarity) that detail the sum of analysis points needed for computation of critical strains. The computation of analysis points is completed with the use of the included layered elastic pavement response model (JULEA), and in this case the documentation reflects the computational points as JULEA would provide.

For the case of this thesis research, Figure 4 was created to demonstrate only the necessary user inputs for analysis using ALVA, and the MATLAB codes are provided in the Appendices of this thesis. Figure 4 does not included further details as to how ALVA takes said inputs and applies the principle of superposition to calculation critical response points.

Axle Spacing User Input Guide:

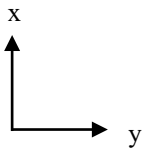

Single Axles:

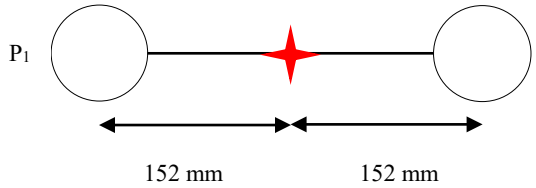

Tandem Axles:

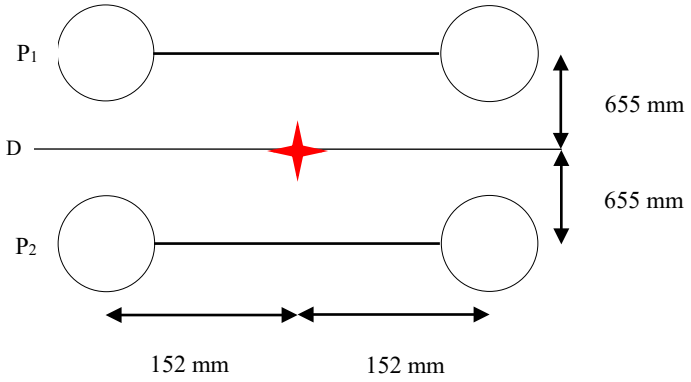

Tridem Axles:

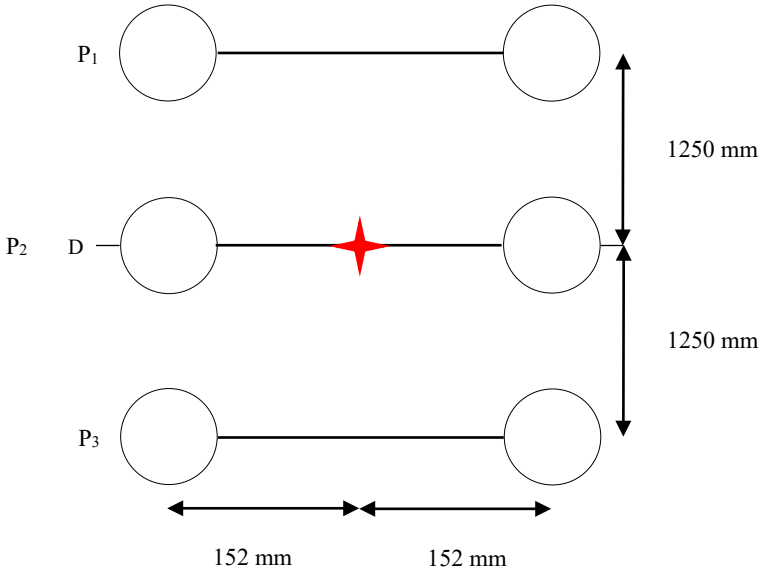

Quad Axles:

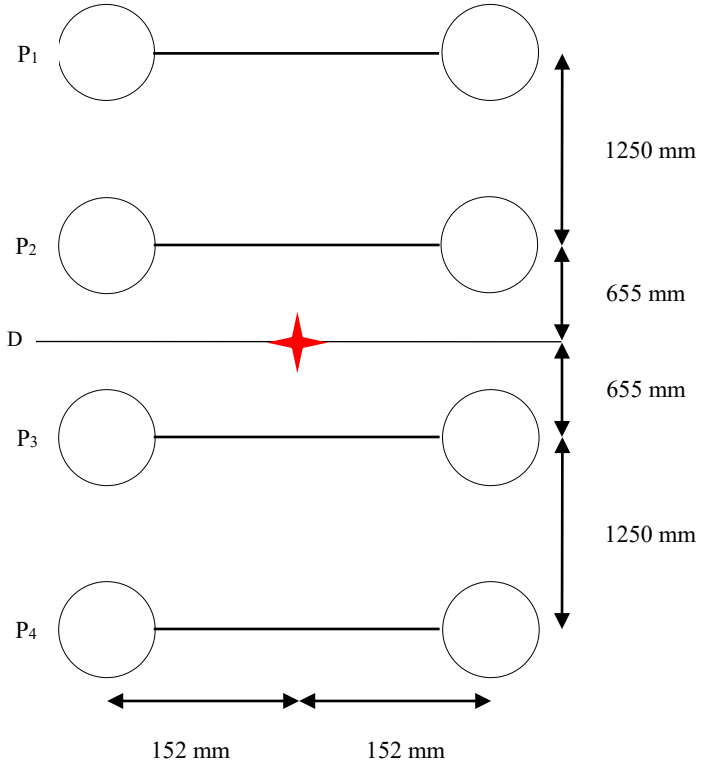

Figure 4: Axle Spacing User Input Guidance

Figure 4 represents the load positioning that was necessary for input into the ALVA MATLAB function. Figure 4 represents a set of dual wheels divided by axle configuration, with a specific load positioning configuration for each axle group. It is important to note, much like for the computational point calculation method used for the MEPDG, that critical locations based off the inputs in Figure 4 are only computed for dual wheels only, and not the entire wheel configuration per axle type (ARA Inc, ERES Division (2), 2004). For analysis inputs, it was necessary for us to define wheel locations where loads are applied. To reiterate, it is only necessary to input the because the ALVA software operates like the MEPDG's JULEA by computing critical response points (ARA Inc, ERES Division (2), 2004). One important note is that regardless of whichever layered elastic analysis software is used for strain prediction,

responses at analysis locations (like the Y locations in Figure 4) are computed for dual wheels. Stresses and strains that affect a pavement structure will only be measured at the dual wheel locations. The measurements in the x and y directions in Figure 4 are affected by axle spacing in the x-direction (AASHTO, 2020). The following are axle spacing defaults given in the MEPDG:

- Tandem Axles: 1318 mm
- Tridem/Quad Axles: 1250 mm

Similarly, the control in the y-direction is the default spacing between dual wheels, which is 152 mm. The final portion of understanding Figure 4 is examining the Datum for each axle configuration. Vertical total strains were calculated at the center of each axle configuration, therefore each datum (represented by the 'D' symbol in Figure 4) are placed accordingly. Also, the red crosses in the center of each datum represent the point where total strain is calculated.

According to Boussinesq theory when a single load from a tire is applied to a pavement surface, 2-3 inches down in the first pavement layer the load is applied at a 35-degree angle relative to the rest of the pavement layer (Papagiannakis & Masad, 2017). Because we calculate dual tires whenever we compute elastic and plastic strains, the loading spread from both tires at 2-3 inches below the surface interact. At certain computational points, the measured stresses and strains will be positive due to a force acting equal and opposite the load(s) applied by the dual tires. Essentially, positive strain means that the pavement is pushing back against the tire with a measurable stress and strain. Otherwise, there is a measured negative stress or strain, which is where damage to the pavement structure begins to occur.

Adaptive Layered Viscoelastic Analysis Software (ALVA)

The adaptive layered viscoelastic analysis software is an alternative to layered elastic analysis software. Traditionally, layered elastic analyses based on Layered Elastic Theory (LET), are used to compute stresses and strains at depth within AC and unbound layers. The foundation of LET analyses are based in Boussinesq theory (single layer systems), and Burmister theory (two-layer systems) (Huang, 2003). The assumptions built into LET models are that pavement structural layers are homogenous, isotropic, and linearly elastic, materials are not stressed beyond elastic ranges, and the subgrade extends infinitely in the vertical direction. Programs like JULEA in the MEPDG are based in LET; ALVA is a true viscoelastic analysis for asphalt pavements. In many cases, LEA models may not be able to compute stresses and strains as efficiently as a viscoelastic-based model, which can calculate both vertical and shear stresses from traffic loading. The ALVA function is fundamentally described by Figure 5, which is from (Skar & Andersen, 2020).

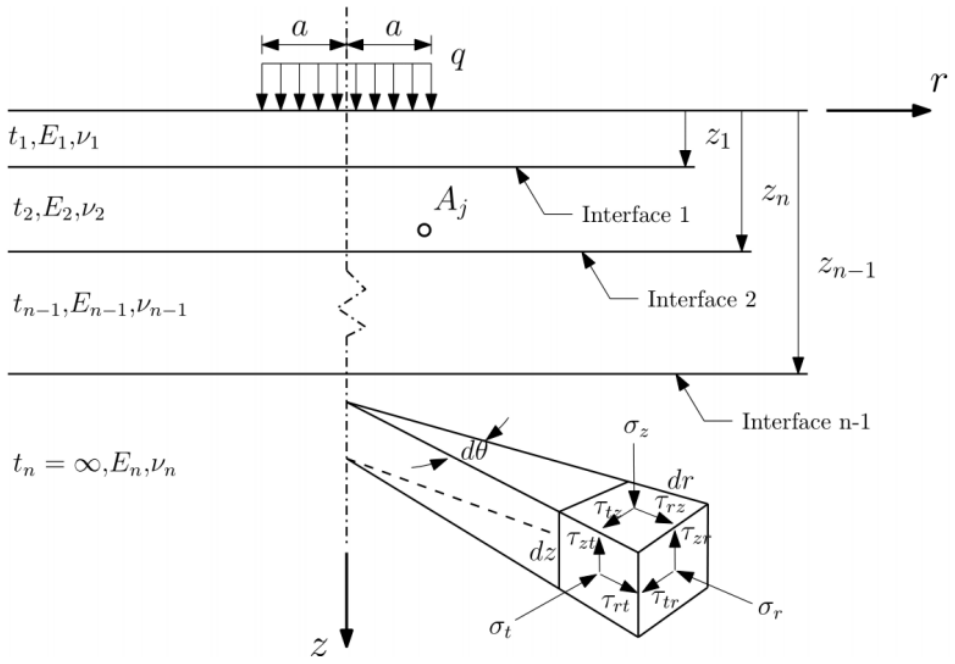

Figure 5: N-Layered Half-Space Model that Forms the Basis of the ALVA Function; Provided by (Skar & Andersen, 2020)[1]

[1]Figure 5, obtained from the original work in the Journal of Open-Source Software, is useable under terms of that are outlined in Appendix B.

Although the ALVA function is a viscoelastic software, the model is based in LET (Skar & Andersen, 2020). At the core of the ALVA function are the assumptions that all layers in the N layered half space model are weightless, elastic, linear, homogenous, isotropic. Essentially, viscoelastic response from pavement loading in the ALVA model is estimate based upon LET computations. Pavement layers are viscoelastic in the ALVA model because they are directly time controlled. Specifically, AC pavement layers in ALVA are controlled by time compliances, as well as shape parameters that control the transition between time compliances. Burgers model represents viscoelasticity and is made up of a component representing elastic behavior of solids,

and a viscous component representing behavior of liquids (Huang, 2003). As there is a viscous (unrecoverable) component to viscoelastic materials, their behavior is time dependent.

Discussion

This chapter detailed the approach needed to determine pavement deformation inputs for analysis. We demonstrated the approaches taken to determine sublayering of pavement layers, and load positioning. Furthermore, we reviewed information about the ALVA model, and how it differs from LEA. Overall, the inputs/processes obtained from this section were modified and/or processed further to be used with ALVA for analysis.

CHAPTER 4: ATMOSPHERIC CLIMATE MODEL SELECTION

Introduction

The analysis portion of this thesis was constructed using two major climate components: current and future climate. The current climate was based in historical data and was obtained from the LTPP database. To account for future climate, a source and method of obtaining/downscaling climate data was required. This chapter discusses the need for altering EICM temperature inputs, as well as the tool and data source for the future climate model.

Pavement Temperature Prediction in the EICM

The EICM provides an assumed normal frequency distribution as a function of time and depth, with a time step of six minutes (0.1 hours) over the specified analysis period for temperature values (ARA, Inc., ERES Consultants Division, 2004). Furthermore, within the MEPDG a unit of one month is used as a default for temperature distributions, while the unit is changed to half month (15 day) durations during periods of freeze-thaw periods. By providing a frequency distribution of temperatures, the EICM deviates from other methods that assume average monthly, or semi-monthly temperatures. Specifically, once a temperature distribution is created at a specified base unit and time step, divisions are then made that divide the distribution into five quintiles that represent 20% of the frequency distribution of the total pavement temperatures for each time period. As a side note, the quintiles also represent 20% of the traffic for the time. The MEPDG accounts for changes temperatures and frequencies throughout pavement depth by completing a sublayering process that is described in the analysis portion of this thesis. By creating frequency distributions for temperatures and specified time steps and periods, the EICM accounts for extreme temperatures where assumptions of average time periods do not.

Because we assume anthropogenic climate change, it is unacceptable to consider historical climate data for temperature in an analysis that does not change temperature with time. Since the EICM projects climate over a specified analysis period, any analysis assuming anthropogenic climate change will not be able to use historical climate data as a valid input. Previously, researchers attempted to create new climate model data sets that specifically assume anthropogenic climate change (Meagher et al., 2012). That research attempted to quantify the effects of climate change on long-term pavement performance and reliability using a climate change forecast. (Qiao et al., 2020).

Emission Scenarios

Climate change forecasts are comprised of atmosphere-ocean general circulation models (AOGGCMs), which distinctly differ based upon emissions scenarios (Meagher et al., 2012). Emissions scenarios vary based on defined "storylines" from the IPCC (IPCC, 2000). The IPCC provides a set of emissions scenarios in the IPCC Fourth Assessment Report (AR4) uses the Special Report on Emissions (SRES) family. The SRES family is divided into four distinct storylines: A1, A2, B1, and B2. Each storyline contains a family, which is simply a grouping of possible emission scenario groups that are family and storyline specific. For example, if one were interested in examining the A1 storyline, one would see that the A1 family is included in the storyline, with emission paths A1F1, A1T, and A1B included. These storylines are described on more detail in the following paragraphs.

Overall, the SRES framework provides six possible emission scenarios, drawn from four main families (IPCC, 2000). The goal of any possible emission scenario is to quantify energy usage leading to GHG emissions, and subsequently climate change by the end of the century. The emission scenarios are a complex collection of future changes that could be possible based

on changes in demographics, economic characteristics, cultural and social interactions, and changes in technology. The key is that all these emission scenarios are attempting to capture the world that we could see by 2100, and even though respective scenarios range in complexity and are distinctly different from one another, all scenarios begin by extrapolating technological, social, and economic trends that presently exist.

Each respective storyline has different outcomes based on factors already described, but fundamentally the A1 storyline can be quantified by continued economic growth, implementation of environmentally efficient technologies that reduce GHG emissions, and a global population that peaks around the mid-century, and then slowly declines through 2100 (IPCC, 2000). The individual scenarios within the A1 family differ based on the technologies used to produce energy: A1B is a balance across all energy sources (fossil fuel and non-fossil fuel), A1T is a scenario with non-fossil fuel energy sources being implemented globally by 2100, and conversely A1F1 is the opposite of A1T with wide-spread fossil fuel usage continuing by 2100. The A2 family is characterized by a future world of continued self-reliance (limited global convergence), continuing global population growth, and technological and economic growth that are heavily regionally controlled, which leads to less global technological convergence. These characteristics make the implications of the A2 family for future climate change very serious, with the only emission scenario, A2, containing the highest number of projected emissions by 2100.

The B1 and B2 families differ from the A1 and A2 mainly by a greater emphasis on global/local solutions to the environmental, economic, and social portions of the triple bottom line of sustainability (IPCC, 2000). Both the B1 and B2 families each contain one emission scenario each, those being scenarios B1 and B2, respectively. The B1 scenario shares a

characteristic with the A1 family of emission scenarios by having global population estimates that peak around mid-century and decline to 2100, but this scenario places a greater emphasis on a global solution to climate change. Because of this, B1 has the most rapidly declining emissions by 2100, with decline in raw material uptake, green energy technologies, and global solutions to balancing the triple bottom line of sustainability. The B2 emission scenario differs from the B1 scenario in terms of global population, and the approach to ensuring sustainability. Like in scenario A2, global population is projected to continue to increase until 2100, but the rate of the increase is lower. Similarly, to scenario B1, B2 projects that sustainability will become a priority across the globe, but in this case all sustainable priorities are projected to occur on a local and regional basis. Outcomes are more diverse changes in technology and economic development compared to B1 and A1 scenarios. That point aside, the B2 scenario still prioritizes equity and protection in the social and environmental aspects of the triple bottom line.

Generally, the ranking for the most-preferable emission scenarios to occur for the reduction of GHG emissions (ranked best case to worst case) are B1, B2, A1T, A1B, A1F1, and A2 (IPCC, 2000). This ranking originates from examining Figure 3 of the IPCC Special Emissions Report, with data for global carbon dioxide emissions from 1990 to 2100 being provided for each emission scenario.

Representative Concentration Pathways

The ICPP Fifth Assessment Report (AR5) includes Representative Concentration Pathways (RCPs) as standard emissions scenarios, which differ from the emission scenarios originating from the SRES framework from the AR4 report (IPCC, 2000; IPCC, 2014). The RCPs consist of four distinct 21st century GHG pathways based on land use, air pollution, and atmospheric conditions. These RCPs cover, as well as expand upon the SRES emission

scenarios. The RCPs are divided by the approach to mitigation of GHG emissions, with the possible RCP pathways being RCP2.6, RCP4.5, RCP6.0, and RCP8.5. RCP2.6 represents the scenario where substantial, and sustained GHG mitigation occurs throughout the remainder of the current century to 2100. RCP4.5 and RCP6.0 are considered intermediate scenarios of mitigation of GHG emissions, where RCP8.5 is the scenario where high emissions of GHGs continue throughout the remainder of 2100 and into the 22nd century. In terms of compatibility to the previous SRES emission scenarios, RCP4.5 and RCP6.0 are most compatible with emission scenarios B1 and B2, respectively, while RCP8.5 is most compatible with emission scenarios A2 and A1F1. There is no compatible SRES emission scenario with RCP2.6. The fundamental differences between the SRES emission scenarios and the RCPs are the inclusion of a more extensive range of adiabatic emissions evaluated by the AR5 report. The RCPs in AR5 represent a better understanding of the risks from climate change compared to the AR4 assessment. Because the AR5 RCPs are the state-of-the-art for GHG projections, RCPs are utilized in the analysis portion of this thesis.

USDOT CMIP Climate Data Processing Tool

The USDOT Coupled Model Intercomparison Project (CMIP) Climate Data Processing Tool is a resource for obtaining climate data that is built as a decision support tool to transportation engineers and planners. The main function of the CMIP Climate Data Processing tool is to statistically downscale climate data from the World Research Climate Research Programme (WCRP) (ICF International, 2006), (Brekke et al., 2013). The downscaled CMIP3 and CMIP5 Climate Hydrology Projections (DCHP) website from the U.S. Bureau of Reclamation houses the data necessary for the USDOT CMIP Tool to function (ICF

International, 2006). Specifically, this tool has the capability to process CMIP3 and CMIP5 data from the WCRP's CMIP Tool.

Every five to seven years the WCRP develops climate projections through their own CMIP Tool (Brekke et al., 2013). These climate projections inform the assessment reports completed by the IPCC, which were previously discussed in this thesis, and an amalgam of other research and assessment activities. The CMIP3 tool supported the IPCC AR4 report, while the CMIP5 tool supported the IPCC AR5 report (ICF International, 2006). The two fundamental statistical downscaling techniques used to process CMIP5 data differ based on whether users want to acquire daily or monthly climate information (Brekke et al., 2013). The daily-bias correction and constructed analogs (BCCA), and the monthly-bias correction and spatial disaggregation (BCSD) methods provide processed daily and monthly climate data, respectively.

Guidance within the USDOT CMIP User guide suggests using the CMIP3 version of the tool as a default option instead of using the CMIP5 tool (ICF International, 2006). CMIP5 data originates from the IPCC AR5 report and contains a more comprehensive approach for calculation emissions projections (IPCC, 2014). Although the CMIP5 tool is the state-of-the-art for emissions projections, the CMIP user guide claims that there is not sufficient scientific evidence that the CMIP5 data is more reliable, or useful than the CMIP3 data (ICF International, 2006). Although there are doubts as to whether the CMIP5 database is more reliable than the already verified CMIP3 data, there are a few distinct advantages for the CMIP5 tool. Table 1 details key differences between the CMIP3 and CMIP5 tools.

Table 1: Key Differences Between the CMIP3 and CMIP5 Tool, Adapted from (ICF International, 2006)

CMIP Tool	Report Basis	Time Range	Emissions Scenario	Number of Climate Models
CMIP3	IPCC AR4	1961-2000; 2046-2065; 2081-2099	B1, A1B, A2	9
CMIP5	IPCC AR5	1950-2099	RCP2.6, RCP4.5, RCP6.0 RCP8.5	21

We see that the fundamental differences between the CMIP3 and the CMIP5 tools are the reports that they are sourced from, but also Table 1 specifically lists with emission scenarios are available per tool. Here we see that the CMIP3 tool contains the B1, A1B, and A2 emission scenarios, while the CMIP5 contains the full set of RCP scenarios. Outside of the already discussed differences between the SRES and RCP scenarios, the CMIP5 tool contains a greater number of climate models and time ranges compared to the CMIP3. The CMIP user guide recommends using the maximum amount of climate models possible when formulating analysis runs, so the CMIP5 model offering more climate models is a distinct advantage (ICF International, 2006). Furthermore, the time availability ranges are limited with the CMIP3 tool; both baseline time periods for the CMIP3 and CMIP5 tools end in 1999, however the start dates are 1961 and 1950, respectively. The other time periods available for analysis greatly differ based on the selected tool; the CMIP3 tool has time availability past the baseline of 2046-2065 and 2081-2099, and the CMIP5 tool has time availability from 1950-2099, which is 2000-2099 for the period past the baseline.

The CMIP user guide further summarizes the differences between the CMIP3 and CMIP5 emission projections, and the implications of each projection. Although there are relevant metrics for CMIP3 data, for the purpose of this thesis it is most important to highlight that changes that will occur according to the RCPs of the CMIP5 tool. Table 2 summarizes some of the projected effects of the RCPs included within the CMIP5 tool from the IPCC AR5 report.

Table 2: Description of RCP Impacts Within the CMIP5 tool, Adapted from (ICF International, 2006)

Representative Concentration Pathway	RCP2.6	RCP4.5	RCP6.0	RCP8.5
Projection Description	Significant reduction in global emissions	High global emission stabilization	Moderate global emission stabilization	Global emissions increase and continue
2000-2100 Global Surface Temperature Increase	0.5 - 3.0 °F	2.0 - 4.7 °F	2.5 - 5.6 °F	4.7 - 8.6 °F
2000-2100 Mean Global Sea Level Rise	0.85 - 1.8 ft.	1.0- 2.1 ft.	1.1 – 2.1 ft.	1.5 – 2.7 ft.

Table 2 captures the severity of the RCP projections, which goes beyond the differences between how the models were designed. In the best case with RCP2.6, we see a significant increase in global surface temperature of 0.5 – 3.0 °F by the end of the century. Similarly, in the worst-case scenario, RCP8.5, we see an increase of 4.7 – 8.6 °F. This is quite significant and shows the severity of the consequences based on the response to mitigating emissions. Furthermore, there are significant differences in projected SLR between the RCPs. When we further examine the best and worst RCP scenarios, we see that there is projected SLR of 0.85 – 1.8 ft. for RCP2.6, and 1.5 – 2.7 ft. for RCP8.5. For the effects of the two climate stressors that are captured in Table 2 alone, selecting and RCP for analysis should be done carefully.

Discussion

The EICM provides an assumed normal frequency distribution of temperatures at time and depth, which is purpose-built to account for variations in high temperatures. Traditionally, the EICM is used with static climate inputs, so accounting for high temperatures is limited by historical climate observations. This research considers future climate resulting from anthropogenic climate change with the use of RCP6.0, which is simply an updated emission projection for 2100 based on the SRES emission projections from the IPCC. We detailed that we

obtained future climate data from the USDOT CMIP5 tool, which contains data for the RCP2.6, RCP4.5, RCP6.0, and RCP8.5 representative concentration pathways. Furthermore, we discussed the fundamental differences between each of the RCPs for the USDOT CMIP5 tool.

CHAPTER 5: NUMERICAL ANALYSIS AND RESULTS

Introduction

This chapter outlines analysis methods and documents all relevant results. Many sections in this chapter focus on preparing inputs for input into MATLAB software for analysis, including sample calculation tables that detail how data was modified to become an analysis input.

The goal of this analysis was to quantify the differences in vertical total strain throughout pavement depths of an analysis section over a 1-year analysis period by using the numbered information below. Refer to page 52 for more information.

1. Temperature prediction over the analysis period using the current EICM (Dempsey & Thompson, 1970), and Modern-Era Retrospective analysis for Research and Applications, Version 2 (MERRA-2) (current climate) temperature data.
    - Analysis 1: Current Climate Dempsey Model (CCDM)
2. Temperature predication over the analysis period using the revised EICM proposed by Bryce & Ihnat (2020), and MERRA-2 (current climate) temperature data.
    - Analysis 2: Current Climate Revised Model (CCRM)
3. Temperature prediction over the analysis period using the revised EICM proposed by Bryce & Ihnat (2020) and CMIP5 (future climate) temperature data.
    - Analysis 3: Future Climate Revised Model (FCRM)

Bryce & Ihnat (2020) have already demonstrated the improvements of their revised EICM in previous research, but what remains to be examined is the effect of the revised EICM on total strain calculation. The major products of this thesis are three runs of total strain calculation, but the sources for, and processing of necessary pavement temperatures differ. The Dempsey Model (Dempsey & Thompson, 1970) is the original model that is currently widely

accepted and modified by researchers. We have already established the revised EICM from Bryce & Ihnat (2020), and discussed the advantages and corrections compared to Dempsey's model (Dempsey & Thompson, 1970). The addition to this analysis that gives the resiliency focus is the use of CMIP5 projections for the analysis location to modify the already available temperature data from the LTPP SMP Database. Additionally, an important analysis point is the fact that the CMIP5 data was processed using Bryce & Ihnat (2020)'s revised EICM.

Updates, Implementation, and Implications for the Revised EICM

Modified heat transfer models and global energy balance equations were coded into MATLAB for analysis (Bryce & Ihnat, 2020). Furthermore, the models capture the effects for the pavement layers for each site, one-dimensional finite element modeling was created for the LTPP SMP data for each pavement analysis section.

After analysis, it was discovered that the main cause of errors within the EICM were associated with characteristics of surface temperature and wind speed (Bryce & Ihnat, 2020). This was a direct indication that those characteristics were poorly defined within the original EICM. Errors in the downwelling longwave radiation formulation (Dempsey & Thompson, 1970) were shown to cause a decrease in downwelling longwave radiation in predictions where cloud cover was present (Bryce & Ihnat, 2020). Furthermore, the source of hourly shortwave radiation was taken from the LTPP database, as opposed to using shortwave radiation present in Dempsey's work (Dempsey & Thompson, 1970) (Bryce & Ihnat, 2020).

Using field data from the LTPP database, Bryce & Ihnat (2020) were able to show that the primary error in the convection coefficient lies with the free convection term, which the convection coefficient severely underpredicts (Bryce & Ihnat, 2020). The implication of this

error is that high temperatures at surfaces are overpredicted during no wind conditions, and in periods of high and extreme heat.

Using bi-modal distributions, Bryce & Ihnat (2020) demonstrated that the proposed solutions to the errors found within the EICM improved temperature prediction (Bryce & Ihnat, 2020). While there were demonstrated improvements to temperature prediction, there is evidence to suggest that there are still heterogeneities present within the proposed revised version of the EICM that would need to be addressed in future research. Furthermore, Bryce & Ihnat (2020) concluded that the convection coefficient included in the revised EICM provided significant functional improvements when compared to the version used in the original EICM. To summarize, the four main components of the revised EICM proposed by Bryce & Ihnat (2020) are revised downwelling longwave radiation equations, removal of the cloud cover portion of the ground upwelling radiation, the adoption of MERRA-2 shortwave radiation values, and a corrected model for calculating the convection coefficient.

LTPP Site Selection, and Data Sources

The site used for analysis was one of the sites used by Bryce & Ihnat (2020) in their validation of proposed changes to the EICM. The analysis location is LTPP site 51-0113, which is on state highway 93 of the Danville Expressway north of Danville, VA; Table 3 and Table 4 contain the section information for the analysis location.

Table 3: General Site Information for LTPP Section 51-0113

LTPP Section 51-0113	
State	Virginia
GPS Coordinates – Lat., Long. (°)	36.62313, -79.36509
Class	Rural Principal Arterial - Other
LTPP SMP Thermistor Depths (m)	0.025, 0.052, 0.079, 0.137, 0.214

Table 4: Pavement Layer Information for LTPP Section 51-0113

Layer Number	Layer Type	Thicknesses [mm]
1	Asphalt concrete layer (upper)	43.2
2	Asphalt concrete layer (lower)	58.4
3	Unbound (granular) base	200.7
4	Bound (treated) subbase	152.4
5	Subgrade (treated)	Infinite

Traffic Processing

Fundamental data for traffic analysis obtained from the LTPP database were Pavement ME axle distributions, and Pavement ME Traffic Characteristics. The Pavement ME input data were obtained by downloading data for section 51-0113. Data obtained and used is listed in Appendix J. Table 5 contains the MEPDG truck volume parameters needed for completing traffic analysis. The vehicle class percentage distributions, traffic growth functions and rates per class, combined Average Annual Daily Truck Traffic (AADTT) for the first year of LTPP analysis were all necessary for framing the traffic analysis portion. AADTT and Average Annual Monthly Truck Traffic (MADTT) per vehicle class were computed using the combined AADTT for the base year of LTPP study, and the vehicle class distribution percentages.

Table 6 shows the computed MADTT values for 12 months of the base year of LTPP study in 1996.

Table 5: LTPP Section 51-0113 MEPDG Truck Volume Parameters

Vehicle Class	Vehicle Class Distribution [%]	Vehicle Class Growth Rate [%]	Vehicle Class Growth Function	Combined Base Year AADTT	AADTT per Vehicle Class
4	2.93	-5.41	Compound	687	20
5	14.93	6	Linear	687	103
6	8.55	-1.0	Linear	687	59
7	0.39	3.25	Linear	687	3
8	6.67	0.8	Compound	687	46
9	62.15	1.46	Compound	687	427
10	0.87	0.21	Compound	687	6
11	3.06	2.23	Compound	687	21
12	0.43	4.32	Compound	687	3
13	0	-26.41	Compound	687	0

Table 6: MADTT Per Calendar Month and Vehicle Class

	MADTT Split											
Class	Jan	Feb	Mar	Apr	May	Jun	Jul	Aug	Sep	Oct	Nov	Dec
4	624	584	624	604	624	604	624	624	604	624	604	624
5	3180	2975	3180	3077	3180	3077	3180	3180	3077	3180	3077	3180
6	1821	1703	1821	1762	1821	1762	1821	1821	1762	1821	1762	1821
7	83	78	83	80	83	80	83	83	80	83	80	83
8	1421	1329	1421	1375	1421	1375	1421	1421	1375	1421	1375	1421
9	13236	12382	13236	12809	13236	12809	13236	13236	12809	13236	12809	13236
10	185	173	185	179	185	179	185	185	179	185	179	185
11	654	612	654	633	654	633	654	654	633	654	633	654
12	92	86	92	89	92	89	92	92	89	92	89	92
13	0	0	0	0	0	0	0	0	0	0	0	0

The last traffic input from LTPP data were the MEPDG axle load distribution factors for the base year of the experiment section. The factors used for analysis from this section of the LTPP data are the MEPDG loading group percentages per class and month of the base year for which the data was collected. This data is further divided by WIM quality (Best or Better) and the axle grouping that the data was collected for. For example, in the data selected there are two entries for FHWA class 4 in the month of February for all 39 loading groups. One of the entries

corresponds to data collection for tandem axles, and the second entry corresponds to data collection for single axles. There is an example format of the data provided by the LTPP database for the MEPDG axle load distribution factors in Table 7 for the month of December, with load groups 1, 19, and 39.

The LTPP database provided data for the full 12 months of the start of the experiment year for the section, as well as the exact configuration of classes and axle groups seen in the example month of December in Table 7. The only addition is that there are 36 other columns of MEPDG loading bin percentages for each class, month, and configuration. Once the data was obtained and sorted, the data was inserted into MATLAB and modified to obtain the base year number of traffic loading applications per class and axle grouping. Appendix B contains the MATLAB code formulated to obtain the base year traffic. This code, named traffcode.m, operates by modifying a matrix that contains MEPDG Axle loading bin percentages per class, month, and loading group from the LTPP database. The base year traffic output was rounded to the nearest integer, then input into traffcode.m where it was grown over a 20-year analysis period with given growth functions from the analysis section. For the purposes of this thesis, only the base year traffic was required for strain computation. Traffic data corresponding to year one was extracted from the MATLAB code into Excel and was used later in analysis.

Table 7: Format for the MEPDG Axle Load Distribution Factor data table for LTPP Section 51-0113

Axle Group	Vehicle Class	MEPDG LG01 [%]	MEPDG LG19 [%]	MEPDG LG39 [%]
Tandem axle	4	0.00	0.50	0.00
Single axle	4	0.05	0.42	0.00
Tandem axle	5	54.4	0.00	0.00
Single axle	5	1.05	0.18	0.00
Tandem axle	6	0.17	0.41	0.00
Single axle	6	0.00	0.09	0.00
Quad axle	7	0.00	1.51	0.00
Tridem axle	7	0.00	0.64	0.00
Single axle	7	0.13	1.43	0.00
Tandem axle	7	0.00	9.7	0.00
Single axle	8	3.4	0.42	0.00
Tandem axle	8	0.56	0.00	0.00
Single axle	9	0.17	0.29	0.00
Tandem axle	9	0.06	0.10	0.00
Single axle	10	0.42	0.08	0.00
Quad axle	10	0.25	3.4	0.00
Tandem axle	10	0.28	1.1	0.00
Tridem axle	10	0.31	1.0	0.00
Single axle	11	0.05	0.46	0.00
Tandem axle	12	0.00	0.00	0.00
Single axle	12	0.02	0.02	0.00
Single axle	13	6.3	1.1	0.00
Tandem axle	13	1.7	2.6	0.00
Tridem axle	13	1.7	1.4	0.00

Temperature Downscaling Method

Temperature is a fundamental input for the calculation of total strain within AC layers; specifically, temperature either increases or decreases stiffness in AC pavement layers by affecting AC layer moduli. Temperature downscaling of climate data previously obtained by Bryce & Ihnat (2020) was completed for the analysis location of LTPP site 51-0113 (Bryce & Ihnat, 2020). Recall that LTPP SMP data was collected from the LTPP climate tool, as well as MERRA-2 data. The LTPP SMP and MERRA-2 climatic data for LTPP site 51-0113 were modified to extend through a 20-year analysis; these are the two datasets that are the foundation for the current climate analyses. Both current climate analyses were ran starting in 1997 and ending in 2017. The temperature data were predicted using both the Dempsey EICM (Dempsey

& Thompson, 1970) and the revised EICM (Bryce & Ihnat, 2020). The other analysis in this study is one that presumes current climate is not adequate and predicts future climate according to CMIP5 RCP6.0. While we discussed the different future climate predictions, we could make based on the RCP scenarios, we assumed that the RCP6.0 seems to be the most likely pathway to take place given the current state of global climate mitigation. Recall that RCP6.0 is a concentration pathway predicated on the analysis that global emissions will continue to rise, but stabilization will slowly occur that reduces emissions as the century progresses.

Studies that produce temperature projections focused on quantifying future climate have had two main goals thus far (Qiao et al., 2020):

1. Quantifying the effects of climate change and the damage to future pavement infrastructure
2. Improving the methods and reliability of statistical downscaling procedures

Work completed by Meagher et al. (2012) proposes a method for using historical climate data to reduce the magnitude of bias when using regional climate models (RCMs) and global climate models (GCMs) (Meagher et al., 2012; Qiao et al., 2020). The outcomes of the methods proposed are a better representation and understanding of extreme climate activity on the local level. The downscaling technique that is presented in their research is the technique that was used to account for a future climate scenario using the revised EICM.

The downscaling technique presented by Meagher et al. (2012) matches the Cumulative Distribution Function (CDF) of observed climate data (or historical) with the CDF of a climate model projection Qiao et al., 2020.

Beyond completing a 20-year analysis period or using different analyses to account for current and future climate with the revised EICM, the fundamental outcome of the temperature prediction and analysis portion is the prediction of temperatures at pavement sublayers.

Table 8: Temperature Sublayering and Additional Analysis Locations Defined by Depth

Analysis Layer Number	Depth [mm]
1	0.0
2	6.4
3	19.1
4	34.3
5	43.2
6	58.4
7	68.6
8	81.3
9	97.8
10	101.6
11	127.0
12	152.4
13	177.8
14	203.2
15	228.6
16	279.4
17	302.3
18	330.2
19	355.6
20	381.0
21	406.4
22	431.8
23	454.7

These sublayering locations in Table 8 (with additional analysis locations input) gave 23 locations where temperature data was recorded. These locations were consistent throughout all three analyses, regardless of current or future climate considerations. In addition to the depths where temperatures were recorded, each climate model contained a set of variables that were used to compute the temperatures at depth. The two fundamental variables included in the current and future climate MATLAB .mat data files were tmv1c and div1c matrices. The tmv1c matrices had a similar structure to what is seen in Table 9. Also, Table 10 contains an example of

the base structure of the tmv1c matrices. Note that the number of rows in a div1c matrix correspond with the number of columns in a tmv1c matrix. Therefore, there are 23 temperature readings at different pavement depths recorded per hour of the analysis period for both current climate and future climate scenarios.

Table 9: Example of div1c1 Matrix Parameters and Structure for Traffic Calculation

Analysis Year	Month	Day	Hour
1997	2	1	12
1997	2	1	13
1997	2	1	14
1997	2	1	15

Table 10: Example of tmv1c1 Matrix Parameters and Structure for Traffic Calculation

	(div1c) Hours			
Depth [mm]	12 [°C]	13 [°C]	14 [°C]	15 [°C]
0.0	17.9	19.6	19.5	18.3
6.4	17.1	18.8	18.9	17.9
19.1	15.4	17.3	17.7	17.2
34.3	13.6	15.6	16.4	16.3
43.2	12.7	14.7	15.7	15.7
58.4	11.3	13.3	14.4	14.8
68.6	10.6	12.4	13.7	14.2
81.3	9.7	11.5	12.8	13.5
97.8	8.8	10.4	11.8	12.6
101.6	8.6	10.2	11.6	12.4
127.0	7.6	9.0	10.2	11.2
152.4	6.8	7.9	9.1	10.1
177.8	6.3	7.2	8.2	9.1
203.2	6.0	6.7	7.5	8.3
228.6	5.8	6.3	6.9	7.7
279.4	5.6	5.8	6.3	6.7
302.3	5.6	5.8	6.1	6.5
330.2	5.6	5.7	5.9	6.2
355.6	5.7	5.7	5.8	6.1
381.0	5.7	5.7	5.8	5.9
406.4	5.7	5.7	5.8	5.8
431.8	5.8	5.7	5.8	5.8
454.7	5.8	5.8	5.8	5.8

Calculation of Dynamic Moduli

Computation of total strains require dynamic moduli values as an input. The dynamic modulus of a pavement is a value that defines stiffness in HMA mixtures as both a function of HMA temperature and loading (Elkins & Ostrom, 2019). These values are fundamental inputs needed to complete mix designs and understand stiffnesses of AC Layers. The LTPP database

provides Dynamic moduli for some sections, as well as the building blocks needed to compute dynamic moduli directly when they are otherwise unavailable. The tables within the LTPP database were designed with Dynamic moduli values and computational parts that are ready to be utilized to satisfy level one analysis criteria of the MEPDG. The key pieces of the dynamic modulus calculation are provided entirely by the LTPP database and documentation. The following equation is used for calculating dynamic moduli values in the LTPP database:

$$\log|E^*| = \delta + \frac{\alpha}{1+e^{\beta+\gamma*\log(t_r)}} \quad [1]$$

Where,

δ = Sigmoidal Coefficient 1

α = Sigmoidal Coefficient 2

β = Sigmoidal Coefficient 3

y = Sigmoidal Coefficient 4

t_r = Inverse of reduced frequency of loading [1/Hz]

Furthermore, we also require the equation for computing the time-temperature shift factor, a function that is necessary for computing $|E^*|$. The following equation is used for computing that factor:

$$\log a_T = \alpha_1 T^2 + \alpha_2 T + \alpha_3 \quad [2]$$

Where,

a_T = Mixture time-temperature shift factor

T = Temperature of interest for analysis

α_1 = Shift Factor 1

α_2 = Shift Factor 2

α_3 = Shift Factor 3

Also, we need to define the functions needed for calculating t_r:

$$f_R[hz] = f[hz] * 10^{\log a_T} \quad [3]$$

Where,

$f_R[hz]$ = The reduced frequency of loading

$f[hz]$ = Frequency

$\log a_T$ = Time temperature factor

Once all these factors are computed, only one function remains in order to calculate $|E^*|$ values for AC layers:

$$t_r = 1/f_R[hz] \quad [4]$$

Where:

t_r = Inverse of reduced frequency of loading [1/Hz]

$f_R[hz]$ = The reduced frequency of loading

The sigmoidal coefficients needed to calculate dynamic moduli values are all listed in order of appearance in each respective function within the LTPP database for the analysis section. The sigmoidal coefficients needed for the calculation of $|E^*|$ are given as SIGMOIDAL_COEFF_1, SIGMOIDAL_COEFF_2, SIGMOIDAL_COEFF_3, and SIGMOIDAL_COEFF_4 in Appendix K. These coefficients are simply number by their order of appearance in the $|E^*|$ equation. These data were collected from laboratory tests and made available by section download within the LTPP database.

Once the sigmoidal coefficients were obtained from the LTPP database, fundamental functions were defined, and the collection of base/subbase and subgrade moduli was completed, the next step was to compute the dynamic moduli. From the completed temperature data

conversion, T (temperature) was used in the $|E^*|$ function. Because there are three separate sources for temperature data in this analysis, there were three total runs completed that corresponded to dynamic moduli data for the CCDM, CCRM, and FCRM. Moreover, a fundamental goal of this moduli analysis was not just to calculate dynamic moduli for the AC layer, but also to define the depths at which future analysis to calculate strains would be.

Based on the pavement sublayering completed, we needed six AC layers, one unbound granular base (crushed stone) depth, and one treated bound subbase depth. Therefore, when the MATLAB code was complete for all the temperature models, the number of rows in the output matrix matched the number of moduli values needed for estimation of strains at the mid-depths of pavement sublayers. Therefore, because there were eight tmv1c matrices for each temperature dataset (both the LTPP SMP sources and the future climate data), there were eight corresponding output matrices that contained the necessary data for strain analysis.

In Appendix D, the code for obtained moduli values for the CCDM model included. Furthermore, Appendix E includes the code for calculating moduli values for the CCRM model. Appendix F contains the code for calculating the moduli values associated with the FCRM model. Furthermore, the number of columns for each output modulus matrix matched the number of rows of the individual temperature .mat files. Because of the similarity in data structure, simple matrix mathematics and the power of MATLAB allowed us to quickly compile moduli values at critical depth for the analysis period.

More important than the actual data structure itself for the moduli values are the assumptions built in that shape the outputs. In this research, we compute the moduli values recognizing that the moduli change as a function of temperature over time. However, a few key assumptions that we made was that base/subbase and subgrade moduli do not change as a

function of temperature. Although literature reviewed in the background portion of this thesis explores that possibility, no conclusive evidence has been released to date that influenced our research to consider non-AC layers to have resilient moduli that change with temperature over time. Because AC layers are a viscoelastic material, changes in temperature have a direct impact on layer stiffness. Unbound layers, although they are affected by pavement deformation, do not have the same characteristics as AC layers that cause temperature-induced changes to stiffness.

Calculation of Base/Subbase and Subgrade Moduli

LTPP section 51-0113 contains average resilient modulus testing data for the base/subbase layer(s) that was obtained from the test section and lab tested. From selected pavement layer and characteristic data from the LTPP, Appendix L and Appendix K contain the average resilient modulus values needed to apply to the CCDM, CCRM, and FCRM values for the base/subbase and subgrade.

The subgrade moduli data were not as easily obtainable. Data availability varies for the LTPP database, so data for the computation of resilient moduli values was obtained from LTPP Section 51-2004, which is only 6.9 miles from LTPP section 51-1003. The resilient moduli values for the subgrade in Appendix L were obtained from the LTPP database, with the base/subbase data. Like the base/subbase data, an average resilient modulus was obtained from a set of resilient moduli values from data that originated from the site and were defined through a series of lab tests.

Calculation of Total Strain

Once the temperature, traffic, and dynamic and resilient moduli inputs were computed, another MATLAB code, named strainfunct.m was created that calculated strains through the analysis period in tandem with the ALVA software. An analycomp.m file that served as the

buffer in-between the final MATLAB code that was created to pull together all the inputs and store strains, as well as communicate with the internal functions of ALVA itself; this is in Appendix G.

The next analysis step was determining the MEPDG bin loads per axle group. The loading ranges were provided by the LTPP database. The MEPDG load bins are set as a minimum and maximum range of loads [lbs.] for each axle configuration of each loading group. For 39 loading groups, there are three ranges of loading corresponding to three axle configurations (with tridem and quad) combined. The method to calculating the real load per axle per loading bin was simply taking the midpoint of the load range given. Table 12 contains the average loads between the given load ranges that were used in strain computation.

Table 11: MEPDG Load Bin Loads Per Axle and Bin Grouping

Bins	Single Axle [N]			Tandem Axle [N]			Tridem & Quad Axles [N]		
1	0	6670	13340	0	13342	26684	0	26686	53372
2	13344	15566	17788	26688	31134	35580	53376	60046	66716
3	17792	20014	22236	35584	40030	44476	66720	73390	80060
4	22240	24462	26684	44480	48926	53372	80064	86734	93404
5	26688	28910	31132	53376	57822	62268	93408	100078	106748
6	31136	33358	35580	62272	66718	71164	106752	113422	120092
7	35584	37806	40028	71168	75614	80060	120096	126766	133436
8	40032	42254	44476	80064	84510	88956	133440	140110	146780
9	44480	46702	48924	88960	93406	97852	146784	153454	160124
10	48928	51150	53372	97856	102302	106748	160128	166798	173468
11	53376	55598	57820	106752	111198	115644	173472	180142	186812
12	57824	60046	62268	115648	120094	124540	186816	193486	200156
13	62272	64494	66716	124544	128990	133436	200160	206830	213500
14	66720	68942	71164	133440	137886	142332	213504	220174	226844
15	71168	73390	75612	142336	146782	151228	226848	233518	240188
16	75616	77838	80060	151232	155678	160124	240192	246862	253532
17	80064	82286	84508	160128	164574	169020	253536	260206	266876
18	84512	86734	88956	169024	173470	177916	266880	273550	280220
19	88960	91182	93404	177920	182366	186812	280224	286894	293564
20	93408	95630	97852	186816	191262	195708	293568	306910	320252
21	97856	100078	102300	195712	200158	204604	320256	326926	333596
22	102304	104526	106748	204608	209054	213500	333600	340270	346940
23	106752	108974	111196	213504	217950	222396	346944	353614	360284
24	111200	113422	115644	222400	226846	231292	360288	366958	373628
25	115648	117870	120092	231296	235742	240188	373632	380302	386972
26	120096	122318	124540	240192	244638	249084	386976	393646	400316
27	124544	126766	128988	249088	253534	257980	400320	406990	413660
28	128992	131214	133436	257984	262430	266876	413664	420334	427004
29	133440	135662	137884	266880	271326	275772	427008	433678	440348
30	137888	140110	142332	275776	280222	284668	440352	447022	453692
31	142336	144558	146780	284672	289118	293564	0	0	0
32	146784	149006	151228	293568	298014	302460	0	0	0
33	151232	153454	155676	302464	306910	311356	0	0	0
34	155680	157902	160124	311360	315806	320252	0	0	0
35	160128	162350	164572	320256	324702	329148	0	0	0
36	164576	166798	169020	329152	333598	338044	0	0	0
37	169024	171246	173468	338048	342494	346940	0	0	0
38	173472	175694	177916	346944	351390	355836	0	0	0
39	177920	180142	182364	355840	360286	364732	0	0	0

One input that the ALVA Code requires is contact radii per axle configuration. The equation for contact radii was gathered from Papagiannakis (Papagiannakis & Masad, 2017):

$$a = \sqrt{\frac{P}{i*\pi}} \quad [5]$$

Where,

a = contact radius [mm]

i = inflation/contact pressure [MPa]

P = vertical load carried per tire [N]

To calculate the contact radius, P [Newtons] was computed by dividing the load per axle per loading group by the number of tires per axle. Table 12 contains sample calculations for P for 5 loading groups.

Table 12: Calculation of P for each Sample Axle Group

Axle Configuration	MEPDG LG01	MEPDG LG02	MEPDG LG03	MEPDG LG04	MEPDG LG05
	Total Load [N]				
Single Axle	6672	15568	20016	24464	28912
Tandem Axle	13344	31136	40032	48928	57824
Tridem Axle	26688	60048	73392	86736	100080
Quad Axle	26688	60048	73392	86736	100080
	P [N]				
Single Axle	3336	7784	10008	12232	14456
Tandem Axle	3336	7784	10008	12232	14456
Tridem Axle	4448	10008	12232	14456	16680
Quad Axle	3336	7504	9172	10840	12508

Once the P values were obtained for each axle configuration, computing contact radii only required converting P [lbs.] to P[Newtons] and solving for contact radii. See Appendix I for documentation on these calculations.

Table 13: Sample Contact Radii Per Tire Axle Configuration and Loading Group

Axle Configuration	MEPDG LG01	MEPDG LG02	MEPDG LG03	MEPDG LG04	MEPDG LG05
	Contact Radii [mm]				
Single	36.4	55.6	63.1	69.8	75.8
Tandem	36.4	55.7	63.1	69.8	75.8
Tridem	42.1	63.1	69.8	75.8	81.5
Quad	36.4	54.6	60.4	65.7	70.6

With contact radii computed at this step of the analysis, the analycomp.m function needed inputs to effectively work between the ALVA functions and strainfunct.m. The first major input was the design thicknesses based off the sublayering completed for the temperature input portion. Layer thickness input into the analycomp.m function was simple because of this; Table 14 contains the thicknesses that were input. One caveat is that ALVA requires all thicknesses to be input as distances from the main surface of the pavement. Additionally, Table 14 contains the actual layer thicknesses, and what was input into ALVA.

Table 14: Layer thickness Inputs vs. ALVA Layer Inputs

Layer Number	Actual Layer Thickness [mm]	Layer Number	ALVA Layer Depth [mm]
1	12.7	1	12.7
2	12.7	2	25.4
3	17.8	3	43.2
4	25.4	4	68.6
5	25.4	5	93.9
6	7.62	6	101.6
7	200.7	7	302.3
8	152.4	8	454.7

The next input into ALVA was Poisson Ratio, which needed an array with the amount of Poisson ratio value matching the number of layer thicknesses + 1 for the subgrade. We assumed the standard MEPDG values for Poisson ratio. Refer to Appendix G for the analycomp.m code that ran that ran in parallel with the strainfunct.m code. Load positioning was described in Chapter 3, but the actual input values for the strainfunct.m code are listed in Table 15.

Table 15: Load Position Analysis Inputs

Analysis Position [x, y] [mm]	Single Axles		Tandem Axles		Tridem Axles		Quad Axles	
P_1	[0, -152]	[0, 152]	[655, -152]	[655, 152]	[1250, -152]	[1250, 152]	[1875, -152]	[1875, 152]
P_2			[-655, -152]	[-655, 152]	[0, -152]	[0, 152]	[625, -152]	[625, 152]
P_3					[-1250, -152]	[-1250, 152]	[-625, -152]	[-625, 152]
P_4							[-1875, -152]	[-1875, 152]

The final input into the analycomp.m code was the location of evaluation points, which differ from the layer thicknesses beginning at the surface, and the critical evaluation points. For all items and axle-specific functions, refer to the strainfunct.m code in Appendix H. The evaluation points are directly under the centerline of a wheelbase, which has x and y coordinates

set to 0. These evaluation points are the mid-depth locations of the respective pavement layers. Furthermore, for this analysis the ALVA code was only set-up to solve for micro-strain in the z direction, epsz. The computation of micro strains in the z-direction through pavement depths is consistent with the procedure used in the MEPDG (ARA Inc, ERES Division (2), 2004). The evaluation points that were input into ALVA are in Table 16.

Table 16: Evaluation Point Analysis Inputs

Evaluation Point	Depth from Surface [mm]
1	0
2	6.4
3	19.1
4	34.2
5	43.2
6	68.6
7	81.3
8	97.8
9	101.6
10	302.3
11	454.7

Gaussian Distribution Models

Once analysis using the ALVA function, analycomp.m, and strainfunct.m was completed, the gathered strains were in a matrix format. Completing analysis results in three resultant matrices, each corresponding to the EICM and/or climate consideration. In previous research, Bryce & Ihnat (2020) determined that normal distributions did not sufficiently capture the errors in data. Therefore Bryce & Ihnat (2020) used a gaussian mixture model that found a better fit between data using Bayes Information Criteria. Bayes Information Criteria better accounts for errors because it is assumed that there are heterogeneities in the output models that are not accounted with the base model itself (Bryce & Ihnat, 2020).

We fit gaussian mixture models to the strain data from the three analysis runs and studied how they shifted. This raises the question of how many underlying distributions make up the mixture model. In theory, there could be just one single distribution that fits the mixture model best, or there could be 100 distributions. Obtaining the optimal number of underlying distributions that fit the mixture model is completed by maximizing the log likelihood. To maximize the log-likelihood of our gaussian mixture models, we completed 10 trials, each with a different number of gaussian distributions that were added together to create a gaussian mixture model. The number of gaussian distributions for each trial equal the trial number. In our analysis we found that Trial 9 (nine gaussian distributions) maximized our log-likelihood, and we subsequently obtained our mixture models with that configuration of distributions. Furthermore, our mixture models were formulated for strains at Depth 11, as that depth clearly demonstrated multiple distributions in the form of peaks across the CCDM, CCRM, and FCRM.

Figure 6, Figure 7, and Figure 8 show the gaussian mixture models for the CCDM, CCRM, and FCRM scenarios.

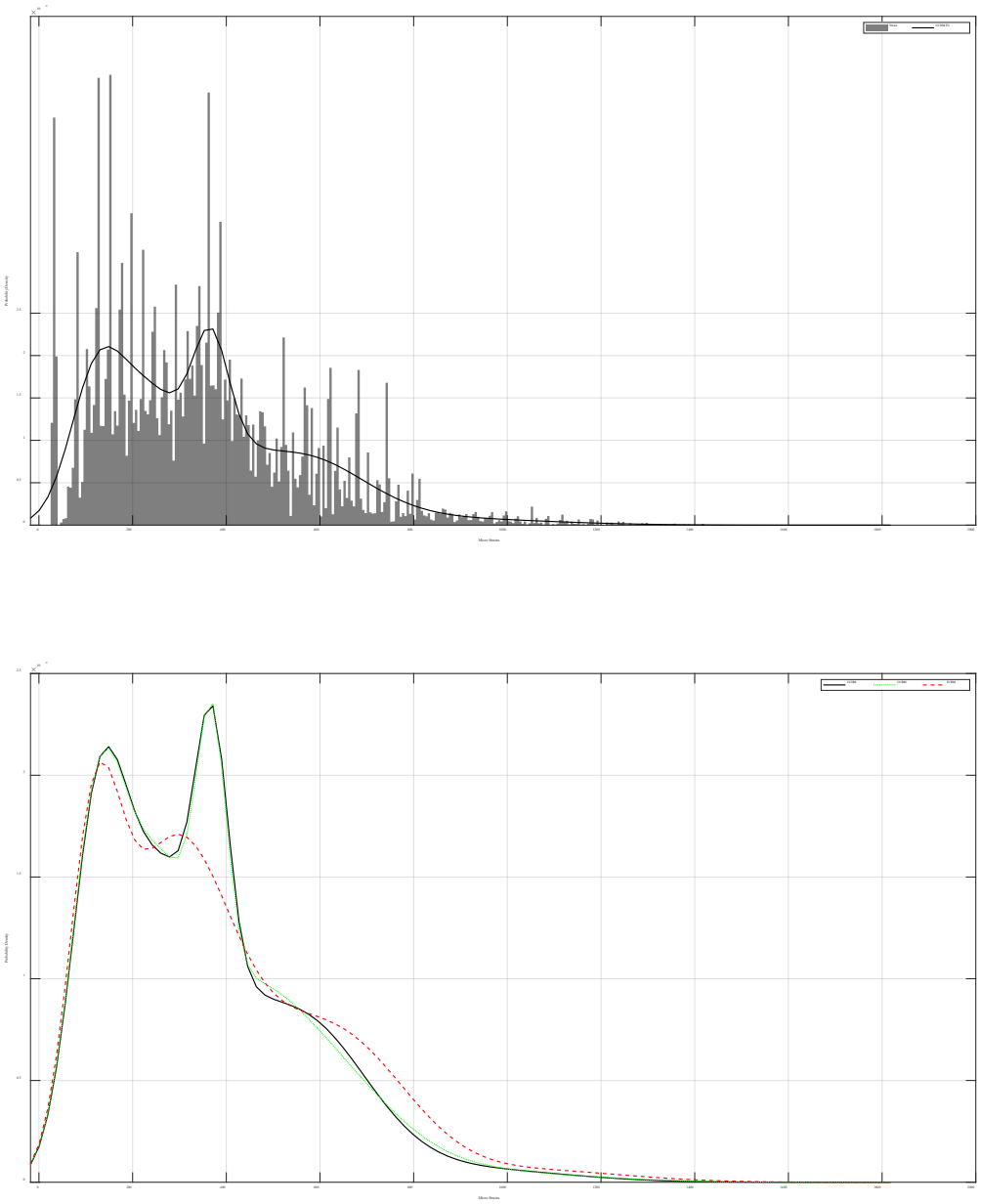

Figure 6: CCDM Gaussian Mixture Model

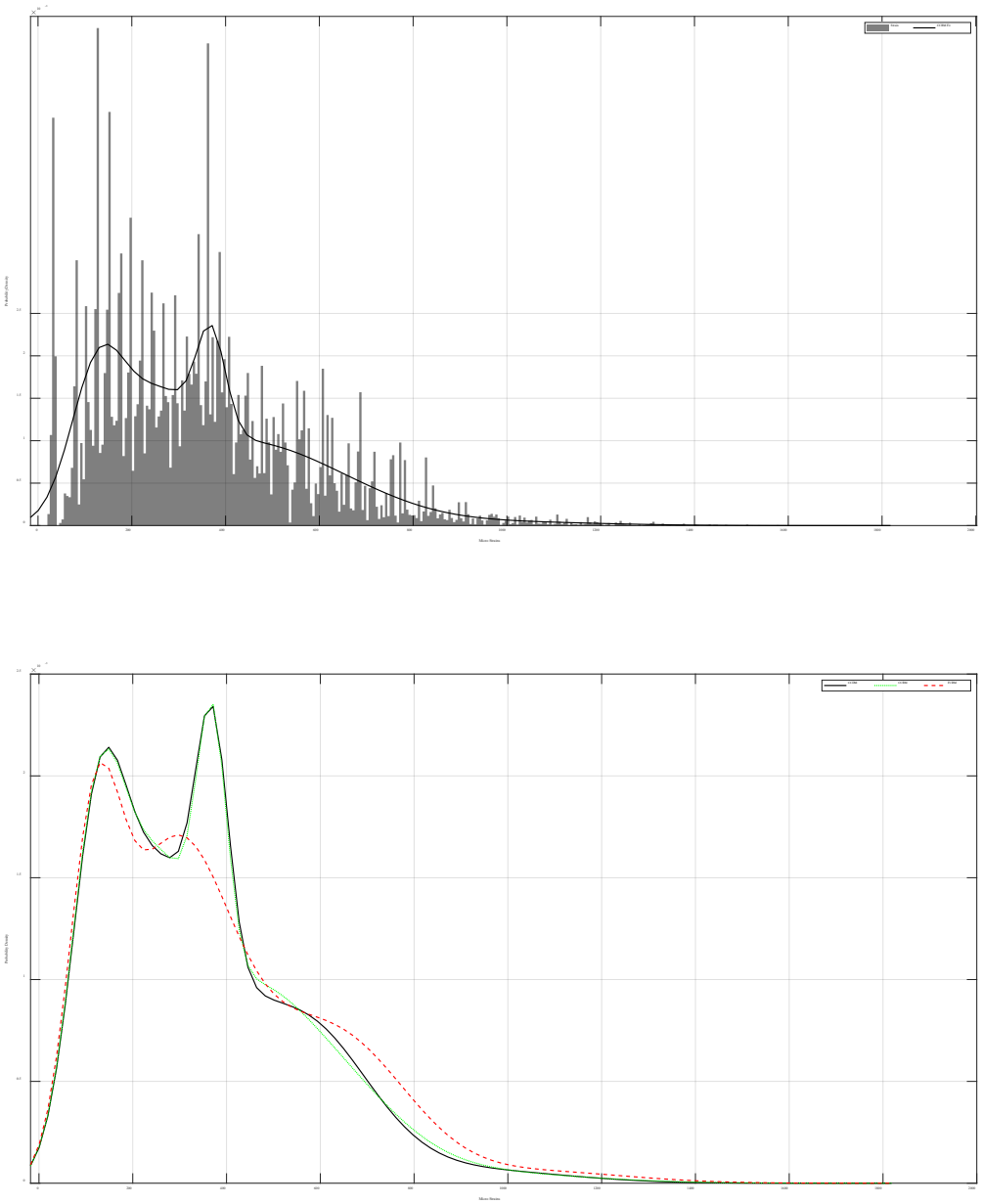

Figure 7: CCRM Gaussian Mixture Model

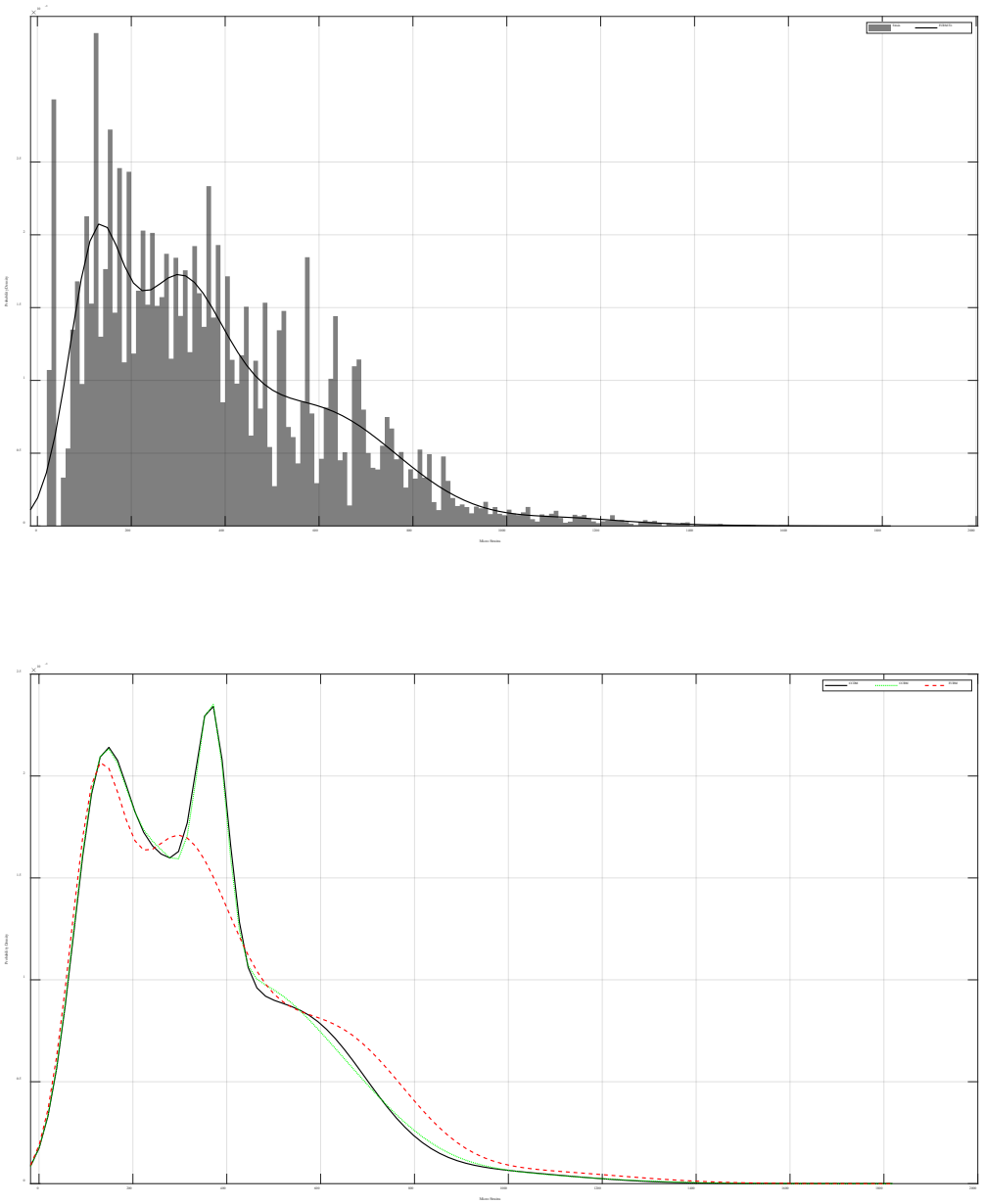

Figure 8: FCRM Gaussian Mixture Model

Strain, Dynamic Moduli, and Temperature Percentiles

Beyond obtaining gaussian mixture models from the assembled gathered_strain_epsz_v3 data, we examined the differences between the 5^{th}, 50^{th}, and 95^{th} percentiles of each model. Each model contains three metrics: dynamic moduli, temperature, and total strain at the mid-depth of each sublayer. The data in each of the metrics are divided into 5^{th}, 50^{th}, and 95^{th} percentiles for the CCDM, CCRM, and FCRM. For the dynamic moduli and temperature metrics, values are listed by AC pavement layer, which are defined in Table 14; there were six defined AC pavement layers. The vertical total strain metric values are listed per evaluation point, which are defined in Table 16. An important caveat about the vertical total strain results is that the sign convention for vertical total strain is opposite what one might expect. A strain with a negative (-) sign convention in Table 16 denotes a strain representing tension; this would otherwise be noted with a positive sign convention. Similarly, a strain with a positive (+) sign convention in Table 16 denotes a strain representing compression. This is because the evaluation points in ALVA must be input as positive numbers, therefore the sign convention for strains is inverse.

Another relevant output from our research would be examples of how temperatures shift over time for the CCDM, CCRM, and FCRM. Figure 9, Figure 10, and Figure 11 show shifts in temperature distributions between the models across the analysis period. Figure 12 contains a model that shows the differences in temperature distributions at 2 meters above the pavement surface between the mean air temperature from 1997-2017 and future climate (2050).

Table 17: Analysis Metric Percentiles

	CCDM			CCRM			FCRM		
	Dynamic Moduli [Mpa]			Dynamic Moduli [Mpa]			Dynamic Moduli [Mpa]		
Depth	Highest Moduli			Lower Moduli			Lowest Moduli		
[mm]	5th	50th	95th	5th	50th	95th	5th	50th	95th
6.4	1620	7711	19348	1277	7711	19507	980	5337	15615
19.1	1728	7663	19085	1391	7610	19214	1052	5249	15232
34.3	1848	7614	18821	1528	7513	18914	1136	5159	14842
81.3	2093	7555	18335	1814	7399	18358	1315	5032	14154
97.8	2170	7543	18187	1906	7377	18190	1377	5016	13950
101.6	2266	7538	18040	2023	7356	17995	1450	5001	13723
	Temperature [°C]			Temperature [°C]			Temperature [°C]		
Depth	Lowest Temperatures			Higher Temperatures			Highest Temperatures		
[mm]	5th	50th	95th	5th	50th	95th	5th	50th	95th
6.4	0.6	21.1	45.0	0.6	21.1	49.4	7.2	26.7	55.0
19.1	1.1	21.1	43.9	1.1	21.1	47.8	7.8	26.7	53.3
34.3	1.7	21.1	42.8	1.7	21.7	46.1	8.3	27.2	51.7
81.3	2.2	21.1	40.6	2.2	21.7	42.8	9.4	27.8	48.9
97.8	2.8	21.1	40.0	2.8	21.7	42.2	10.0	27.8	47.8
101.6	2.8	21.1	39.4	3.3	21.7	41.1	10.0	27.8	46.7
	Vertical Total Strain [epsz]			Vertical Total Strain [epsz]			Vertical Total Strain [epsz]		
Depth									
[mm]	5th	50th	95th	5th	50th	95th	5th	50th	95th
0	-375	-49	1	-395	-48	1	-450	-57	0
6.4	-343	-43	-1	-357	-43	-1	-412	-50	-1
19.1	-262	-31	-2	-279	-31	-2	-330	-37	-2
34.3	-156	-19	-2	-170	-20	-2	-203	-26	-2
43.2	-90	-15	-2	-101	-15	-2	-121	-19	-2
68.6	-20	16	106	-21	16	106	-30	20	124
81.3	-24	28	197	-25	29	202	-35	34	236
97.8	-28	44	309	-30	44	323	-41	53	364
101.6	-30	47	338	-31	48	352	-43	58	396
302.3	52	272	849	50	272	862	45	274	958
454.7	75	324	745	76	325	771	71	331	832

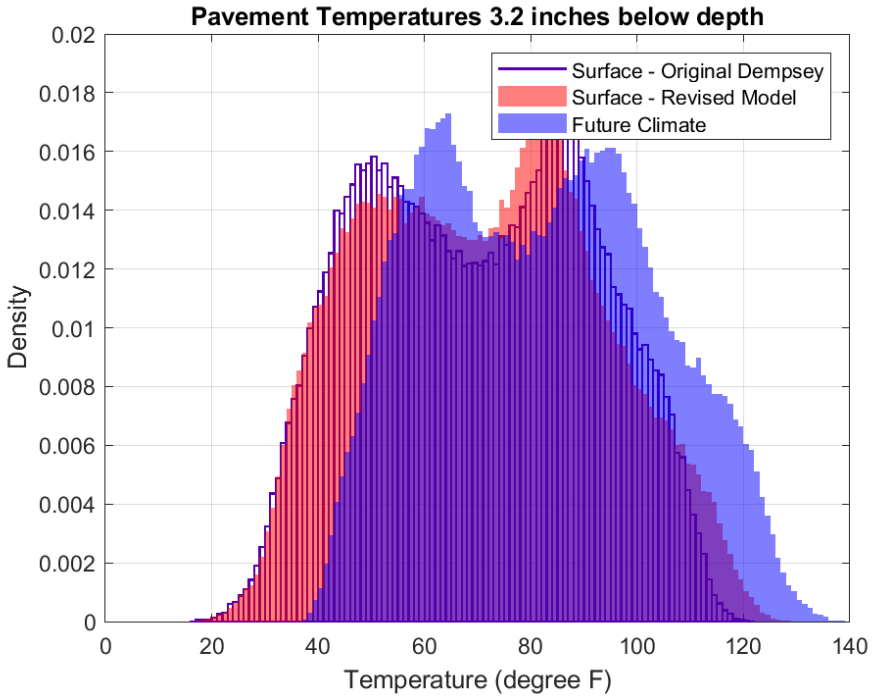

Figure 9: Analysis Period 3.2-Inch Depth Temperature Distributions

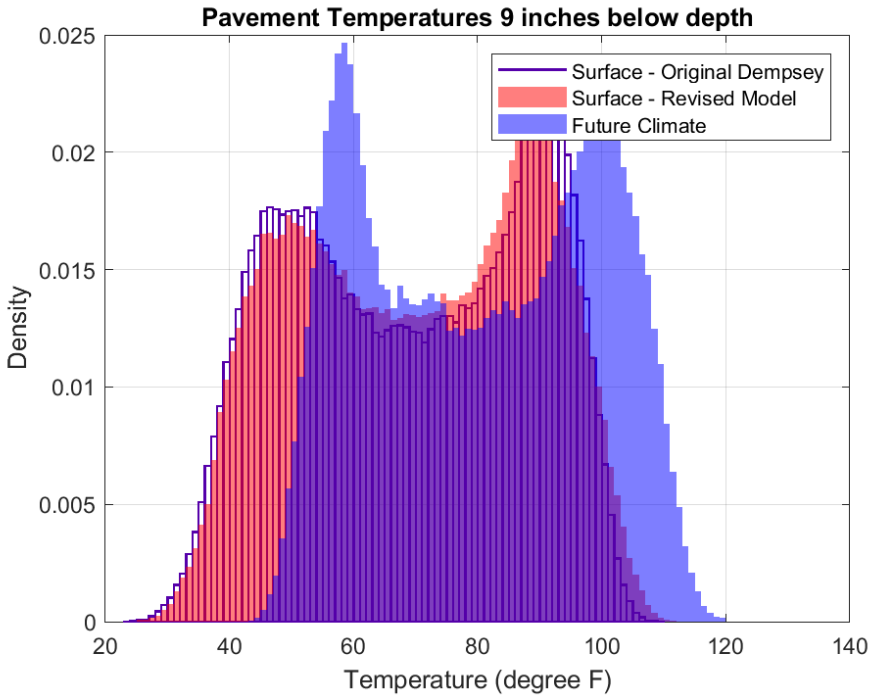

Figure 10: Analysis Period 9-Inch Depth Temperature Distributions

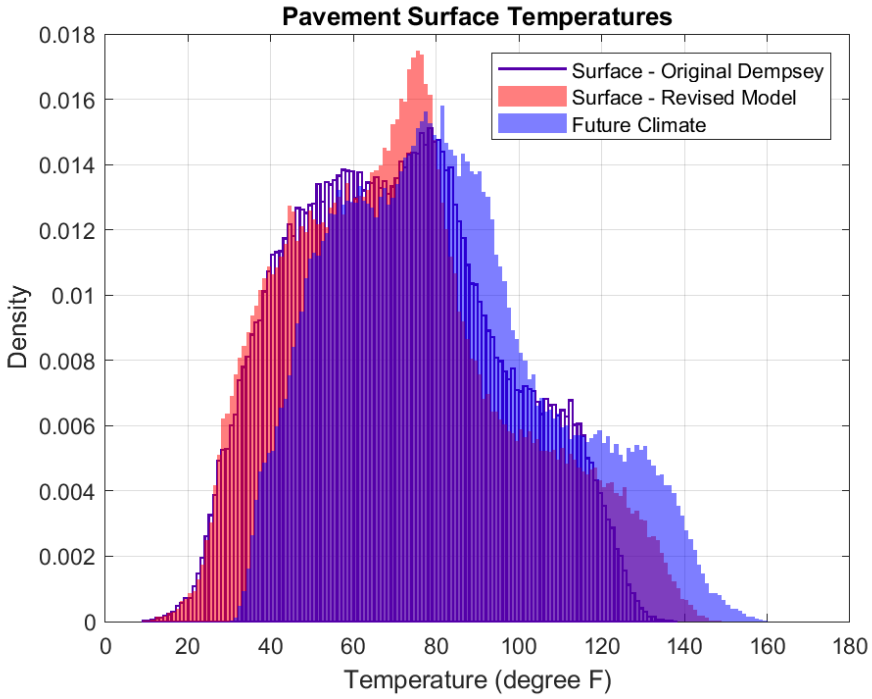

Figure 11: Analysis Period Pavement Surface Temperature Distributions

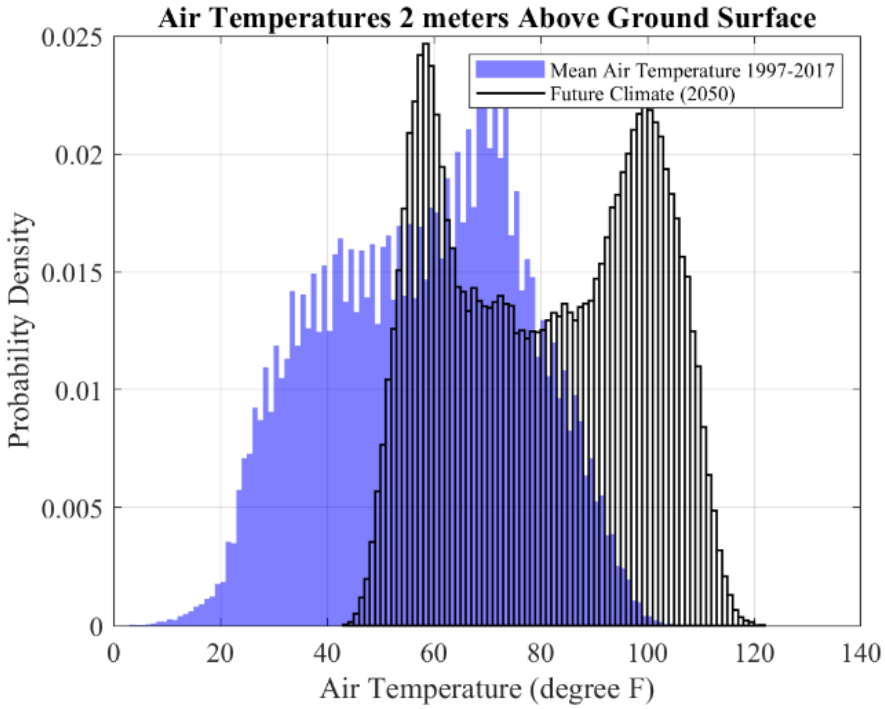

Figure 12: Analysis Mean Air Temperature vs. Future Climate Temperature

CHAPTER 6: DISCUSSION AND CONCLUSIONS

Temperature Assessment

The first item of discussion of note before the discussion of total strain is temperature. Our research has captured a clear shift in temperature distributions for our chosen analysis period, regardless of which pavement layer is examined. Our results in Figure 9 and Figure 10 show a clear shift in the temperature distributions of each model towards higher temperatures at depths of 3.2 and 9 inches in the pavement structure. Interestingly, this same trend is present in Figure 11 and Figure 12, which capture the shift in distributions at locations either at, or directly above the pavement surface. Figure 12 is of particular interest, because in that figure the differences in temperature distributions for the analysis period, and future climate by 2050 are noted. The clear shift that occurs towards increased temperatures in this case is particularly alarming; we see a clear shift in the 5^{th}, 50^{th}, and 95^{th} percentiles from the mean air temperature. Most alarmingly, the percentile shifting for the 5^{th} and 95^{th} percentiles from roughly 5°F to 42°F and 105°F to 122°F from mean air temperature to future climate by 2050 is an unprecedented increase in air temperature. Furthermore, there is a clear skew in the FCRM distribution towards higher probability densities at 58°F and 101°F. While Figure 12 captures the clear skew towards increased temperatures the best, it is true that this skew is captured for all temperature distribution figures in our results.

We also observe a measurable shift between the EICM proposed by Dempsey et al. (1970), and the revised EICM from Bryce & Ihnat (2020). While the FCRM captures severe shifting between the 5^{th} and 95^{th} percentiles in Figure 9, Figure 10, and Figure 11, interestingly we also see differences in temperature prediction for the CCDM and CCRM regardless of pavement depth. Starting at the 5^{th} percentile location and then following the left side of the

distributions in Figure 9 and Figure 10, there is a slight increase in temperatures for the CCRM. Additionally, starting at the 95th percentile on the right side of the distribution and looking toward the 50th percentile we see that there is evidence of an improvement in temperature prediction for cases of high heat between the CCDM and CCRM, but the CCRM still predicts higher densities of temperatures at the highest percentiles. Bryce at al. (2020) contended that there would be an improvement in pavement surface temperature prediction in windless, high-heat conditions, so the improvement in temperature prediction in high-heat conditions that are not extreme is validated. To be clear, the improvements in temperature prediction noted in Figure 9 and Figure 10 are still observable in Figure 11, however it is important to note that the revised EICM still predicts higher temperatures at higher temperature percentiles.

These temperature distributions validate our hypothesis that pavement temperatures are increasing, and our analysis used a revised version of the EICM to do so. In summary, temperature distributions are skewing towards increased temperatures at a variety of pavement depth locations between each model version both over the analysis period, as well as between mean air temperature and future climate. As discussed in Chapters 1 and 2 of this thesis, we contend that increased temperatures lead directly to a higher level of pavement deformation in flexible pavements, specifically leading to increases in total strain. Our analysis results validate that contention.

Total Strain Assessment

Refer to Table 16 of Chapter 5 for following paragraphs. Table 16 shows the following relationships: For lower temperatures, one will observe higher dynamic moduli values, and smaller strain values at depth in pavement layers. Similarly, for higher temperatures one will observe lower dynamic moduli values, and higher strain values at depth in pavement layers.

Higher total strain values are a direct indicator of increases in pavement deformation. For the case of dynamic moduli values, we captured a clear decrease in 5th percentile dynamic moduli values (those corresponding to 95th percentile high temperatures) across the CCDM, CCRM, and FCRM. While there was a clear decrease in 5th percentile moduli values between the CCDM and CCRM, there was notably less change between the 50th and 95th percentile values (those corresponding to the 5th and 50th percentile low and mid-range temperatures). The shifting in dynamic moduli values for the FCRM are a different case; here there is a clear decrease in 5th, 50th, and 95th percentile moduli values when compared to the CCDM and CCRM.

The magnitude of micro strains at pavement depth is inversely proportional to the dynamic moduli values at those depths. Therefore, 95th percentile dynamic moduli values are proportional to 5th percentile micro strains, 5th percentile dynamic moduli values are proportional to 95th percentile micro stains, and the 50th percentile categories of both metrics are directly proportional. We see that depths 1-5 are in tension across all models, but starting at depth 6, or pavement sublayer 3 (see Table 14 and Table 16) our strains transform from strains in tension to compression. Note that for strains in the 5th percentile, this shift from tension to compression starting at depth 6 does not occur; at higher dynamic moduli ranges this is a probable outcome. However, starting at depth 6 and increasing to depth 11 we see a clear increase in compressive micro strains for the 50th and 95th percentiles (the 95th percentile strains corresponding to 95th percentile temperature values). Interestingly the shift in values is slight between the CCDM and CCRM, which corresponds to the slight shift in temperatures and dynamic moduli values, but this shift increases become more linear at depths 10 and 11. The shifts between 95th percentile values become even more linear from depths 6 through 11 for the FCRM model, especially between depths 10 and 11. Finally, we also see an increase in tensile strains between the CCDM,

CCRM, and FCRM that correlates with decreasing 95th percentile moduli values between the same models.

Implications

In summary, our total strain results and temperature distribution results clearly demonstrate the following:

1. There is a measured decrease in dynamic moduli in pavement layers at high temperatures.
2. There is a corresponding increase in compressive and tensive stains.
3. Decreases in dynamic moduli and increases in compressive and tensive strains at pavement depths are directly proportional to temperature distribution shifting to increased temperatures.
4. The use of static climate inputs alone for flexible pavement design is no longer valid.
    - Decision support tools that consider future climate are necessary to ensure resilient, sustainable flexible pavement designs through 2100.
5. There is a strong argument between the outcomes of research from Bryce & Ihnat (2020) and this thesis research that suggests that the revised EICM model (CCRM) more accurately predicts temperature compared to the Dempsey EICM (Dempsey & Thompson, 1970).

Based on our analysis, there is clear evidence that climate change will indeed cause drastic increases in flexible pavement deformation, and the revised EICM model from Bryce & Ihnat (2020) provides a needed update in predicting the temperatures that will cause a negative impact to total strain. The increase in total strain and therefore pavement degradation become especially prevalent when the revised EICM model is applied to future climate utilizing the CMIP5 RCP6.0

concentration pathway. If our assumption that RCP6.0 is the most likely pathway to occur is correct, the increases in total strain in flexible pavement layers are shown to be drastic for our scenario analysis.

Naysayers may doubt the reliability of climate projections, and subsequently the reliability of the data sets from which they originate. It is true that there are levels of uncertainty in datasets that transportation engineers and practitioners use in engineering design, but Choate et al. (2017) suggest that this fact should not be a deterrent from utilizing climate projections as design inputs, and ultimately decision support tools. Climate projections should be utilized how they are in this research: utilize a variety of emission scenarios/representative concentration pathways, use the maximum number of climate models per emissions path as possible, and assess/reassess climate outputs as needed (Choate, et al., 2017). This approach does not guarantee a robust solution, but with more robust climate tools, emission pathways, and improvements expected over time, this approach could serve as a very reliable input into flexible pavement design.

Results from the FCRM analysis suggest that increases in extreme increased temperatures will occur, and therefore starkly increase the risk of pavement deformation, therefore creating a need for widespread resilient adaptation plans to protect flexible pavement assets. Furthermore, flexible pavement designers should immediately move away from static climate assumptions and utilize resilient design principles in adaptation strategies to produce flexible pavement designs that are sustainable and adapted for climate change.

One item that needs to be discussed is a series of caveats for resilient adaptation strategies (Choate, et al., 2017). These caveats consist of common themes from multiple engineering disciplines: first and foremost, climate stressors have non-linear effects, and climate change does not mean that engineering design standards must change. Also, small, and large changes in climate stressors should both be considered by practitioners when forming adaptation plans, as well as noting

the complex interactions among various climate stressors. Furthermore, a selected adaptation strategy may be very similar to current practices for the practitioner's agency; this should not be a deterrent. Finally, one of the possible benefits from adaptation planning is reducing economic impacts by managing uncertainty and risk.

It is wise to entertain the outcomes of all possible RCP scenarios, which ranges from continuing high emissions to full emission mitigation. Pavement designers need to familiarize, and educate themselves on the ramifications of RCP scenarios, and use the information from said scenarios as decision support. As we progress through this decade to 2100 and climate change occurs with no guarantee of which RCP scenario will be the most accurate for predicting actual emissions behavior by 2100, practitioner ability to effectively balance the triple bottom line could be called into question. The amount of economic, social, and especially environmental ramifications for continuing to only complete flexible pavement designs with static climate inputs, therefore disregarding future climate projections will almost certainly result in catastrophe. If total stain at pavement depths increases at rates (not accounted for when the infrastructure was originally designed) that are captured in our analysis results, accelerated maintenance timing, and increased agency costs will be necessary, which will cause a significant negative economic impact, as well as increased optimal aggregate usage that also occurs at an accelerated rate.

While the negative environmental and economic impacts alone would have tremendous negative social impacts on the micro level for our scenario analysis, if similar trends in total strain (not accounted for in design) are observed for pavement infrastructure on the macro level, catastrophic infrastructure failures may result. A not-so-well understood effect of macro level infrastructure failures is demographic (traffic) changes that result from climate-related migrations (Qiao et al., 2020). These migrations could not only be considered a social catastrophe for American

citizens on its own, but this phenomenon could also have an indirect impact on further pavement degradation, and therefore contain environmental and economic impacts.

Future Research

Future research needs to explore/examine the following:

1. Future climate scenarios that use the other RCP scenarios (2.6, 4.5, and 8.5) to further quantify the magnitude of increase in compressive and tensive total strain.
2. A sustainability-focused scenario pavement design complete with a Lifecycle assessment (LCA), Life Cycle Cost Analysis (LCCA), and social rating system that examine the environmental, economic, and social impacts of the results of this thesis.
3. A scenario analysis that quantifies the increases in rutting (accumulation of plastic strains) using the CCDM, CCRM, and FCRM, and a corresponding analysis as described in bullet 2.
4. Resilient adaptation strategies that prevent increases in total strain due to increased temperature that have open-access, transparent metrics on the associated environmental, economic, and social impacts from said strategies.
5. Optimal ways of providing stakeholder education to pavement designers as to the risks of climate change for flexible pavements.

REFERENCES

AASHTO. (2020). *Mechanistic-Empirical Pavement Design Guide: A Manual of Practice (Third ed.).* Washington, D.C. : American Association of State Highway Transportation Officials.

ARA Inc, ERES Division (2). (2004). *NCHRP 1-37A Guide for Mechanistic-Empirical Design of New and Rehabilitated Pavement Structures Appendix GG-1: Calibration of Permanent Deformation Models for Flexible Pavements.* Champaign: National Cooperative Highway Research Council.

ARA, Inc., ERES Consultants Division. (2004). *NCHRP 1-37A Guide for Mechanistic Design of New and Rehabilitated Pavement Structures Part 2. Design Inputs Chapter 3. Environmental Effects.* National Cooperative Highway Research Program.

Brekke, L., Trasher, B., Maurer, E., & Pruitt, T. (2013). *Downscaled CMIP3 and CMIP5 Climate Projections: Release of Downscaled CMIP5 Climate Projections, Comparison with Preceding Information, and Summary of User Needs.* Denver: US Department of the Interior, Bureau of Reclamation, Technical Service Center.

Bryce, J., & Ihnat, Z. (2020). Improved Models of Solar Radiation and Convective Heat Transfer for Pavement Temperature Prediction. *International Journal of Pavement Engineering* .

Choate, A., Dix, B., Wong, A., Rodehorst, B., Jaglom, W., & Keller, J. D. (2017). *Synthesis of Approaches for Addressing Resilience in Project Development* . Washington, D.C.: Federal Highway Administration.

Dempsey, B. J., & Thompson, M. R. (1970). A Heat Transfer Model For Evaluating Frost Action and Temperature-Related Effects In Multilayered Pavement Systems. *Highway Research Record*.

Elkins, G., & Ostrom, B. (2019). *Long Term Pavemenet Performance Information Management System User Guide* . Washington, D.C.: Federal Highway Administration.

Gudipudi, P., Underwood, B., & Zalghout, A. (2017). Impact of Climate Change on Pavement Structural Performance in the United States. *Transport Res. Part D*.

Huang, Y. (2003). *Pavement Design and Analysis.* Pearson.

ICF International. (2006). *U.S. DOT CMIP Climate Data Processing Tool User's Guide.* Washington, D.C.: U.S. DOT.

IPCC. (2000). *IPCC Special Report: Emissions Scenarios Summary for Policymakers, A Special Report of IPCC Working Group III.* IPCC.

IPCC. (2014). *Climate Change 2014: Synthesis Report. Contribution of Working Groups I, II, and III to the Fifth Assessment Report of the Intergovernmental Panel on Climate Change.* Geneva: IPCC.

Knott, J. F., Sias, J. E., Dave, E. V., & Jacobs, J. M. (2019). Seasonal and Long-Term Changes to Pavement Life Caused by Rising Temperatures from Climate Change. . *Transportation Research Record*.

Li, Q., Mills, L., & McNeil, S. (2011). *The Implications of Climate Change on Pavement Performance and Design; UDUTC Final Report.* Newark : Delaware University Transportation Center.

Meagher, W., Daniel, J. S., Jacobs, J., & Linder, E. (2012). Method for Evaluating Implications of Climate Change for Design and Performance of Flexible Pavements. *Transportation Research Record*.

Mills, B. N., Tighe, S. L., Andrey, J., Smith, J. T., Parm, S., & Huen, K. (2007). *Road well-traveled: Implications of climate change for pavement infrastructure in southern Canada.* Waterloo: Environment Canada.

National Academies of Sciences, Engineering, and Medicine. (2019). *Critical Issues in Transportation, 2019.* Washington, D.C. : The National Academies Press.

Obama, B. (2011). Presidential Policy Directive 8; PPD 8. Washington, DC., United States: White House Office.

Papagiannakis, A. T., & Masad, E. (2017). *Pavement Design and Materials.* John Wiley & Sons.

Qiao, Y. (2015). Flexible Pavements and Climate Change: Impact of Climate Change on the Performance, Maintenance, and Life-cycle Costs of Flexible Pavements. *Ph.D. Thesis, University of Nottingham, UK, 2015*.

Qiao, Y., Dawson, A. R., Parry, T., Flintsch, G., & Wang, W. (2020). Flexible Pavements and Climate Change: A Comprehensive Review and Implications. *MDPI Sustainability*.

Schwartz, C., Li, R., Kim, S., Ceylan, H., & Gopalakrishnan, K. (2011). Sensitivity Evaluation of MEPDG Performance Prediction. *Civil and Environmental Engineering Commons*.

Shafiee, M., Maadani, O., & Shirkhani, H. (2019). Evaluation of Climate Impacts on Jointed Plain Concrete Pavement Structures. *National Research Council Canada.* Ottawa: National Research Council Canada.

Skar, A., & Andersen, S. (2020). ALVA: An adaptive MATLAB package for layered viscoelastic analysis . *Journal of Open Source Software*.

Stempihar, J., Underwood, S., & Kaloush, K. (2015). *Resilient Modulus to Dynamic Modulus Relationship and Pavement Analysis with the Mechanistic-Empirical Pavement Design Guide.* Arizona State University.

Stoner, A. M., Daniel, J. S., Jacobs, J. M., Hayhoe, K., & Scott-Fleming, I. (2019). Quantifying the Impact of Climate Change on Flexible Pavement Performance and Lifetime in the United States. *Transportation Research Record*.

Van Dam, T. J., Harvey, J., Muench, S. T., Smith, K. D., Snyder, M. B., & Al-Qadi, I. L. (2015). *Towards sustainable pavement systems: a reference document.* Washington, D.C.: Federal Highway Administration .

APPENDIX A: APPROVAL LETTER

MARSHALL UNIVERSITY
www.marshall.edu

Office of Research Integrity

November 3, 2020

Austin Jarrell
5993 East Pea Ridge Rd.
Huntington, WV 25705

Dear Mr. Jarrell:

This letter is in response to the submitted thesis abstract entitled *"Climate Resilience: Examination of Revised Heat Transfer Models in the Enhanced Integrated Climatic Model for Pavement Temperature Prediction."* After assessing the abstract, it has been deemed not to be human subject research and therefore exempt from oversight of the Marshall University Institutional Review Board (IRB). The Code of Federal Regulations (45CFR46) has set forth the criteria utilized in making this determination. Since the information in this study does not involve human subjects as defined in the above referenced instruction, it is not considered human subject research. If there are any changes to the abstract you provided then you would need to resubmit that information to the Office of Research Integrity for review and a determination.

I appreciate your willingness to submit the abstract for determination. Please feel free to contact the Office of Research Integrity if you have any questions regarding future protocols that may require IRB review.

Sincerely,

Bruce F. Day, ThD, CIP
Director

APPENDIX B: JOURNAL OF OPEN-SOURCE SOFTWARE COPYRIGHT PERMISSION

This page is available in the following languages: 

Creative Commons License Deed

Attribution 4.0 International (CC BY 4.0)

This is a human-readable summary of (and not a substitute for) the license.

You are free to:

Share — copy and redistribute the material in any medium or format

Adapt — remix, transform, and build upon the material

for any purpose, even commercially.

The licensor cannot revoke these freedoms as long as you follow the license terms.

Under the following terms:

Attribution — You must give appropriate credit, provide a link to the license, and indicate if changes were made. You may do so in any reasonable manner, but not in any way that suggests the licensor endorses you or your use.

No additional restrictions — You may not apply legal terms or technological measures that legally restrict others from doing anything the license permits.

Notices:

You do not have to comply with the license for elements of the material in the public domain or where your use is permitted by an applicable exception or limitation.

No warranties are given. The license may not give you all of the permissions necessary for your intended use. For example, other rights such as publicity, privacy, or moral rights may limit how you use the material.

APPENDIX C: MATLAB CODE - TRAFFCODE.M

```
aadtt = 687;
split =
xlsread('DanvilleVAdatabucket.v2.xlsx','MEPDG_TRUCK_VOL_PARAMETERS','p2:p11')
;
grwth =
xlsread('DanvilleVAdatabucket.v2.xlsx','MEPDG_TRUCK_VOL_PARAMETERS','h2:h11')
;
traff = xlsread('DanvilleVAdatabucket.v2.xlsx','Truck_Calculations
','m2:ay300');

linea = [2, 3, 4];
comp = [1; 5; 6; 7; 8; 9; 10];

traff = traff./100;
grwth = grwth./100;
annualTraff = aadtt.*split.*365;

%Analysis period
new_mat = zeros(size(traff,1),size(traff,2),20);

cls4 = 1:2;
cls5 = 3:4;
cls6 = 5:6;
cls7 = 7:10;
cls8 = 11:12;
cls9 = 13:14;
cls10 = 15:18;
cls11 = 19;
cls12 = 20:21;
cls13 = 22:24;

ind = [1; 1; 2; 2; 3; 3; 4; 4; 4; 4; 5; 5; 6; 6; 7; 7; 7; 7; 8; 9; 9; 10; 10;
10];

% ind2 = [1,26, 51, 76; 101; 126; 151; 176; 201; etc.

trf = zeros(24,1);
trf(:,1) = annualTraff(ind);


for i=1:20
    count2 = 0;

    for j=1:12
        count = 0;
        for k=1:24
            new_mat(k+count2,:,i) = trf(k).*traff(k+count2,:,1);
        end
        count2 = count2 + 25;
    end

    for m = 1:24
```

```
        GR = grwth(ind(m));
        l = find(ind(m)==linea);
        if ~isempty(l)
            %linear
            trf(m,1) = trf(m,1) + GR*i;
        else
            %compound
            trf(m,1) = trf(m,1)*((1+GR)^i);
        end
    end

end
```

APPENDIX D: MATLAB CODE - E_STAR_CCDM.M

```
%This script calculates |E*| values as a function of temperature and depth
for AC sublayers using the current climate Dempsey model.

load('currentclimate_DEMPSEYmodel.mat')

%% Inputs from LTPP Database

% Inputs
S1A =
readmatrix('DanvilleVAmodulidata','Sheet','TST_ESTAR_MODULUS_COEFF','Range','
G17:G17'); %SIGMOIDAL_COEFF_1_A
S2A =
readmatrix('DanvilleVAmodulidata','Sheet','TST_ESTAR_MODULUS_COEFF','Range','
H17:H17'); %SIGMOIDAL_COEFF_2_A
S3A =
readmatrix('DanvilleVAmodulidata','Sheet','TST_ESTAR_MODULUS_COEFF','Range','
I17:I17'); %SIGMOIDAL_COEFF_3_A
S4A =
readmatrix('DanvilleVAmodulidata','Sheet','TST_ESTAR_MODULUS_COEFF','Range','
J17:J17'); %SIGMOIDAL_COEFF_4_A

SF1A =
readmatrix('DanvilleVAmodulidata','Sheet','TST_ESTAR_MODULUS_COEFF','Range','
K17:K17'); %SHIFT_FACTOR_COEFF_1_A
SF2A =
readmatrix('DanvilleVAmodulidata','Sheet','TST_ESTAR_MODULUS_COEFF','Range','
L17:L17'); %SHIFT_FACTOR_COEFF_2_A
SF3A =
readmatrix('DanvilleVAmodulidata','Sheet','TST_ESTAR_MODULUS_COEFF','Range','
M17:M17'); %SHIFT_FACTOR_COEFF_3_A

F_hz =
readmatrix('DanvilleVAmodulidata','Sheet','TST_ESTAR_MODULUS_COEFF','Range','
C20:C20'); %Frequency in hertz. (Assumed to be constant)
Mr_base_MPa =
readmatrix('DanvilleVAmodulidata','Sheet','TST_UG07_SS07_WKSHT_SUM','Range','
R48:R48'); %Average Resilient Modulus for the base/subbase
Mr_subg_MPa =
readmatrix('DanvilleVAsubgrademodulidata','Sheet','TST_UG07_SS07_WKSHT_SUM','
Range','R18:R18'); %Average Resilient Modulus for the subgrade

%Selecting required layers for analysis

A_CCDM = tmv1c1([2,3,4,7,8,9],:);
B_CCDM = tmv1c2([2,3,4,7,8,9],:);
C_CCDM = tmv1c3([2,3,4,7,8,9],:);
D_CCDM = tmv1c4([2,3,4,7,8,9],:);
E_CCDM = tmv1c5([2,3,4,7,8,9],:);
F_CCDM = tmv1c6([2,3,4,7,8,9],:);
G_CCDM = tmv1c7([2,3,4,7,8,9],:);
H_CCDM = tmv1c8([2,3,4,7,8,9],:);

% Temperature Conversion to Degrees Celsius
```

```
tmv1c1c_CCDM = (A_CCDM - 32).*(5/9);
tmv1c2c_CCDM = (B_CCDM - 32).*(5/9);
tmv1c3c_CCDM = (C_CCDM - 32).*(5/9);
tmv1c4c_CCDM = (D_CCDM - 32).*(5/9);
tmv1c5c_CCDM = (E_CCDM - 32).*(5/9);
tmv1c6c_CCDM = (F_CCDM - 32).*(5/9);
tmv1c7c_CCDM = (G_CCDM - 32).*(5/9);
tmv1c8c_CCDM = (H_CCDM - 32).*(5/9);

%% Calculation of log(aT)

logat_c1_A_CCDM = zeros(6,length(tmv1c1c_CCDM));

for i = 1:length(tmv1c1c_CCDM)

T_sel_c1_A_CCDM = tmv1c1c_CCDM(:,i);
T_calc_c1_A_CCDM = SF1A.*T_sel_c1_A_CCDM.^2 + SF2A.*T_sel_c1_A_CCDM + SF3A;

logat_c1_A_CCDM(:,i) = T_calc_c1_A_CCDM;

end

logat_c2_A_CCDM = zeros(6,length(tmv1c2c_CCDM));

for i = 1:length(tmv1c2c_CCDM)

T_sel_c2_A_CCDM = tmv1c2c_CCDM(:,i);
T_calc_c2_A_CCDM = SF1A.*T_sel_c2_A_CCDM.^2 + SF2A.*T_sel_c2_A_CCDM + SF3A;

logat_c2_A_CCDM(:,i) = T_calc_c2_A_CCDM;

end

logat_c3_A_CCDM = zeros(6,length(tmv1c3c_CCDM));

for i = 1:length(tmv1c3c_CCDM)

T_sel_c3_A_CCDM = tmv1c3c_CCDM(:,i);
T_calc_c3_A_CCDM = SF1A.*T_sel_c3_A_CCDM.^2 + SF2A.*T_sel_c3_A_CCDM + SF3A;

logat_c3_A_CCDM(:,i) = T_calc_c3_A_CCDM;

end

logat_c4_A_CCDM = zeros(6,length(tmv1c4c_CCDM));

for i = 1:length(tmv1c4c_CCDM)

T_sel_c4_A_CCDM = tmv1c4c_CCDM(:,i);
T_calc_c4_A_CCDM = SF1A.*T_sel_c4_A_CCDM.^2 + SF2A.*T_sel_c4_A_CCDM + SF3A;

logat_c4_A_CCDM(:,i) = T_calc_c4_A_CCDM;

end

logat_c5_A_CCDM = zeros(6,length(tmv1c5c_CCDM));
```

```
for i = 1:length(tmv1c5c_CCDM)

T_sel_c5_A_CCDM = tmv1c5c_CCDM(:,i);
T_calc_c5_A_CCDM = SF1A.*T_sel_c5_A_CCDM.^2 + SF2A.*T_sel_c5_A_CCDM + SF3A;

logat_c5_A_CCDM(:,i) = T_calc_c5_A_CCDM;

end

logat_c6_A_CCDM = zeros(6,length(tmv1c6c_CCDM));

for i = 1:length(tmv1c6c_CCDM)

T_sel_c6_A_CCDM = tmv1c6c_CCDM(:,i);
T_calc_c6_A_CCDM = SF1A.*T_sel_c6_A_CCDM.^2 + SF2A.*T_sel_c6_A_CCDM + SF3A;

logat_c6_A_CCDM(:,i) = T_calc_c6_A_CCDM;

end

logat_c7_A_CCDM = zeros(6,length(tmv1c7c_CCDM));

for i = 1:length(tmv1c7c_CCDM)

T_sel_c7_A_CCDM = tmv1c7c_CCDM(:,i);
T_calc_c7_A_CCDM = SF1A.*T_sel_c7_A_CCDM.^2 + SF2A.*T_sel_c7_A_CCDM + SF3A;

logat_c7_A_CCDM(:,i) = T_calc_c7_A_CCDM;

end

logat_c8_A_CCDM = zeros(6,length(tmv1c8c_CCDM));

for i = 1:length(tmv1c8c_CCDM)

T_sel_c8_A_CCDM = tmv1c8c_CCDM(:,i);
T_calc_c8_A_CCDM = SF1A.*T_sel_c8_A_CCDM.^2 + SF2A.*T_sel_c8_A_CCDM + SF3A;

logat_c8_A_CCDM(:,i) = T_calc_c8_A_CCDM;

end

%% Calculation of fr [hz]

fr_c1_A_CCDM = F_hz*10.^(logat_c1_A_CCDM);
fr_c2_A_CCDM = F_hz*10.^(logat_c2_A_CCDM);
fr_c3_A_CCDM = F_hz*10.^(logat_c3_A_CCDM);
fr_c4_A_CCDM = F_hz*10.^(logat_c4_A_CCDM);
fr_c5_A_CCDM = F_hz*10.^(logat_c5_A_CCDM);
fr_c6_A_CCDM = F_hz*10.^(logat_c6_A_CCDM);
fr_c7_A_CCDM = F_hz*10.^(logat_c7_A_CCDM);
fr_c8_A_CCDM = F_hz*10.^(logat_c8_A_CCDM);

%% Calculation of tr

tr_c1_A_CCDM = 1 ./ fr_c1_A_CCDM;
tr_c2_A_CCDM = 1 ./ fr_c2_A_CCDM;
```

```
tr_c3_A_CCDM = 1 ./ fr_c3_A_CCDM;
tr_c4_A_CCDM = 1 ./ fr_c4_A_CCDM;
tr_c5_A_CCDM = 1 ./ fr_c5_A_CCDM;
tr_c6_A_CCDM = 1 ./ fr_c6_A_CCDM;
tr_c7_A_CCDM = 1 ./ fr_c7_A_CCDM;
tr_c8_A_CCDM = 1 ./ fr_c8_A_CCDM;

%% Calculation of log|E*|

log_abs_Estar_C1A_CCDM = S1A + (S2A)./(1+exp((S3A +
S4A.*(log10(tr_c1_A_CCDM)))));
log_abs_Estar_C2A_CCDM = S1A + (S2A)./(1+exp((S3A +
S4A.*(log10(tr_c2_A_CCDM)))));
log_abs_Estar_C3A_CCDM = S1A + (S2A)./(1+exp((S3A +
S4A.*(log10(tr_c3_A_CCDM)))));
log_abs_Estar_C4A_CCDM = S1A + (S2A)./(1+exp((S3A +
S4A.*(log10(tr_c4_A_CCDM)))));
log_abs_Estar_C5A_CCDM = S1A + (S2A)./(1+exp((S3A +
S4A.*(log10(tr_c5_A_CCDM)))));
log_abs_Estar_C6A_CCDM = S1A + (S2A)./(1+exp((S3A +
S4A.*(log10(tr_c6_A_CCDM)))));
log_abs_Estar_C7A_CCDM = S1A + (S2A)./(1+exp((S3A +
S4A.*(log10(tr_c7_A_CCDM)))));
log_abs_Estar_C8A_CCDM = S1A + (S2A)./(1+exp((S3A +
S4A.*(log10(tr_c8_A_CCDM)))));

%% Calculation of Asphalt Moduli Values  Units: [psi -> Mpa]

% Removing the log base

psi_Estar_C1A_CCDM = 10.^(log_abs_Estar_C1A_CCDM);
psi_Estar_C2A_CCDM = 10.^(log_abs_Estar_C2A_CCDM);
psi_Estar_C3A_CCDM = 10.^(log_abs_Estar_C3A_CCDM);
psi_Estar_C4A_CCDM = 10.^(log_abs_Estar_C4A_CCDM);
psi_Estar_C5A_CCDM = 10.^(log_abs_Estar_C5A_CCDM);
psi_Estar_C6A_CCDM = 10.^(log_abs_Estar_C6A_CCDM);
psi_Estar_C7A_CCDM = 10.^(log_abs_Estar_C7A_CCDM);
psi_Estar_C8A_CCDM = 10.^(log_abs_Estar_C8A_CCDM);

% Conversion to [MPa]

AC_mod_C1A_CCDM = (psi_Estar_C1A_CCDM.*0.00689475729);
AC_mod_C2A_CCDM = (psi_Estar_C2A_CCDM.*0.00689475729);
AC_mod_C3A_CCDM = (psi_Estar_C3A_CCDM.*0.00689475729);
AC_mod_C4A_CCDM = (psi_Estar_C4A_CCDM.*0.00689475729);
AC_mod_C5A_CCDM = (psi_Estar_C5A_CCDM.*0.00689475729);
AC_mod_C6A_CCDM = (psi_Estar_C6A_CCDM.*0.00689475729);
AC_mod_C7A_CCDM = (psi_Estar_C7A_CCDM.*0.00689475729);
AC_mod_C8A_CCDM = (psi_Estar_C8A_CCDM.*0.00689475729);

%% Calculation of Unbound Moduli Values

%Base/Subbase Moduli Values

Emp_base1_mod1_CCDM = ones(1,length(tmv1c1c_CCDM));
Emp_base1_mod2_CCDM = ones(1,length(tmv1c2c_CCDM));
Emp_base1_mod3_CCDM = ones(1,length(tmv1c3c_CCDM));
```

```
Emp_base1_mod4_CCDM = ones(1,length(tmv1c4c_CCDM));
Emp_base1_mod5_CCDM = ones(1,length(tmv1c5c_CCDM));
Emp_base1_mod6_CCDM = ones(1,length(tmv1c6c_CCDM));
Emp_base1_mod7_CCDM = ones(1,length(tmv1c7c_CCDM));
Emp_base1_mod8_CCDM = ones(1,length(tmv1c8c_CCDM));

Base1_mod1_MPa_CCDM = Mr_base_MPa*Emp_base1_mod1_CCDM;
Base1_mod2_MPa_CCDM = Mr_base_MPa*Emp_base1_mod2_CCDM;
Base1_mod3_MPa_CCDM = Mr_base_MPa*Emp_base1_mod3_CCDM;
Base1_mod4_MPa_CCDM = Mr_base_MPa*Emp_base1_mod4_CCDM;
Base1_mod5_MPa_CCDM = Mr_base_MPa*Emp_base1_mod5_CCDM;
Base1_mod6_MPa_CCDM = Mr_base_MPa*Emp_base1_mod6_CCDM;
Base1_mod7_MPa_CCDM = Mr_base_MPa*Emp_base1_mod7_CCDM;
Base1_mod8_MPa_CCDM = Mr_base_MPa*Emp_base1_mod8_CCDM;

% Treated Subbase

Emp_base2_mod1_CCDM = ones(1,length(tmv1c1c_CCDM));
Emp_base2_mod2_CCDM = ones(1,length(tmv1c2c_CCDM));
Emp_base2_mod3_CCDM = ones(1,length(tmv1c3c_CCDM));
Emp_base2_mod4_CCDM = ones(1,length(tmv1c4c_CCDM));
Emp_base2_mod5_CCDM = ones(1,length(tmv1c5c_CCDM));
Emp_base2_mod6_CCDM = ones(1,length(tmv1c6c_CCDM));
Emp_base2_mod7_CCDM = ones(1,length(tmv1c7c_CCDM));
Emp_base2_mod8_CCDM = ones(1,length(tmv1c8c_CCDM));

Base2_mod1_MPa_CCDM = Mr_base_MPa*Emp_base2_mod1_CCDM;
Base2_mod2_MPa_CCDM = Mr_base_MPa*Emp_base2_mod2_CCDM;
Base2_mod3_MPa_CCDM = Mr_base_MPa*Emp_base2_mod3_CCDM;
Base2_mod4_MPa_CCDM = Mr_base_MPa*Emp_base2_mod4_CCDM;
Base2_mod5_MPa_CCDM = Mr_base_MPa*Emp_base2_mod5_CCDM;
Base2_mod6_MPa_CCDM = Mr_base_MPa*Emp_base2_mod6_CCDM;
Base2_mod7_MPa_CCDM = Mr_base_MPa*Emp_base2_mod7_CCDM;
Base2_mod8_MPa_CCDM = Mr_base_MPa*Emp_base2_mod8_CCDM;

%Subgrade Moduli Values

Emp_subg_mod1_CCDM = ones(1,length(tmv1c1c_CCDM));
Emp_subg_mod2_CCDM = ones(1,length(tmv1c2c_CCDM));
Emp_subg_mod3_CCDM = ones(1,length(tmv1c3c_CCDM));
Emp_subg_mod4_CCDM = ones(1,length(tmv1c4c_CCDM));
Emp_subg_mod5_CCDM = ones(1,length(tmv1c5c_CCDM));
Emp_subg_mod6_CCDM = ones(1,length(tmv1c6c_CCDM));
Emp_subg_mod7_CCDM = ones(1,length(tmv1c7c_CCDM));
Emp_subg_mod8_CCDM = ones(1,length(tmv1c8c_CCDM));

Subg_mod1_MPa_CCDM = Mr_subg_MPa*Emp_subg_mod1_CCDM;
Subg_mod2_MPa_CCDM = Mr_subg_MPa*Emp_subg_mod2_CCDM;
Subg_mod3_MPa_CCDM = Mr_subg_MPa*Emp_subg_mod3_CCDM;
Subg_mod4_MPa_CCDM = Mr_subg_MPa*Emp_subg_mod4_CCDM;
Subg_mod5_MPa_CCDM = Mr_subg_MPa*Emp_subg_mod5_CCDM;
Subg_mod6_MPa_CCDM = Mr_subg_MPa*Emp_subg_mod6_CCDM;
Subg_mod7_MPa_CCDM = Mr_subg_MPa*Emp_subg_mod7_CCDM;
Subg_mod8_MPa_CCDM = Mr_subg_MPa*Emp_subg_mod8_CCDM;

%% Calculation of the Combined Moduli Values
```

```
Mod_MPa_C1A_CCDM =
vertcat(AC_mod_C1A_CCDM,Base1_mod1_MPa_CCDM,Base2_mod1_MPa_CCDM,Subg_mod1_MPa
_CCDM);
Mod_MPa_C2A_CCDM =
vertcat(AC_mod_C2A_CCDM,Base1_mod2_MPa_CCDM,Base2_mod2_MPa_CCDM,Subg_mod2_MPa
_CCDM);
Mod_MPa_C3A_CCDM =
vertcat(AC_mod_C3A_CCDM,Base1_mod3_MPa_CCDM,Base2_mod3_MPa_CCDM,Subg_mod3_MPa
_CCDM);
Mod_MPa_C4A_CCDM =
vertcat(AC_mod_C4A_CCDM,Base1_mod4_MPa_CCDM,Base2_mod4_MPa_CCDM,Subg_mod4_MPa
_CCDM);
Mod_MPa_C5A_CCDM =
vertcat(AC_mod_C5A_CCDM,Base1_mod5_MPa_CCDM,Base2_mod5_MPa_CCDM,Subg_mod5_MPa
_CCDM);
Mod_MPa_C6A_CCDM =
vertcat(AC_mod_C6A_CCDM,Base1_mod6_MPa_CCDM,Base2_mod6_MPa_CCDM,Subg_mod6_MPa
_CCDM);
Mod_MPa_C7A_CCDM =
vertcat(AC_mod_C7A_CCDM,Base1_mod7_MPa_CCDM,Base2_mod7_MPa_CCDM,Subg_mod7_MPa
_CCDM);
Mod_MPa_C8A_CCDM =
vertcat(AC_mod_C8A_CCDM,Base1_mod8_MPa_CCDM,Base2_mod8_MPa_CCDM,Subg_mod8_MPa
_CCDM);

newmat = [Mod_MPa_C1A_CCDM Mod_MPa_C2A_CCDM Mod_MPa_C3A_CCDM Mod_MPa_C4A_CCDM
Mod_MPa_C5A_CCDM Mod_MPa_C6A_CCDM Mod_MPa_C7A_CCDM Mod_MPa_C8A_CCDM];

mod_mat_CCDM = vertcat(newmat, commat);
```

APPENDIX E: MATLAB CODE - E_STAR_CCRM.M

```
%This script calculates the |E*| Curve as a function of temperature and depth
for the current climate revised model.

load('currentclimate_revisedmodel.mat')

%% Inputs from LTPP Database

% Run A Inputs
S1A =
readmatrix('DanvilleVAmodulidata','Sheet','TST_ESTAR_MODULUS_COEFF','Range','
G17:G17'); %SIGMOIDAL_COEFF_1_A
S2A =
readmatrix('DanvilleVAmodulidata','Sheet','TST_ESTAR_MODULUS_COEFF','Range','
H17:H17'); %SIGMOIDAL_COEFF_2_A
S3A =
readmatrix('DanvilleVAmodulidata','Sheet','TST_ESTAR_MODULUS_COEFF','Range','
I17:I17'); %SIGMOIDAL_COEFF_3_A
S4A =
readmatrix('DanvilleVAmodulidata','Sheet','TST_ESTAR_MODULUS_COEFF','Range','
J17:J17'); %SIGMOIDAL_COEFF_4_A

SF1A =
readmatrix('DanvilleVAmodulidata','Sheet','TST_ESTAR_MODULUS_COEFF','Range','
K17:K17'); %SHIFT_FACTOR_COEFF_1_A
SF2A =
readmatrix('DanvilleVAmodulidata','Sheet','TST_ESTAR_MODULUS_COEFF','Range','
L17:L17'); %SHIFT_FACTOR_COEFF_2_A
SF3A =
readmatrix('DanvilleVAmodulidata','Sheet','TST_ESTAR_MODULUS_COEFF','Range','
M17:M17'); %SHIFT_FACTOR_COEFF_3_A

% Common Inputs
F_hz =
readmatrix('DanvilleVAmodulidata','Sheet','TST_ESTAR_MODULUS_COEFF','Range','
C20:C20'); %Frequency in hertz. (Assumed to be constant)
Mr_base_MPa =
readmatrix('DanvilleVAmodulidata','Sheet','TST_UG07_SS07_WKSHT_SUM','Range','
R48:R48'); %Average Resilient Modulus for the base/subbase
Mr_subg_MPa =
readmatrix('DanvilleVAsubgrademodulidata','Sheet','TST_UG07_SS07_WKSHT_SUM','
Range','R18:R18'); %Average Resilient Modulus for the subgrade

%Selecting required layers for analysis

A_CCRM = tmv1c1([2,3,4,7,8,9],:);
B_CCRM = tmv1c2([2,3,4,7,8,9],:);
C_CCRM = tmv1c3([2,3,4,7,8,9],:);
D_CCRM = tmv1c4([2,3,4,7,8,9],:);
E_CCRM = tmv1c5([2,3,4,7,8,9],:);
F_CCRM = tmv1c6([2,3,4,7,8,9],:);
G_CCRM = tmv1c7([2,3,4,7,8,9],:);
H_CCRM = tmv1c8([2,3,4,7,8,9],:);

% Temperature Conversion to Degrees Celsius
```

```
tmv1c1c_CCRM = (A_CCRM - 32).*(5/9);
tmv1c2c_CCRM = (B_CCRM - 32).*(5/9);
tmv1c3c_CCRM = (C_CCRM - 32).*(5/9);
tmv1c4c_CCRM = (D_CCRM - 32).*(5/9);
tmv1c5c_CCRM = (E_CCRM - 32).*(5/9);
tmv1c6c_CCRM = (F_CCRM - 32).*(5/9);
tmv1c7c_CCRM = (G_CCRM - 32).*(5/9);
tmv1c8c_CCRM = (H_CCRM - 32).*(5/9);

%% Calculation of log(aT)

%This calculation will have to be performed 8 times, due to there being 8
%runs, and 8 subsequently stored matrices of data

%L_at = ((SF1A)*(T^2)) + ((SF2A)*(T)) + SF3A

% Run A

logat_c1_A_CCRM = zeros(6,length(tmv1c1c_CCRM));

for i = 1:length(tmv1c1c_CCRM)

T_sel_c1_A_CCRM = tmv1c1c_CCRM(:,i);
T_calc_c1_A_CCRM = SF1A.*T_sel_c1_A_CCRM.^2 + SF2A.*T_sel_c1_A_CCRM + SF3A;

logat_c1_A_CCRM(:,i) = T_calc_c1_A_CCRM;

end

logat_c2_A_CCRM = zeros(6,length(tmv1c2c_CCRM));

for i = 1:length(tmv1c2c_CCRM)

T_sel_c2_A_CCRM = tmv1c2c_CCRM(:,i);
T_calc_c2_A_CCRM = SF1A.*T_sel_c2_A_CCRM.^2 + SF2A.*T_sel_c2_A_CCRM + SF3A;

logat_c2_A_CCRM(:,i) = T_calc_c2_A_CCRM;

end

logat_c3_A_CCRM = zeros(6,length(tmv1c3c_CCRM));

for i = 1:length(tmv1c3c_CCRM)

T_sel_c3_A_CCRM = tmv1c3c_CCRM(:,i);
T_calc_c3_A_CCRM = SF1A.*T_sel_c3_A_CCRM.^2 + SF2A.*T_sel_c3_A_CCRM + SF3A;

logat_c3_A_CCRM(:,i) = T_calc_c3_A_CCRM;

end

logat_c4_A_CCRM = zeros(6,length(tmv1c4c_CCRM));

for i = 1:length(tmv1c4c_CCRM)

T_sel_c4_A_CCRM = tmv1c4c_CCRM(:,i);
```

```
T_calc_c4_A_CCRM = SF1A.*T_sel_c4_A_CCRM.^2 + SF2A.*T_sel_c4_A_CCRM + SF3A;

logat_c4_A_CCRM(:,i) = T_calc_c4_A_CCRM;

end

logat_c5_A_CCRM = zeros(6,length(tmv1c5c_CCRM));

for i = 1:length(tmv1c5c_CCRM)

T_sel_c5_A_CCRM = tmv1c5c_CCRM(:,i);
T_calc_c5_A_CCRM = SF1A.*T_sel_c5_A_CCRM.^2 + SF2A.*T_sel_c5_A_CCRM + SF3A;

logat_c5_A_CCRM(:,i) = T_calc_c5_A_CCRM;

end

logat_c6_A_CCRM = zeros(6,length(tmv1c6c_CCRM));

for i = 1:length(tmv1c6c_CCRM)

T_sel_c6_A_CCRM = tmv1c6c_CCRM(:,i);
T_calc_c6_A_CCRM = SF1A.*T_sel_c6_A_CCRM.^2 + SF2A.*T_sel_c6_A_CCRM + SF3A;

logat_c6_A_CCRM(:,i) = T_calc_c6_A_CCRM;

end

logat_c7_A_CCRM = zeros(6,length(tmv1c7c_CCRM));

for i = 1:length(tmv1c7c_CCRM)

T_sel_c7_A_CCRM = tmv1c7c_CCRM(:,i);
T_calc_c7_A_CCRM = SF1A.*T_sel_c7_A_CCRM.^2 + SF2A.*T_sel_c7_A_CCRM + SF3A;

logat_c7_A_CCRM(:,i) = T_calc_c7_A_CCRM;

end

logat_c8_A_CCRM = zeros(6,length(tmv1c8c_CCRM));

for i = 1:length(tmv1c8c_CCRM)

T_sel_c8_A_CCRM = tmv1c8c_CCRM(:,i);
T_calc_c8_A_CCRM = SF1A.*T_sel_c8_A_CCRM.^2 + SF2A.*T_sel_c8_A_CCRM + SF3A;

logat_c8_A_CCRM(:,i) = T_calc_c8_A_CCRM;

end

%% Calculation of fr [hz]

% Run A

fr_c1_A_CCRM = F_hz*10.^(logat_c1_A_CCRM);
fr_c2_A_CCRM = F_hz*10.^(logat_c2_A_CCRM);
fr_c3_A_CCRM = F_hz*10.^(logat_c3_A_CCRM);
```

```
fr_c4_A_CCRM = F_hz*10.^(logat_c4_A_CCRM);
fr_c5_A_CCRM = F_hz*10.^(logat_c5_A_CCRM);
fr_c6_A_CCRM = F_hz*10.^(logat_c6_A_CCRM);
fr_c7_A_CCRM = F_hz*10.^(logat_c7_A_CCRM);
fr_c8_A_CCRM = F_hz*10.^(logat_c8_A_CCRM);

%% Calculation of tr

% Run A

tr_c1_A_CCRM = 1 ./ fr_c1_A_CCRM;
tr_c2_A_CCRM = 1 ./ fr_c2_A_CCRM;
tr_c3_A_CCRM = 1 ./ fr_c3_A_CCRM;
tr_c4_A_CCRM = 1 ./ fr_c4_A_CCRM;
tr_c5_A_CCRM = 1 ./ fr_c5_A_CCRM;
tr_c6_A_CCRM = 1 ./ fr_c6_A_CCRM;
tr_c7_A_CCRM = 1 ./ fr_c7_A_CCRM;
tr_c8_A_CCRM = 1 ./ fr_c8_A_CCRM;

%% Calculation of log|E*|

% Run A

log_abs_Estar_C1A_CCRM = S1A + (S2A)./(1+exp((S3A +
S4A.*(log10(tr_c1_A_CCRM)))));
log_abs_Estar_C2A_CCRM = S1A + (S2A)./(1+exp((S3A +
S4A.*(log10(tr_c2_A_CCRM)))));
log_abs_Estar_C3A_CCRM = S1A + (S2A)./(1+exp((S3A +
S4A.*(log10(tr_c3_A_CCRM)))));
log_abs_Estar_C4A_CCRM = S1A + (S2A)./(1+exp((S3A +
S4A.*(log10(tr_c4_A_CCRM)))));
log_abs_Estar_C5A_CCRM = S1A + (S2A)./(1+exp((S3A +
S4A.*(log10(tr_c5_A_CCRM)))));
log_abs_Estar_C6A_CCRM = S1A + (S2A)./(1+exp((S3A +
S4A.*(log10(tr_c6_A_CCRM)))));
log_abs_Estar_C7A_CCRM = S1A + (S2A)./(1+exp((S3A +
S4A.*(log10(tr_c7_A_CCRM)))));
log_abs_Estar_C8A_CCRM = S1A + (S2A)./(1+exp((S3A +
S4A.*(log10(tr_c8_A_CCRM)))));

%% Calculation of Asphalt Moduli Values  Units: [psi -> Mpa]

% Removing the log base

% Run A

psi_Estar_C1A_CCRM = 10.^(log_abs_Estar_C1A_CCRM);
psi_Estar_C2A_CCRM = 10.^(log_abs_Estar_C2A_CCRM);
psi_Estar_C3A_CCRM = 10.^(log_abs_Estar_C3A_CCRM);
psi_Estar_C4A_CCRM = 10.^(log_abs_Estar_C4A_CCRM);
psi_Estar_C5A_CCRM = 10.^(log_abs_Estar_C5A_CCRM);
psi_Estar_C6A_CCRM = 10.^(log_abs_Estar_C6A_CCRM);
psi_Estar_C7A_CCRM = 10.^(log_abs_Estar_C7A_CCRM);
psi_Estar_C8A_CCRM = 10.^(log_abs_Estar_C8A_CCRM);

% Conversion to [MPa]
```

```
% Run A

AC_mod_C1A_CCRM = (psi_Estar_C1A_CCRM.*0.00689475729);
AC_mod_C2A_CCRM = (psi_Estar_C2A_CCRM.*0.00689475729);
AC_mod_C3A_CCRM = (psi_Estar_C3A_CCRM.*0.00689475729);
AC_mod_C4A_CCRM = (psi_Estar_C4A_CCRM.*0.00689475729);
AC_mod_C5A_CCRM = (psi_Estar_C5A_CCRM.*0.00689475729);
AC_mod_C6A_CCRM = (psi_Estar_C6A_CCRM.*0.00689475729);
AC_mod_C7A_CCRM = (psi_Estar_C7A_CCRM.*0.00689475729);
AC_mod_C8A_CCRM = (psi_Estar_C8A_CCRM.*0.00689475729);

%% Calculation of Unbound Moduli Values

%Base/Subbase Moduli Values

% Granular (untreated) Base

Emp_base1_mod1_CCRM = ones(1,length(tmv1c1c_CCRM));
Emp_base1_mod2_CCRM = ones(1,length(tmv1c2c_CCRM));
Emp_base1_mod3_CCRM = ones(1,length(tmv1c3c_CCRM));
Emp_base1_mod4_CCRM = ones(1,length(tmv1c4c_CCRM));
Emp_base1_mod5_CCRM = ones(1,length(tmv1c5c_CCRM));
Emp_base1_mod6_CCRM = ones(1,length(tmv1c6c_CCRM));
Emp_base1_mod7_CCRM = ones(1,length(tmv1c7c_CCRM));
Emp_base1_mod8_CCRM = ones(1,length(tmv1c8c_CCRM));

Base1_mod1_MPa_CCRM = Mr_base_MPa*Emp_base1_mod1_CCRM;
Base1_mod2_MPa_CCRM = Mr_base_MPa*Emp_base1_mod2_CCRM;
Base1_mod3_MPa_CCRM = Mr_base_MPa*Emp_base1_mod3_CCRM;
Base1_mod4_MPa_CCRM = Mr_base_MPa*Emp_base1_mod4_CCRM;
Base1_mod5_MPa_CCRM = Mr_base_MPa*Emp_base1_mod5_CCRM;
Base1_mod6_MPa_CCRM = Mr_base_MPa*Emp_base1_mod6_CCRM;
Base1_mod7_MPa_CCRM = Mr_base_MPa*Emp_base1_mod7_CCRM;
Base1_mod8_MPa_CCRM = Mr_base_MPa*Emp_base1_mod8_CCRM;

% Treated Subbase

Emp_base2_mod1_CCRM = ones(1,length(tmv1c1c_CCRM));
Emp_base2_mod2_CCRM = ones(1,length(tmv1c2c_CCRM));
Emp_base2_mod3_CCRM = ones(1,length(tmv1c3c_CCRM));
Emp_base2_mod4_CCRM = ones(1,length(tmv1c4c_CCRM));
Emp_base2_mod5_CCRM = ones(1,length(tmv1c5c_CCRM));
Emp_base2_mod6_CCRM = ones(1,length(tmv1c6c_CCRM));
Emp_base2_mod7_CCRM = ones(1,length(tmv1c7c_CCRM));
Emp_base2_mod8_CCRM = ones(1,length(tmv1c8c_CCRM));

Base2_mod1_MPa_CCRM = Mr_base_MPa*Emp_base2_mod1_CCRM;
Base2_mod2_MPa_CCRM = Mr_base_MPa*Emp_base2_mod2_CCRM;
Base2_mod3_MPa_CCRM = Mr_base_MPa*Emp_base2_mod3_CCRM;
Base2_mod4_MPa_CCRM = Mr_base_MPa*Emp_base2_mod4_CCRM;
Base2_mod5_MPa_CCRM = Mr_base_MPa*Emp_base2_mod5_CCRM;
Base2_mod6_MPa_CCRM = Mr_base_MPa*Emp_base2_mod6_CCRM;
Base2_mod7_MPa_CCRM = Mr_base_MPa*Emp_base2_mod7_CCRM;
Base2_mod8_MPa_CCRM = Mr_base_MPa*Emp_base2_mod8_CCRM;

%Subgrade Moduli Values
```

```
Emp_subg_mod1_CCRM = ones(1,length(tmv1c1c_CCRM));
Emp_subg_mod2_CCRM = ones(1,length(tmv1c2c_CCRM));
Emp_subg_mod3_CCRM = ones(1,length(tmv1c3c_CCRM));
Emp_subg_mod4_CCRM = ones(1,length(tmv1c4c_CCRM));
Emp_subg_mod5_CCRM = ones(1,length(tmv1c5c_CCRM));
Emp_subg_mod6_CCRM = ones(1,length(tmv1c6c_CCRM));
Emp_subg_mod7_CCRM = ones(1,length(tmv1c7c_CCRM));
Emp_subg_mod8_CCRM = ones(1,length(tmv1c8c_CCRM));

Subg_mod1_MPa_CCRM = Mr_subg_MPa*Emp_subg_mod1_CCRM;
Subg_mod2_MPa_CCRM = Mr_subg_MPa*Emp_subg_mod2_CCRM;
Subg_mod3_MPa_CCRM = Mr_subg_MPa*Emp_subg_mod3_CCRM;
Subg_mod4_MPa_CCRM = Mr_subg_MPa*Emp_subg_mod4_CCRM;
Subg_mod5_MPa_CCRM = Mr_subg_MPa*Emp_subg_mod5_CCRM;
Subg_mod6_MPa_CCRM = Mr_subg_MPa*Emp_subg_mod6_CCRM;
Subg_mod7_MPa_CCRM = Mr_subg_MPa*Emp_subg_mod7_CCRM;
Subg_mod8_MPa_CCRM = Mr_subg_MPa*Emp_subg_mod8_CCRM;

%% Calculation of the Combined Moduli Values

% Run A

Mod_MPa_C1A_CCRM =
vertcat(AC_mod_C1A_CCRM,Base1_mod1_MPa_CCRM,Base2_mod1_MPa_CCRM,Subg_mod1_MPa
_CCRM);
Mod_MPa_C2A_CCRM =
vertcat(AC_mod_C2A_CCRM,Base1_mod2_MPa_CCRM,Base2_mod2_MPa_CCRM,Subg_mod2_MPa
_CCRM);
Mod_MPa_C3A_CCRM =
vertcat(AC_mod_C3A_CCRM,Base1_mod3_MPa_CCRM,Base2_mod3_MPa_CCRM,Subg_mod3_MPa
_CCRM);
Mod_MPa_C4A_CCRM =
vertcat(AC_mod_C4A_CCRM,Base1_mod4_MPa_CCRM,Base2_mod4_MPa_CCRM,Subg_mod4_MPa
_CCRM);
Mod_MPa_C5A_CCRM =
vertcat(AC_mod_C5A_CCRM,Base1_mod5_MPa_CCRM,Base2_mod5_MPa_CCRM,Subg_mod5_MPa
_CCRM);
Mod_MPa_C6A_CCRM =
vertcat(AC_mod_C6A_CCRM,Base1_mod6_MPa_CCRM,Base2_mod6_MPa_CCRM,Subg_mod6_MPa
_CCRM);
Mod_MPa_C7A_CCRM =
vertcat(AC_mod_C7A_CCRM,Base1_mod7_MPa_CCRM,Base2_mod7_MPa_CCRM,Subg_mod7_MPa
_CCRM);
Mod_MPa_C8A_CCRM =
vertcat(AC_mod_C8A_CCRM,Base1_mod8_MPa_CCRM,Base2_mod8_MPa_CCRM,Subg_mod8_MPa
_CCRM);

newmat = [Mod_MPa_C1A_CCRM Mod_MPa_C2A_CCRM Mod_MPa_C3A_CCRM Mod_MPa_C4A_CCRM
Mod_MPa_C5A_CCRM Mod_MPa_C6A_CCRM Mod_MPa_C7A_CCRM Mod_MPa_C8A_CCRM];

mod_mat_CCRM = vertcat(newmat, commat);
```

APPENDIX F: MATLAB CODE - E_STAR_FCRM.M

```
%This script calculates the |E*| Curve as a function of temperature and depth
for the current climate revised model.

load('futureclimate_revisedmodel.mat')

%% Inputs from LTPP Database

% Run A Inputs
S1A =
readmatrix('DanvilleVAmodulidata','Sheet','TST_ESTAR_MODULUS_COEFF','Range','
G17:G17'); %SIGMOIDAL_COEFF_1_A
S2A =
readmatrix('DanvilleVAmodulidata','Sheet','TST_ESTAR_MODULUS_COEFF','Range','
H17:H17'); %SIGMOIDAL_COEFF_2_A
S3A =
readmatrix('DanvilleVAmodulidata','Sheet','TST_ESTAR_MODULUS_COEFF','Range','
I17:I17'); %SIGMOIDAL_COEFF_3_A
S4A =
readmatrix('DanvilleVAmodulidata','Sheet','TST_ESTAR_MODULUS_COEFF','Range','
J17:J17'); %SIGMOIDAL_COEFF_4_A

SF1A =
readmatrix('DanvilleVAmodulidata','Sheet','TST_ESTAR_MODULUS_COEFF','Range','
K17:K17'); %SHIFT_FACTOR_COEFF_1_A
SF2A =
readmatrix('DanvilleVAmodulidata','Sheet','TST_ESTAR_MODULUS_COEFF','Range','
L17:L17'); %SHIFT_FACTOR_COEFF_2_A
SF3A =
readmatrix('DanvilleVAmodulidata','Sheet','TST_ESTAR_MODULUS_COEFF','Range','
M17:M17'); %SHIFT_FACTOR_COEFF_3_A

% Common Inputs
F_hz =
readmatrix('DanvilleVAmodulidata','Sheet','TST_ESTAR_MODULUS_COEFF','Range','
C20:C20'); %Frequency in hertz. (Assumed to be constant)
Mr_base_MPa =
readmatrix('DanvilleVAmodulidata','Sheet','TST_UG07_SS07_WKSHT_SUM','Range','
R48:R48'); %Average Resilient Modulus for the base/subbase
Mr_subg_MPa =
readmatrix('DanvilleVAsubgrademodulidata','Sheet','TST_UG07_SS07_WKSHT_SUM','
Range','R18:R18'); %Average Resilient Modulus for the subgrade

%Selecting required layers for analysis

A_FCRM = tmv1c1([2,3,4,7,8,9],:);
B_FCRM = tmv1c2([2,3,4,7,8,9],:);
C_FCRM = tmv1c3([2,3,4,7,8,9],:);
D_FCRM = tmv1c4([2,3,4,7,8,9],:);
E_FCRM = tmv1c5([2,3,4,7,8,9],:);
F_FCRM = tmv1c6([2,3,4,7,8,9],:);
G_FCRM = tmv1c7([2,3,4,7,8,9],:);
H_FCRM = tmv1c8([2,3,4,7,8,9],:);

% Temperature Conversion to Degrees Celcius
```

```
tmv1c1c_FCRM = (A_FCRM - 32).*(5/9);
tmv1c2c_FCRM = (B_FCRM - 32).*(5/9);
tmv1c3c_FCRM = (C_FCRM - 32).*(5/9);
tmv1c4c_FCRM = (D_FCRM - 32).*(5/9);
tmv1c5c_FCRM = (E_FCRM - 32).*(5/9);
tmv1c6c_FCRM = (F_FCRM - 32).*(5/9);
tmv1c7c_FCRM = (G_FCRM - 32).*(5/9);
tmv1c8c_FCRM = (H_FCRM - 32).*(5/9);

%% Calculation of log(aT)

%This calculation will have to be performed 8 times, due to there being 8
%runs, and 8 subsequently stored matrices of data

%L_at = ((SF1A)*(T^2)) + ((SF2A)*(T)) + SF3A

% Run A

logat_c1_A_FCRM = zeros(6,length(tmv1c1c_FCRM));

for i = 1:length(tmv1c1c_FCRM)

T_sel_c1_A_FCRM = tmv1c1c_FCRM(:,i);
T_calc_c1_A_FCRM = SF1A.*T_sel_c1_A_FCRM.^2 + SF2A.*T_sel_c1_A_FCRM + SF3A;

logat_c1_A_FCRM(:,i) = T_calc_c1_A_FCRM;

end

logat_c2_A_FCRM = zeros(6,length(tmv1c2c_FCRM));

for i = 1:length(tmv1c2c_FCRM)

T_sel_c2_A_FCRM = tmv1c2c_FCRM(:,i);
T_calc_c2_A_FCRM = SF1A.*T_sel_c2_A_FCRM.^2 + SF2A.*T_sel_c2_A_FCRM + SF3A;

logat_c2_A_FCRM(:,i) = T_calc_c2_A_FCRM;

end

logat_c3_A_FCRM = zeros(6,length(tmv1c3c_FCRM));

for i = 1:length(tmv1c3c_FCRM)

T_sel_c3_A_FCRM = tmv1c3c_FCRM(:,i);
T_calc_c3_A_FCRM = SF1A.*T_sel_c3_A_FCRM.^2 + SF2A.*T_sel_c3_A_FCRM + SF3A;

logat_c3_A_FCRM(:,i) = T_calc_c3_A_FCRM;

end

logat_c4_A_FCRM = zeros(6,length(tmv1c4c_FCRM));

for i = 1:length(tmv1c4c_FCRM)

T_sel_c4_A_FCRM = tmv1c4c_FCRM(:,i);
```

```
T_calc_c4_A_FCRM = SF1A.*T_sel_c4_A_FCRM.^2 + SF2A.*T_sel_c4_A_FCRM + SF3A;

logat_c4_A_FCRM(:,i) = T_calc_c4_A_FCRM;

end

logat_c5_A_FCRM = zeros(6,length(tmv1c5c_FCRM));

for i = 1:length(tmv1c5c_FCRM)

T_sel_c5_A_FCRM = tmv1c5c_FCRM(:,i);
T_calc_c5_A_FCRM = SF1A.*T_sel_c5_A_FCRM.^2 + SF2A.*T_sel_c5_A_FCRM + SF3A;

logat_c5_A_FCRM(:,i) = T_calc_c5_A_FCRM;

end

logat_c6_A_FCRM = zeros(6,length(tmv1c6c_FCRM));

for i = 1:length(tmv1c6c_FCRM)

T_sel_c6_A_FCRM = tmv1c6c_FCRM(:,i);
T_calc_c6_A_FCRM = SF1A.*T_sel_c6_A_FCRM.^2 + SF2A.*T_sel_c6_A_FCRM + SF3A;

logat_c6_A_FCRM(:,i) = T_calc_c6_A_FCRM;

end

logat_c7_A_FCRM = zeros(6,length(tmv1c7c_FCRM));

for i = 1:length(tmv1c7c_FCRM)

T_sel_c7_A_FCRM = tmv1c7c_FCRM(:,i);
T_calc_c7_A_FCRM = SF1A.*T_sel_c7_A_FCRM.^2 + SF2A.*T_sel_c7_A_FCRM + SF3A;

logat_c7_A_FCRM(:,i) = T_calc_c7_A_FCRM;

end

logat_c8_A_FCRM = zeros(6,length(tmv1c8c_FCRM));

for i = 1:length(tmv1c8c_FCRM)

T_sel_c8_A_FCRM = tmv1c8c_FCRM(:,i);
T_calc_c8_A_FCRM = SF1A.*T_sel_c8_A_FCRM.^2 + SF2A.*T_sel_c8_A_FCRM + SF3A;

logat_c8_A_FCRM(:,i) = T_calc_c8_A_FCRM;

end

%% Calculation of fr [hz]

% Run A

fr_c1_A_FCRM = F_hz*10.^(logat_c1_A_FCRM);
fr_c2_A_FCRM = F_hz*10.^(logat_c2_A_FCRM);
fr_c3_A_FCRM = F_hz*10.^(logat_c3_A_FCRM);
```

```
fr_c4_A_FCRM = F_hz*10.^(logat_c4_A_FCRM);
fr_c5_A_FCRM = F_hz*10.^(logat_c5_A_FCRM);
fr_c6_A_FCRM = F_hz*10.^(logat_c6_A_FCRM);
fr_c7_A_FCRM = F_hz*10.^(logat_c7_A_FCRM);
fr_c8_A_FCRM = F_hz*10.^(logat_c8_A_FCRM);

%% Calculation of tr

% Run A

tr_c1_A_FCRM = 1 ./ fr_c1_A_FCRM;
tr_c2_A_FCRM = 1 ./ fr_c2_A_FCRM;
tr_c3_A_FCRM = 1 ./ fr_c3_A_FCRM;
tr_c4_A_FCRM = 1 ./ fr_c4_A_FCRM;
tr_c5_A_FCRM = 1 ./ fr_c5_A_FCRM;
tr_c6_A_FCRM = 1 ./ fr_c6_A_FCRM;
tr_c7_A_FCRM = 1 ./ fr_c7_A_FCRM;
tr_c8_A_FCRM = 1 ./ fr_c8_A_FCRM;

%% Calculation of log|E*|

% Run A

log_abs_Estar_C1A_FCRM = S1A + (S2A)./(1+exp((S3A +
S4A.*(log10(tr_c1_A_FCRM)))));
log_abs_Estar_C2A_FCRM = S1A + (S2A)./(1+exp((S3A +
S4A.*(log10(tr_c2_A_FCRM)))));
log_abs_Estar_C3A_FCRM = S1A + (S2A)./(1+exp((S3A +
S4A.*(log10(tr_c3_A_FCRM)))));
log_abs_Estar_C4A_FCRM = S1A + (S2A)./(1+exp((S3A +
S4A.*(log10(tr_c4_A_FCRM)))));
log_abs_Estar_C5A_FCRM = S1A + (S2A)./(1+exp((S3A +
S4A.*(log10(tr_c5_A_FCRM)))));
log_abs_Estar_C6A_FCRM = S1A + (S2A)./(1+exp((S3A +
S4A.*(log10(tr_c6_A_FCRM)))));
log_abs_Estar_C7A_FCRM = S1A + (S2A)./(1+exp((S3A +
S4A.*(log10(tr_c7_A_FCRM)))));
log_abs_Estar_C8A_FCRM = S1A + (S2A)./(1+exp((S3A +
S4A.*(log10(tr_c8_A_FCRM)))));

%% Calculation of Asphalt Moduli Values  Units: [psi -> Mpa]

% Removing the log base

% Run A

psi_Estar_C1A_FCRM = 10.^(log_abs_Estar_C1A_FCRM);
psi_Estar_C2A_FCRM = 10.^(log_abs_Estar_C2A_FCRM);
psi_Estar_C3A_FCRM = 10.^(log_abs_Estar_C3A_FCRM);
psi_Estar_C4A_FCRM = 10.^(log_abs_Estar_C4A_FCRM);
psi_Estar_C5A_FCRM = 10.^(log_abs_Estar_C5A_FCRM);
psi_Estar_C6A_FCRM = 10.^(log_abs_Estar_C6A_FCRM);
psi_Estar_C7A_FCRM = 10.^(log_abs_Estar_C7A_FCRM);
psi_Estar_C8A_FCRM = 10.^(log_abs_Estar_C8A_FCRM);

% Conversion to [MPa]
```

```
% Run A

AC_mod_C1A_FCRM = (psi_Estar_C1A_FCRM.*0.00689475729);
AC_mod_C2A_FCRM = (psi_Estar_C2A_FCRM.*0.00689475729);
AC_mod_C3A_FCRM = (psi_Estar_C3A_FCRM.*0.00689475729);
AC_mod_C4A_FCRM = (psi_Estar_C4A_FCRM.*0.00689475729);
AC_mod_C5A_FCRM = (psi_Estar_C5A_FCRM.*0.00689475729);
AC_mod_C6A_FCRM = (psi_Estar_C6A_FCRM.*0.00689475729);
AC_mod_C7A_FCRM = (psi_Estar_C7A_FCRM.*0.00689475729);
AC_mod_C8A_FCRM = (psi_Estar_C8A_FCRM.*0.00689475729);

%% Calculation of Unbound Moduli Values

%Base/Subbase Moduli Values

% Granular (untreated) Base

Emp_base1_mod1_FCRM = ones(1,length(tmv1c1c_FCRM));
Emp_base1_mod2_FCRM = ones(1,length(tmv1c2c_FCRM));
Emp_base1_mod3_FCRM = ones(1,length(tmv1c3c_FCRM));
Emp_base1_mod4_FCRM = ones(1,length(tmv1c4c_FCRM));
Emp_base1_mod5_FCRM = ones(1,length(tmv1c5c_FCRM));
Emp_base1_mod6_FCRM = ones(1,length(tmv1c6c_FCRM));
Emp_base1_mod7_FCRM = ones(1,length(tmv1c7c_FCRM));
Emp_base1_mod8_FCRM = ones(1,length(tmv1c8c_FCRM));

Base1_mod1_MPa_FCRM = Mr_base_MPa*Emp_base1_mod1_FCRM;
Base1_mod2_MPa_FCRM = Mr_base_MPa*Emp_base1_mod2_FCRM;
Base1_mod3_MPa_FCRM = Mr_base_MPa*Emp_base1_mod3_FCRM;
Base1_mod4_MPa_FCRM = Mr_base_MPa*Emp_base1_mod4_FCRM;
Base1_mod5_MPa_FCRM = Mr_base_MPa*Emp_base1_mod5_FCRM;
Base1_mod6_MPa_FCRM = Mr_base_MPa*Emp_base1_mod6_FCRM;
Base1_mod7_MPa_FCRM = Mr_base_MPa*Emp_base1_mod7_FCRM;
Base1_mod8_MPa_FCRM = Mr_base_MPa*Emp_base1_mod8_FCRM;

% Treated Subbase

Emp_base2_mod1_FCRM = ones(1,length(tmv1c1c_FCRM));
Emp_base2_mod2_FCRM = ones(1,length(tmv1c2c_FCRM));
Emp_base2_mod3_FCRM = ones(1,length(tmv1c3c_FCRM));
Emp_base2_mod4_FCRM = ones(1,length(tmv1c4c_FCRM));
Emp_base2_mod5_FCRM = ones(1,length(tmv1c5c_FCRM));
Emp_base2_mod6_FCRM = ones(1,length(tmv1c6c_FCRM));
Emp_base2_mod7_FCRM = ones(1,length(tmv1c7c_FCRM));
Emp_base2_mod8_FCRM = ones(1,length(tmv1c8c_FCRM));

Base2_mod1_MPa_FCRM = Mr_base_MPa*Emp_base2_mod1_FCRM;
Base2_mod2_MPa_FCRM = Mr_base_MPa*Emp_base2_mod2_FCRM;
Base2_mod3_MPa_FCRM = Mr_base_MPa*Emp_base2_mod3_FCRM;
Base2_mod4_MPa_FCRM = Mr_base_MPa*Emp_base2_mod4_FCRM;
Base2_mod5_MPa_FCRM = Mr_base_MPa*Emp_base2_mod5_FCRM;
Base2_mod6_MPa_FCRM = Mr_base_MPa*Emp_base2_mod6_FCRM;
Base2_mod7_MPa_FCRM = Mr_base_MPa*Emp_base2_mod7_FCRM;
Base2_mod8_MPa_FCRM = Mr_base_MPa*Emp_base2_mod8_FCRM;

%Subgrade Moduli Values
```

```
Emp_subg_mod1_FCRM = ones(1,length(tmv1c1c_FCRM));
Emp_subg_mod2_FCRM = ones(1,length(tmv1c2c_FCRM));
Emp_subg_mod3_FCRM = ones(1,length(tmv1c3c_FCRM));
Emp_subg_mod4_FCRM = ones(1,length(tmv1c4c_FCRM));
Emp_subg_mod5_FCRM = ones(1,length(tmv1c5c_FCRM));
Emp_subg_mod6_FCRM = ones(1,length(tmv1c6c_FCRM));
Emp_subg_mod7_FCRM = ones(1,length(tmv1c7c_FCRM));
Emp_subg_mod8_FCRM = ones(1,length(tmv1c8c_FCRM));

Subg_mod1_MPa_FCRM = Mr_subg_MPa*Emp_subg_mod1_FCRM;
Subg_mod2_MPa_FCRM = Mr_subg_MPa*Emp_subg_mod2_FCRM;
Subg_mod3_MPa_FCRM = Mr_subg_MPa*Emp_subg_mod3_FCRM;
Subg_mod4_MPa_FCRM = Mr_subg_MPa*Emp_subg_mod4_FCRM;
Subg_mod5_MPa_FCRM = Mr_subg_MPa*Emp_subg_mod5_FCRM;
Subg_mod6_MPa_FCRM = Mr_subg_MPa*Emp_subg_mod6_FCRM;
Subg_mod7_MPa_FCRM = Mr_subg_MPa*Emp_subg_mod7_FCRM;
Subg_mod8_MPa_FCRM = Mr_subg_MPa*Emp_subg_mod8_FCRM;

%% Calculation of the Combined Moduli Values

% Run A

Mod_MPa_C1A_FCRM =
vertcat(AC_mod_C1A_FCRM,Base1_mod1_MPa_FCRM,Base2_mod1_MPa_FCRM,Subg_mod1_MPa
_FCRM);
Mod_MPa_C2A_FCRM =
vertcat(AC_mod_C2A_FCRM,Base1_mod2_MPa_FCRM,Base2_mod2_MPa_FCRM,Subg_mod2_MPa
_FCRM);
Mod_MPa_C3A_FCRM =
vertcat(AC_mod_C3A_FCRM,Base1_mod3_MPa_FCRM,Base2_mod3_MPa_FCRM,Subg_mod3_MPa
_FCRM);
Mod_MPa_C4A_FCRM =
vertcat(AC_mod_C4A_FCRM,Base1_mod4_MPa_FCRM,Base2_mod4_MPa_FCRM,Subg_mod4_MPa
_FCRM);
Mod_MPa_C5A_FCRM =
vertcat(AC_mod_C5A_FCRM,Base1_mod5_MPa_FCRM,Base2_mod5_MPa_FCRM,Subg_mod5_MPa
_FCRM);
Mod_MPa_C6A_FCRM =
vertcat(AC_mod_C6A_FCRM,Base1_mod6_MPa_FCRM,Base2_mod6_MPa_FCRM,Subg_mod6_MPa
_FCRM);
Mod_MPa_C7A_FCRM =
vertcat(AC_mod_C7A_FCRM,Base1_mod7_MPa_FCRM,Base2_mod7_MPa_FCRM,Subg_mod7_MPa
_FCRM);
Mod_MPa_C8A_FCRM =
vertcat(AC_mod_C8A_FCRM,Base1_mod8_MPa_FCRM,Base2_mod8_MPa_FCRM,Subg_mod8_MPa
_FCRM);

newmat = [Mod_MPa_C1A_FCRM Mod_MPa_C2A_FCRM Mod_MPa_C3A_FCRM Mod_MPa_C4A_FCRM
Mod_MPa_C5A_FCRM Mod_MPa_C6A_FCRM Mod_MPa_C7A_FCRM Mod_MPa_C8A_FCRM];

mod_mat_FCRM = vertcat(newmat, commat);
```

APPENDIX G : MATLAB CODE - ANALYCOMP.M

```
function [ux, uy, uz, sigx, sigy, sigz, sigxy, sigyz, sigxz, epsx, epsy,
epsz, epsxy, epsyz, epsxz]=analycomp(Lpres,Lrad,Lpos,mods)


% Inputs
%% Layer thicknesses beginning at surface (mm)
% thks = [12.7 12.7 17.78 25.4 25.4 7.62 200.66 152.4];

thks = [12.7,25.4,43.18,68.58,93.98,101.6,302.26,454.66];

%% Layer Moduli (MPA) - should have 1 more than layer thicknesses...last one
% is the subgrade
% mods = [200 200 200 200];

%% Possoin's ratio for each layer (including subgrade)
prat = [0.35 0.35 0.35 0.35 0.35 0.35 0.35 0.35 0.35];

%% Tire pressure (MPa) - Assumed to be constant - value from MEPDG (120 psi)
% Lpres = [0.8
%          0.8];

%% Load radius (mm) - Contact radius


%
% Lrad = [150
%         150];

%% Position of the load(s) in mm relative to the evaluation. [x1 y1; x2
y2;...]
% for tandem, change y-coordinates - %Changes - Axle configuration affects
% this
% Lpos_S = [-1295 0 ; 1295 0];
% Lpos_tan = [-1295 0; 1295 0; -1295 1318; 1295 1318];
% Lpos_tri = [-1295 0; 1295 0; -1295 1250; 1295 1250; -1295 2500; 1295 2500];

%% Location of evaluation points: [x1 y1 z1; x2 y2 z2;..] in [mm]
evpts = [0      0      0; 0      0     6.35; 0      0      19.05;
         0      0     34.29; 0      0     43.18; 0      0      68.58;
         0      0     81.28; 0      0     97.29; 0      0     101.6;
         0      0    302.26; 0      0     454.66];

[ux, uy, uz, sigx, sigy, sigz, sigxy, sigyz, sigxz, epsx, epsy, epsz, epsxy,
epsyz, epsxz]=alvafunct(thks,mods,prat,Lpres,Lrad,Lpos,evpts);
```

APPENDIX H: MATLAB CODE - STRAINFUNCT.M

```
%break traffic into monthly values

addpath('C:\Users\jarrell123\OneDrive - Marshall
University\Documents\Main\MATLAB\Coding\jmb ALVA\basic')

load('year1traffic.mat');
load('mod_mat_CCDM.mat');
load('mod_mat_CCRM.mat');
load('mod_mat_FCRM.mat');
load('mthly_dist.mat');
load('rads.mat');

%% Current Climate Dempsey Model Strains

mths = zeros(24,39,12);
for i=1:39
    mths(:,i,1) = trafmat(:,i).*mthly_dist(1);
    mths(:,i,2) = trafmat(:,i).*mthly_dist(2);
    mths(:,i,3) = trafmat(:,i).*mthly_dist(3);
    mths(:,i,4) = trafmat(:,i).*mthly_dist(4);
    mths(:,i,5) = trafmat(:,i).*mthly_dist(5);
    mths(:,i,6) = trafmat(:,i).*mthly_dist(6);
    mths(:,i,7) = trafmat(:,i).*mthly_dist(7);
    mths(:,i,8) = trafmat(:,i).*mthly_dist(8);
    mths(:,i,9) = trafmat(:,i).*mthly_dist(9);
    mths(:,i,10) = trafmat(:,i).*mthly_dist(10);
    mths(:,i,11) = trafmat(:,i).*mthly_dist(11);
    mths(:,i,12) = trafmat(:,i).*mthly_dist(12);
end

Lpos_S = [0 -152; 0 152];
Lpos_tan = [655 -152; 655 152; -655 -152; -655 152];
Lpos_tri = [1250 -152; 1250 152; 0 -152; 0 152; -1250 -152; -1250 152];
Lpos_quad = [1875 -152; 1875 152; 625 -152; 625 152; -625 -152; -625 152; -
1875 -152; -1875 152];

Lpres_S = [0.8 0.8]';
Lpres_tan = [0.8 0.8 0.8 0.8]';
Lpres_tri = [0.8 0.8 0.8 0.8 0.8 0.8]';
Lpres_quad = [0.8 0.8 0.8 0.8 0.8 0.8 0.8 0.8]';
count = 1;
for i = 1:12
    for j=1:5
        num_load_app = round(mths(:,:,i)./5);
        %define moduli
        l=find(mod_mat_CCDM(10,:)==i);

        if j==1
            mods_CCDM = prctile(mod_mat_CCDM(1:9,l)',10);
        elseif j==2
            mods_CCDM = prctile(mod_mat_CCDM(1:9,l)',30);
        elseif j==3
            mods_CCDM = prctile(mod_mat_CCDM(1:9,l)',50);
        elseif j==4
```

```
            mods_CCDM = prctile(mod_mat_CCDM(1:9,l)',70);
        elseif j==5
            mods_CCDM = prctile(mod_mat_CCDM(1:9,l)',90);
        end


        for k = 1:39 %k represents loading group
            for m = 1:24
                if m==1 %m represents truck classes, divided based on axle
type per LTPP data
                    %Class 4 Tandem Axles
                    Lrad_S = [rads(1,k) rads(1,k)]';
                    Lrad_tan = [rads(2,k) rads(2,k) rads(2,k) rads(2,k)]';
                    Lrad_tri = [rads(3,k) rads(3,k) rads(3,k) rads(3,k)
rads(3,k) rads(3,k)]';
                    Lrad_quad = [rads(4,k) rads(4,k) rads(4,k) rads(4,k)
rads(4,k) rads(4,k) rads(4,k) rads(4,k)]';
                    [~, ~, ~, ~, ~, ~, ~, ~, ~, ~, ~, epsz, ~, ~,
~]=analycomp(Lpres_tan,Lrad_tan,Lpos_tan,mods_CCDM); %tandem axle
                    ind_num = num_load_app(m,k);
                    if ind_num>0
                        gathered_strain_CCDM(:,count:(count+ind_num)) =
ones(11,size(count:(count+ind_num),2)).*epsz;
                        count = count+ind_num+1;
                    end
                elseif m==2
                    %Class 4 Single Axles
                    Lrad_S = [rads(1,k) rads(1,k)]';
                    Lrad_tan = [rads(2,k) rads(2,k) rads(2,k) rads(2,k)]';
                    Lrad_tri = [rads(3,k) rads(3,k) rads(3,k) rads(3,k)
rads(3,k) rads(3,k)]';
                    Lrad_quad = [rads(4,k) rads(4,k) rads(4,k) rads(4,k)
rads(4,k) rads(4,k) rads(4,k) rads(4,k)]';
                    [~, ~, ~, ~, ~, ~, ~, ~, ~, ~, ~, epsz, ~, ~,
~]=analycomp(Lpres_S,Lrad_S,Lpos_S,mods_CCDM); %single axle
                    ind_num = num_load_app(m,k);
                    if ind_num>0
                        gathered_strain_CCDM(:,count:(count+ind_num)) =
ones(11,size(count:(count+ind_num),2)).*epsz;
                        count = count+ind_num+1;
                    end
                elseif m==3
                    %Class 5 Tandem Axles
                    Lrad_S = [rads(1,k) rads(1,k)];
                    Lrad_tan = [rads(2,k) rads(2,k) rads(2,k) rads(2,k)]';
                    Lrad_tri = [rads(3,k) rads(3,k) rads(3,k) rads(3,k)
rads(3,k) rads(3,k)]';
                    Lrad_quad = [rads(4,k) rads(4,k) rads(4,k) rads(4,k)
rads(4,k) rads(4,k) rads(4,k) rads(4,k)]';
                    [~, ~, ~, ~, ~, ~, ~, ~, ~, ~, ~, epsz, ~, ~,
~]=analycomp(Lpres_tan,Lrad_tan,Lpos_tan,mods_CCDM); %tandem axle
                    ind_num = num_load_app(m,k);
                    if ind_num>0
                        gathered_strain_CCDM(:,count:(count+ind_num)) =
ones(11,size(count:(count+ind_num),2)).*epsz;
                        count = count+ind_num+1;
                    end
```

```
                elseif m==4
                    %Class 5 Single Axles
                    Lrad_S = [rads(1,k) rads(1,k)]';
                    Lrad_tan = [rads(2,k) rads(2,k) rads(2,k) rads(2,k)]';
                    Lrad_tri = [rads(3,k) rads(3,k) rads(3,k) rads(3,k)
rads(3,k) rads(3,k)]';
                    Lrad_quad = [rads(4,k) rads(4,k) rads(4,k) rads(4,k)
rads(4,k) rads(4,k) rads(4,k) rads(4,k)]';
                    [~, ~, ~, ~, ~, ~, ~, ~, ~, ~, ~, epsz, ~, ~,
~]=analycomp(Lpres_S,Lrad_S,Lpos_S,mods_CCDM); %single axle
                    ind_num = num_load_app(m,k);
                    if ind_num>0
                        gathered_strain_CCDM(:,count:(count+ind_num)) =
ones(11,size(count:(count+ind_num),2)).*epsz;
                        count = count+ind_num+1;
                    end
                elseif m==5
                    %Class 6 Tandem Axles
                    Lrad_S = [rads(1,k) rads(1,k)]';
                    Lrad_tan = [rads(2,k) rads(2,k) rads(2,k) rads(2,k)]';
                    Lrad_tri = [rads(3,k) rads(3,k) rads(3,k) rads(3,k)
rads(3,k) rads(3,k)]';
                    Lrad_quad = [rads(4,k) rads(4,k) rads(4,k) rads(4,k)
rads(4,k) rads(4,k) rads(4,k) rads(4,k)]';
                    [~, ~, ~, ~, ~, ~, ~, ~, ~, ~, ~, epsz, ~, ~,
~]=analycomp(Lpres_tan,Lrad_tan,Lpos_tan,mods_CCDM); %tandem axle
                    ind_num = num_load_app(m,k);
                    if ind_num>0
                        gathered_strain_CCDM(:,count:(count+ind_num)) =
ones(11,size(count:(count+ind_num),2)).*epsz;
                        count = count+ind_num+1;
                    end
                elseif m==6
                    %Class 6 Single Axles
                    Lrad_S = [rads(1,k) rads(1,k)]';
                    Lrad_tan = [rads(2,k) rads(2,k) rads(2,k) rads(2,k)]';
                    Lrad_tri = [rads(3,k) rads(3,k) rads(3,k) rads(3,k)
rads(3,k) rads(3,k)]';
                    Lrad_quad = [rads(4,k) rads(4,k) rads(4,k) rads(4,k)
rads(4,k) rads(4,k) rads(4,k) rads(4,k)]';
                    [~, ~, ~, ~, ~, ~, ~, ~, ~, ~, ~, epsz, ~, ~,
~]=analycomp(Lpres_S,Lrad_S,Lpos_S,mods_CCDM); %single axle
                    ind_num = num_load_app(m,k);
                    if ind_num>0
                        gathered_strain_CCDM(:,count:(count+ind_num)) =
ones(11,size(count:(count+ind_num),2)).*epsz;
                        count = count+ind_num+1;
                    end
                elseif m==7
                    %Class 7 Quad Axles
                    Lrad_S = [rads(1,k) rads(1,k)]';
                    Lrad_tan = [rads(2,k) rads(2,k) rads(2,k) rads(2,k)]';
                    Lrad_tri = [rads(3,k) rads(3,k) rads(3,k) rads(3,k)
rads(3,k) rads(3,k)]';
                    Lrad_quad = [rads(4,k) rads(4,k) rads(4,k) rads(4,k)
rads(4,k) rads(4,k) rads(4,k) rads(4,k)]';
```

```
                    [~, ~, ~, ~, ~, ~, ~, ~, ~, ~, ~, epsz, ~, ~,
~]=analycomp(Lpres_quad,Lrad_quad,Lpos_quad,mods_CCDM); %quad axle
                    ind_num = num_load_app(m,k);
                    if ind_num>0
                        gathered_strain_CCDM(:,count:(count+ind_num)) =
ones(11,size(count:(count+ind_num),2)).*epsz;
                        count = count+ind_num+1;
                    end
                elseif m==8
                    %Class 7 Tridem Axles
                    Lrad_S = [rads(1,k) rads(1,k)]';
                    Lrad_tan = [rads(2,k) rads(2,k) rads(2,k) rads(2,k)]';
                    Lrad_tri = [rads(3,k) rads(3,k) rads(3,k) rads(3,k)
rads(3,k) rads(3,k)]';
                    Lrad_quad = [rads(4,k) rads(4,k) rads(4,k) rads(4,k)
rads(4,k) rads(4,k) rads(4,k) rads(4,k)]';
                    [~, ~, ~, ~, ~, ~, ~, ~, ~, ~, ~, epsz, ~, ~,
~]=analycomp(Lpres_tri,Lrad_tri,Lpos_tri,mods_CCDM); %tridem axle
                    ind_num = num_load_app(m,k);
                    if ind_num>0
                        gathered_strain_CCDM(:,count:(count+ind_num)) =
ones(11,size(count:(count+ind_num),2)).*epsz;
                        count = count+ind_num+1;
                    end
                elseif m==9
                    %Class 7 Single Axles
                    Lrad_S = [rads(1,k) rads(1,k)]';
                    Lrad_tan = [rads(2,k) rads(2,k) rads(2,k) rads(2,k)]';
                    Lrad_tri = [rads(3,k) rads(3,k) rads(3,k) rads(3,k)
rads(3,k) rads(3,k)]';
                    Lrad_quad = [rads(4,k) rads(4,k) rads(4,k) rads(4,k)
rads(4,k) rads(4,k) rads(4,k) rads(4,k)]';
                    [~, ~, ~, ~, ~, ~, ~, ~, ~, ~, ~, epsz, ~, ~,
~]=analycomp(Lpres_S,Lrad_S,Lpos_S,mods_CCDM); %single axle
                    ind_num = num_load_app(m,k);
                    if ind_num>0
                        gathered_strain_CCDM(:,count:(count+ind_num)) =
ones(11,size(count:(count+ind_num),2)).*epsz;
                        count = count+ind_num+1;
                    end
                elseif m==10
                    %Class 7 Tandem Axles
                    Lrad_S = [rads(1,k) rads(1,k)]';
                    Lrad_tan = [rads(2,k) rads(2,k) rads(2,k) rads(2,k)]';
                    Lrad_tri = [rads(3,k) rads(3,k) rads(3,k) rads(3,k)
rads(3,k) rads(3,k)]';
                    Lrad_quad = [rads(4,k) rads(4,k) rads(4,k) rads(4,k)
rads(4,k) rads(4,k) rads(4,k) rads(4,k)]';
                    [~, ~, ~, ~, ~, ~, ~, ~, ~, ~, ~, epsz, ~, ~,
~]=analycomp(Lpres_tan,Lrad_tan,Lpos_tan,mods_CCDM); %tandem axle
                    ind_num = num_load_app(m,k);
                    if ind_num>0
                        gathered_strain_CCDM(:,count:(count+ind_num)) =
ones(11,size(count:(count+ind_num),2)).*epsz;
                        count = count+ind_num+1;
                    end
                elseif m==11
```

```
                    %Class 8 Single Axles
                    Lrad_S = [rads(1,k) rads(1,k)]';
                    Lrad_tan = [rads(2,k) rads(2,k) rads(2,k) rads(2,k)]';
                    Lrad_tri = [rads(3,k) rads(3,k) rads(3,k) rads(3,k)
rads(3,k) rads(3,k)]';
                    Lrad_quad = [rads(4,k) rads(4,k) rads(4,k) rads(4,k)
rads(4,k) rads(4,k) rads(4,k) rads(4,k)]';
                    [~, ~, ~, ~, ~, ~, ~, ~, ~, ~, ~, epsz, ~, ~,
~]=analycomp(Lpres_S,Lrad_S,Lpos_S,mods_CCDM); %single axle
                    ind_num = num_load_app(m,k);
                    if ind_num>0
                        gathered_strain_CCDM(:,count:(count+ind_num)) =
ones(11,size(count:(count+ind_num),2)).*epsz;
                        count = count+ind_num+1;
                    end
                elseif m==12
                    %Class 8 Tandem Axles
                    Lrad_S = [rads(1,k) rads(1,k)]';
                    Lrad_tan = [rads(2,k) rads(2,k) rads(2,k) rads(2,k)]';
                    Lrad_tri = [rads(3,k) rads(3,k) rads(3,k) rads(3,k)
rads(3,k) rads(3,k)]';
                    Lrad_quad = [rads(4,k) rads(4,k) rads(4,k) rads(4,k)
rads(4,k) rads(4,k) rads(4,k) rads(4,k)]';
                    [~, ~, ~, ~, ~, ~, ~, ~, ~, ~, ~, epsz, ~, ~,
~]=analycomp(Lpres_tan,Lrad_tan,Lpos_tan,mods_CCDM); %tandem axle
                    ind_num = num_load_app(m,k);
                    if ind_num>0
                        gathered_strain_CCDM(:,count:(count+ind_num)) =
ones(11,size(count:(count+ind_num),2)).*epsz;
                        count = count+ind_num+1;
                    end
                elseif m==13
                    %Class 9 Single Axles
                    Lrad_S = [rads(1,k) rads(1,k)]';
                    Lrad_tan = [rads(2,k) rads(2,k) rads(2,k) rads(2,k)]';
                    Lrad_tri = [rads(3,k) rads(3,k) rads(3,k) rads(3,k)
rads(3,k) rads(3,k)]';
                    Lrad_quad = [rads(4,k) rads(4,k) rads(4,k) rads(4,k)
rads(4,k) rads(4,k) rads(4,k) rads(4,k)]';
                    [~, ~, ~, ~, ~, ~, ~, ~, ~, ~, ~, epsz, ~, ~,
~]=analycomp(Lpres_S,Lrad_S,Lpos_S,mods_CCDM); %single axle
                    ind_num = num_load_app(m,k);
                    if ind_num>0
                        gathered_strain_CCDM(:,count:(count+ind_num)) =
ones(11,size(count:(count+ind_num),2)).*epsz;
                        count = count+ind_num+1;
                    end
                elseif m==14
                    %Class 9 Tandem Axles
                    Lrad_S = [rads(1,k) rads(1,k)]';
                    Lrad_tan = [rads(2,k) rads(2,k) rads(2,k) rads(2,k)]';
                    Lrad_tri = [rads(3,k) rads(3,k) rads(3,k) rads(3,k)
rads(3,k) rads(3,k)]';
                    Lrad_quad = [rads(4,k) rads(4,k) rads(4,k) rads(4,k)
rads(4,k) rads(4,k) rads(4,k) rads(4,k)]';
                    [~, ~, ~, ~, ~, ~, ~, ~, ~, ~, ~, epsz, ~, ~,
~]=analycomp(Lpres_tan,Lrad_tan,Lpos_tan,mods_CCDM); %tandem axle
```

```
                    ind_num = num_load_app(m,k);
                    if ind_num>0
                        gathered_strain_CCDM(:,count:(count+ind_num)) =
ones(11,size(count:(count+ind_num),2)).*epsz;
                        count = count+ind_num+1;
                    end
                elseif m==15
                    %Class 10 Single Axles
                    Lrad_S = [rads(1,k) rads(1,k)]';
                    Lrad_tan = [rads(2,k) rads(2,k) rads(2,k) rads(2,k)]';
                    Lrad_tri = [rads(3,k) rads(3,k) rads(3,k) rads(3,k)
rads(3,k) rads(3,k)]';
                    Lrad_quad = [rads(4,k) rads(4,k) rads(4,k) rads(4,k)
rads(4,k) rads(4,k) rads(4,k) rads(4,k)]';
                    [~, ~, ~, ~, ~, ~, ~, ~, ~, ~, ~, epsz, ~, ~,
~]=analycomp(Lpres_S,Lrad_S,Lpos_S,mods_CCDM); %single axle
                    ind_num = num_load_app(m,k);
                    if ind_num>0
                        gathered_strain_CCDM(:,count:(count+ind_num)) =
ones(11,size(count:(count+ind_num),2)).*epsz;
                        count = count+ind_num+1;
                    end
                elseif m==16
                    %Class 10 Quad Axles
                    Lrad_S = [rads(1,k) rads(1,k)]';
                    Lrad_tan = [rads(2,k) rads(2,k) rads(2,k) rads(2,k)]';
                    Lrad_tri = [rads(3,k) rads(3,k) rads(3,k) rads(3,k)
rads(3,k) rads(3,k)]';
                    Lrad_quad = [rads(4,k) rads(4,k) rads(4,k) rads(4,k)
rads(4,k) rads(4,k) rads(4,k) rads(4,k)]';
                    [~, ~, ~, ~, ~, ~, ~, ~, ~, ~, ~, epsz, ~, ~,
~]=analycomp(Lpres_quad,Lrad_quad,Lpos_quad,mods_CCDM); %quad axle
                    ind_num = num_load_app(m,k);
                    if ind_num>0
                        gathered_strain_CCDM(:,count:(count+ind_num)) =
ones(11,size(count:(count+ind_num),2)).*epsz;
                        count = count+ind_num+1;
                    end
                elseif m==17
                    %Class 10 Tandem Axles
                    Lrad_S = [rads(1,k) rads(1,k)]';
                    Lrad_tan = [rads(2,k) rads(2,k) rads(2,k) rads(2,k)]';
                    Lrad_tri = [rads(3,k) rads(3,k) rads(3,k) rads(3,k)
rads(3,k) rads(3,k)]';
                    Lrad_quad = [rads(4,k) rads(4,k) rads(4,k) rads(4,k)
rads(4,k) rads(4,k) rads(4,k) rads(4,k)]';
                    [~, ~, ~, ~, ~, ~, ~, ~, ~, ~, ~, epsz, ~, ~,
~]=analycomp(Lpres_tan,Lrad_tan,Lpos_tan,mods_CCDM); %tandem axle
                    ind_num = num_load_app(m,k);
                    if ind_num>0
                        gathered_strain_CCDM(:,count:(count+ind_num)) =
ones(11,size(count:(count+ind_num),2)).*epsz;
                        count = count+ind_num+1;
                    end
                elseif m==18
                    %Class 10 Tridem Axles
                    Lrad_S = [rads(1,k) rads(1,k)]';
```

```
                    Lrad_tan = [rads(2,k) rads(2,k) rads(2,k) rads(2,k)]';
                    Lrad_tri = [rads(3,k) rads(3,k) rads(3,k) rads(3,k)
rads(3,k) rads(3,k)]';
                    Lrad_quad = [rads(4,k) rads(4,k) rads(4,k) rads(4,k)
rads(4,k) rads(4,k) rads(4,k) rads(4,k)]';
                    [~, ~, ~, ~, ~, ~, ~, ~, ~, ~, ~, epsz, ~, ~,
~]=analycomp(Lpres_tri,Lrad_tri,Lpos_tri,mods_CCDM); %tridem axle
                    ind_num = num_load_app(m,k);
                    if ind_num>0
                        gathered_strain_CCDM(:,count:(count+ind_num)) =
ones(11,size(count:(count+ind_num),2)).*epsz;
                        count = count+ind_num+1;
                    end
                elseif m==19
                    %Class 11 Single Axles
                    Lrad_S = [rads(1,k) rads(1,k)]';
                    Lrad_tan = [rads(2,k) rads(2,k) rads(2,k) rads(2,k)]';
                    Lrad_tri = [rads(3,k) rads(3,k) rads(3,k) rads(3,k)
rads(3,k) rads(3,k)]';
                    Lrad_quad = [rads(4,k) rads(4,k) rads(4,k) rads(4,k)
rads(4,k) rads(4,k) rads(4,k) rads(4,k)]';
                    [~, ~, ~, ~, ~, ~, ~, ~, ~, ~, ~, epsz, ~, ~,
~]=analycomp(Lpres_S,Lrad_S,Lpos_S,mods_CCDM); %single axle
                    ind_num = num_load_app(m,k);
                    if ind_num>0
                        gathered_strain_CCDM(:,count:(count+ind_num)) =
ones(11,size(count:(count+ind_num),2)).*epsz;
                        count = count+ind_num+1;
                    end
                elseif m==20
                    %Class 12 Tandem Axles
                    Lrad_S = [rads(1,k) rads(1,k)]';
                    Lrad_tan = [rads(2,k) rads(2,k) rads(2,k) rads(2,k)]';
                    Lrad_tri = [rads(3,k) rads(3,k) rads(3,k) rads(3,k)
rads(3,k) rads(3,k)]';
                    Lrad_quad = [rads(4,k) rads(4,k) rads(4,k) rads(4,k)
rads(4,k) rads(4,k) rads(4,k) rads(4,k)]';
                    [~, ~, ~, ~, ~, ~, ~, ~, ~, ~, ~, epsz, ~, ~,
~]=analycomp(Lpres_tan,Lrad_tan,Lpos_tan,mods_CCDM); %tandem axle
                    ind_num = num_load_app(m,k);
                    if ind_num>0
                        gathered_strain_CCDM(:,count:(count+ind_num)) =
ones(11,size(count:(count+ind_num),2)).*epsz;
                        count = count+ind_num+1;
                    end
                elseif m==21
                    %Class 12 Single Axles
                    Lrad_S = [rads(1,k) rads(1,k)]';
                    Lrad_tan = [rads(2,k) rads(2,k) rads(2,k) rads(2,k)]';
                    Lrad_tri = [rads(3,k) rads(3,k) rads(3,k) rads(3,k)
rads(3,k) rads(3,k)]';
                    Lrad_quad = [rads(4,k) rads(4,k) rads(4,k) rads(4,k)
rads(4,k) rads(4,k) rads(4,k) rads(4,k)]';
                    [~, ~, ~, ~, ~, ~, ~, ~, ~, ~, ~, epsz, ~, ~,
~]=analycomp(Lpres_S,Lrad_S,Lpos_S,mods_CCDM); %single axle
                    ind_num = num_load_app(m,k);
                    if ind_num>0
```

```
                        gathered_strain_CCDM(:,count:(count+ind_num)) =
ones(11,size(count:(count+ind_num),2)).*epsz;
                        count = count+ind_num+1;
                    end
                elseif m==22
                    %Class 13 Single Axles
                    Lrad_S = [rads(1,k) rads(1,k)]';
                    Lrad_tan = [rads(2,k) rads(2,k) rads(2,k) rads(2,k)]';
                    Lrad_tri = [rads(3,k) rads(3,k) rads(3,k) rads(3,k)
rads(3,k) rads(3,k)]';
                    Lrad_quad = [rads(4,k) rads(4,k) rads(4,k) rads(4,k)
rads(4,k) rads(4,k) rads(4,k) rads(4,k)]';
                    [~, ~, ~, ~, ~, ~, ~, ~, ~, ~, ~, epsz, ~, ~,
~]=analycomp(Lpres_S,Lrad_S,Lpos_S,mods_CCDM); %single axle
                    ind_num = num_load_app(m,k);
                    if ind_num>0
                        gathered_strain_CCDM(:,count:(count+ind_num)) =
ones(11,size(count:(count+ind_num),2)).*epsz;
                        count = count+ind_num+1;
                    end
                elseif m==23
                    %Class 13 Tandem Axles
                    Lrad_S = [rads(1,k) rads(1,k)]';
                    Lrad_tan = [rads(2,k) rads(2,k) rads(2,k) rads(2,k)]';
                    Lrad_tri = [rads(3,k) rads(3,k) rads(3,k) rads(3,k)
rads(3,k) rads(3,k)]';
                    Lrad_quad = [rads(4,k) rads(4,k) rads(4,k) rads(4,k)
rads(4,k) rads(4,k) rads(4,k) rads(4,k)]';
                    [~, ~, ~, ~, ~, ~, ~, ~, ~, ~, ~, epsz, ~, ~,
~]=analycomp(Lpres_tan,Lrad_tan,Lpos_tan,mods_CCDM); %tandem axle
                    ind_num = num_load_app(m,k);
                    if ind_num>0
                        gathered_strain_CCDM(:,count:(count+ind_num)) =
ones(11,size(count:(count+ind_num),2)).*epsz;
                        count = count+ind_num+1;
                    end
                elseif m==24
                    %Class 13 Tridem Axles
                    Lrad_S = [rads(1,k) rads(1,k)]';
                    Lrad_tan = [rads(2,k) rads(2,k) rads(2,k) rads(2,k)]';
                    Lrad_tri = [rads(3,k) rads(3,k) rads(3,k) rads(3,k)
rads(3,k) rads(3,k)]';
                    Lrad_quad = [rads(4,k) rads(4,k) rads(4,k) rads(4,k)
rads(4,k) rads(4,k) rads(4,k) rads(4,k)]';
                    [~, ~, ~, ~, ~, ~, ~, ~, ~, ~, ~, epsz, ~, ~,
~]=analycomp(Lpres_tri,Lrad_tri,Lpos_tri,mods_CCDM); %tridem axle
                    ind_num = num_load_app(m,k);
                    if ind_num>0
                        gathered_strain_CCDM(:,count:(count+ind_num)) =
ones(11,size(count:(count+ind_num),2)).*epsz;
                        count = count+ind_num+1;
                    end
                end
            end
        end
    end
end
```

```
%% Current Climate Revised Model Strains

count = 1;
for i = 1:12
    for j=1:5
        num_load_app = round(mths(:,:,i)./5);
        %define moduli
        l=find(mod_mat_CCRM(10,:)==i);

        if j==1
            mods_CCRM = prctile(mod_mat_CCRM(1:9,l)',10);
        elseif j==2
            mods_CCRM = prctile(mod_mat_CCRM(1:9,l)',30);
        elseif j==3
            mods_CCRM = prctile(mod_mat_CCRM(1:9,l)',50);
        elseif j==4
            mods_CCRM = prctile(mod_mat_CCRM(1:9,l)',70);
        elseif j==5
            mods_CCRM = prctile(mod_mat_CCRM(1:9,l)',90);
        end


        for k = 1:39 %k represents loading group
            for m = 1:24
                if m==1 %m represents truck classes, divided based on axle
type per LTPP data
                    %Class 4 Tandem Axles
                    Lrad_S = [rads(1,k) rads(1,k)]';
                    Lrad_tan = [rads(2,k) rads(2,k) rads(2,k) rads(2,k)]';
                    Lrad_tri = [rads(3,k) rads(3,k) rads(3,k) rads(3,k)
rads(3,k) rads(3,k)]';
                    Lrad_quad = [rads(4,k) rads(4,k) rads(4,k) rads(4,k)
rads(4,k) rads(4,k) rads(4,k) rads(4,k)]';
                    [~, ~, ~, ~, ~, ~, ~, ~, ~, ~, ~, epsz, ~, ~,
~]=analycomp(Lpres_tan,Lrad_tan,Lpos_tan,mods_CCRM); %tandem axle
                    ind_num = num_load_app(m,k);
                    if ind_num>0
                        gathered_strain_CCRM(:,count:(count+ind_num)) =
ones(11,size(count:(count+ind_num),2)).*epsz;
                        count = count+ind_num+1;
                    end
                elseif m==2
                    %Class 4 Single Axles
                    Lrad_S = [rads(1,k) rads(1,k)]';
                    Lrad_tan = [rads(2,k) rads(2,k) rads(2,k) rads(2,k)]';
                    Lrad_tri = [rads(3,k) rads(3,k) rads(3,k) rads(3,k)
rads(3,k) rads(3,k)]';
                    Lrad_quad = [rads(4,k) rads(4,k) rads(4,k) rads(4,k)
rads(4,k) rads(4,k) rads(4,k) rads(4,k)]';
                    [~, ~, ~, ~, ~, ~, ~, ~, ~, ~, ~, epsz, ~, ~,
~]=analycomp(Lpres_S,Lrad_S,Lpos_S,mods_CCRM); %single axle
                    ind_num = num_load_app(m,k);
                    if ind_num>0
                        gathered_strain_CCRM(:,count:(count+ind_num)) =
ones(11,size(count:(count+ind_num),2)).*epsz;
                        count = count+ind_num+1;
```

```
                    end
                elseif m==3
                    %Class 5 Tandem Axles
                    Lrad_S = [rads(1,k) rads(1,k)];
                    Lrad_tan = [rads(2,k) rads(2,k) rads(2,k) rads(2,k)]';
                    Lrad_tri = [rads(3,k) rads(3,k) rads(3,k) rads(3,k)
rads(3,k) rads(3,k)]';
                    Lrad_quad = [rads(4,k) rads(4,k) rads(4,k) rads(4,k)
rads(4,k) rads(4,k) rads(4,k) rads(4,k)]';
                    [~, ~, ~, ~, ~, ~, ~, ~, ~, ~, ~, epsz, ~, ~,
~]=analycomp(Lpres_tan,Lrad_tan,Lpos_tan,mods_CCRM); %tandem axle
                    ind_num = num_load_app(m,k);
                    if ind_num>0
                        gathered_strain_CCRM(:,count:(count+ind_num)) =
ones(11,size(count:(count+ind_num),2)).*epsz;
                        count = count+ind_num+1;
                    end
                elseif m==4
                    %Class 5 Single Axles
                    Lrad_S = [rads(1,k) rads(1,k)]';
                    Lrad_tan = [rads(2,k) rads(2,k) rads(2,k) rads(2,k)]';
                    Lrad_tri = [rads(3,k) rads(3,k) rads(3,k) rads(3,k)
rads(3,k) rads(3,k)]';
                    Lrad_quad = [rads(4,k) rads(4,k) rads(4,k) rads(4,k)
rads(4,k) rads(4,k) rads(4,k) rads(4,k)]';
                    [~, ~, ~, ~, ~, ~, ~, ~, ~, ~, ~, epsz, ~, ~,
~]=analycomp(Lpres_S,Lrad_S,Lpos_S,mods_CCRM); %single axle
                    ind_num = num_load_app(m,k);
                    if ind_num>0
                        gathered_strain_CCRM(:,count:(count+ind_num)) =
ones(11,size(count:(count+ind_num),2)).*epsz;
                        count = count+ind_num+1;
                    end
                elseif m==5
                    %Class 6 Tandem Axles
                    Lrad_S = [rads(1,k) rads(1,k)]';
                    Lrad_tan = [rads(2,k) rads(2,k) rads(2,k) rads(2,k)]';
                    Lrad_tri = [rads(3,k) rads(3,k) rads(3,k) rads(3,k)
rads(3,k) rads(3,k)]';
                    Lrad_quad = [rads(4,k) rads(4,k) rads(4,k) rads(4,k)
rads(4,k) rads(4,k) rads(4,k) rads(4,k)]';
                    [~, ~, ~, ~, ~, ~, ~, ~, ~, ~, ~, epsz, ~, ~,
~]=analycomp(Lpres_tan,Lrad_tan,Lpos_tan,mods_CCRM); %tandem axle
                    ind_num = num_load_app(m,k);
                    if ind_num>0
                        gathered_strain_CCRM(:,count:(count+ind_num)) =
ones(11,size(count:(count+ind_num),2)).*epsz;
                        count = count+ind_num+1;
                    end
                elseif m==6
                    %Class 6 Single Axles
                    Lrad_S = [rads(1,k) rads(1,k)]';
                    Lrad_tan = [rads(2,k) rads(2,k) rads(2,k) rads(2,k)]';
                    Lrad_tri = [rads(3,k) rads(3,k) rads(3,k) rads(3,k)
rads(3,k) rads(3,k)]';
                    Lrad_quad = [rads(4,k) rads(4,k) rads(4,k) rads(4,k)
rads(4,k) rads(4,k) rads(4,k) rads(4,k)]';
```

```
                    [~, ~, ~, ~, ~, ~, ~, ~, ~, ~, ~, epsz, ~, ~,
~]=analycomp(Lpres_S,Lrad_S,Lpos_S,mods_CCRM); %single axle
                    ind_num = num_load_app(m,k);
                    if ind_num>0
                        gathered_strain_CCRM(:,count:(count+ind_num)) =
ones(11,size(count:(count+ind_num),2)).*epsz;
                        count = count+ind_num+1;
                    end
                elseif m==7
                    %Class 7 Quad Axles
                    Lrad_S = [rads(1,k) rads(1,k)]';
                    Lrad_tan = [rads(2,k) rads(2,k) rads(2,k) rads(2,k)]';
                    Lrad_tri = [rads(3,k) rads(3,k) rads(3,k) rads(3,k)
rads(3,k) rads(3,k)]';
                    Lrad_quad = [rads(4,k) rads(4,k) rads(4,k) rads(4,k)
rads(4,k) rads(4,k) rads(4,k) rads(4,k)]';
                    [~, ~, ~, ~, ~, ~, ~, ~, ~, ~, ~, epsz, ~, ~,
~]=analycomp(Lpres_quad,Lrad_quad,Lpos_quad,mods_CCRM); %quad axle
                    ind_num = num_load_app(m,k);
                    if ind_num>0
                        gathered_strain_CCRM(:,count:(count+ind_num)) =
ones(11,size(count:(count+ind_num),2)).*epsz;
                        count = count+ind_num+1;
                    end
                elseif m==8
                    %Class 7 Tridem Axles
                    Lrad_S = [rads(1,k) rads(1,k)]';
                    Lrad_tan = [rads(2,k) rads(2,k) rads(2,k) rads(2,k)]';
                    Lrad_tri = [rads(3,k) rads(3,k) rads(3,k) rads(3,k)
rads(3,k) rads(3,k)]';
                    Lrad_quad = [rads(4,k) rads(4,k) rads(4,k) rads(4,k)
rads(4,k) rads(4,k) rads(4,k) rads(4,k)]';
                    [~, ~, ~, ~, ~, ~, ~, ~, ~, ~, ~, epsz, ~, ~,
~]=analycomp(Lpres_tri,Lrad_tri,Lpos_tri,mods_CCRM); %tridem axle
                    ind_num = num_load_app(m,k);
                    if ind_num>0
                        gathered_strain_CCRM(:,count:(count+ind_num)) =
ones(11,size(count:(count+ind_num),2)).*epsz;
                        count = count+ind_num+1;
                    end
                elseif m==9
                    %Class 7 Single Axles
                    Lrad_S = [rads(1,k) rads(1,k)]';
                    Lrad_tan = [rads(2,k) rads(2,k) rads(2,k) rads(2,k)]';
                    Lrad_tri = [rads(3,k) rads(3,k) rads(3,k) rads(3,k)
rads(3,k) rads(3,k)]';
                    Lrad_quad = [rads(4,k) rads(4,k) rads(4,k) rads(4,k)
rads(4,k) rads(4,k) rads(4,k) rads(4,k)]';
                    [~, ~, ~, ~, ~, ~, ~, ~, ~, ~, ~, epsz, ~, ~,
~]=analycomp(Lpres_S,Lrad_S,Lpos_S,mods_CCRM); %single axle
                    ind_num = num_load_app(m,k);
                    if ind_num>0
                        gathered_strain_CCRM(:,count:(count+ind_num)) =
ones(11,size(count:(count+ind_num),2)).*epsz;
                        count = count+ind_num+1;
                    end
                elseif m==10
```

```
                    %Class 7 Tandem Axles
                    Lrad_S = [rads(1,k) rads(1,k)]';
                    Lrad_tan = [rads(2,k) rads(2,k) rads(2,k) rads(2,k)]';
                    Lrad_tri = [rads(3,k) rads(3,k) rads(3,k) rads(3,k)
rads(3,k) rads(3,k)]';
                    Lrad_quad = [rads(4,k) rads(4,k) rads(4,k) rads(4,k)
rads(4,k) rads(4,k) rads(4,k) rads(4,k)]';
                    [~, ~, ~, ~, ~, ~, ~, ~, ~, ~, ~, epsz, ~, ~,
~]=analycomp(Lpres_tan,Lrad_tan,Lpos_tan,mods_CCRM); %tandem axle
                    ind_num = num_load_app(m,k);
                    if ind_num>0
                        gathered_strain_CCRM(:,count:(count+ind_num)) =
ones(11,size(count:(count+ind_num),2)).*epsz;
                        count = count+ind_num+1;
                    end
                elseif m==11
                    %Class 8 Single Axles
                    Lrad_S = [rads(1,k) rads(1,k)]';
                    Lrad_tan = [rads(2,k) rads(2,k) rads(2,k) rads(2,k)]';
                    Lrad_tri = [rads(3,k) rads(3,k) rads(3,k) rads(3,k)
rads(3,k) rads(3,k)]';
                    Lrad_quad = [rads(4,k) rads(4,k) rads(4,k) rads(4,k)
rads(4,k) rads(4,k) rads(4,k) rads(4,k)]';
                    [~, ~, ~, ~, ~, ~, ~, ~, ~, ~, ~, epsz, ~, ~,
~]=analycomp(Lpres_S,Lrad_S,Lpos_S,mods_CCRM); %single axle
                    ind_num = num_load_app(m,k);
                    if ind_num>0
                        gathered_strain_CCRM(:,count:(count+ind_num)) =
ones(11,size(count:(count+ind_num),2)).*epsz;
                        count = count+ind_num+1;
                    end
                elseif m==12
                    %Class 8 Tandem Axles
                    Lrad_S = [rads(1,k) rads(1,k)]';
                    Lrad_tan = [rads(2,k) rads(2,k) rads(2,k) rads(2,k)]';
                    Lrad_tri = [rads(3,k) rads(3,k) rads(3,k) rads(3,k)
rads(3,k) rads(3,k)]';
                    Lrad_quad = [rads(4,k) rads(4,k) rads(4,k) rads(4,k)
rads(4,k) rads(4,k) rads(4,k) rads(4,k)]';
                    [~, ~, ~, ~, ~, ~, ~, ~, ~, ~, ~, epsz, ~, ~,
~]=analycomp(Lpres_tan,Lrad_tan,Lpos_tan,mods_CCRM); %tandem axle
                    ind_num = num_load_app(m,k);
                    if ind_num>0
                        gathered_strain_CCRM(:,count:(count+ind_num)) =
ones(11,size(count:(count+ind_num),2)).*epsz;
                        count = count+ind_num+1;
                    end
                elseif m==13
                    %Class 9 Single Axles
                    Lrad_S = [rads(1,k) rads(1,k)]';
                    Lrad_tan = [rads(2,k) rads(2,k) rads(2,k) rads(2,k)]';
                    Lrad_tri = [rads(3,k) rads(3,k) rads(3,k) rads(3,k)
rads(3,k) rads(3,k)]';
                    Lrad_quad = [rads(4,k) rads(4,k) rads(4,k) rads(4,k)
rads(4,k) rads(4,k) rads(4,k) rads(4,k)]';
                    [~, ~, ~, ~, ~, ~, ~, ~, ~, ~, ~, epsz, ~, ~,
~]=analycomp(Lpres_S,Lrad_S,Lpos_S,mods_CCRM); %single axle
```

```
                    ind_num = num_load_app(m,k);
                    if ind_num>0
                        gathered_strain_CCRM(:,count:(count+ind_num)) =
ones(11,size(count:(count+ind_num),2)).*epsz;
                        count = count+ind_num+1;
                    end
                elseif m==14
                    %Class 9 Tandem Axles
                    Lrad_S = [rads(1,k) rads(1,k)]';
                    Lrad_tan = [rads(2,k) rads(2,k) rads(2,k) rads(2,k)]';
                    Lrad_tri = [rads(3,k) rads(3,k) rads(3,k) rads(3,k)
rads(3,k) rads(3,k)]';
                    Lrad_quad = [rads(4,k) rads(4,k) rads(4,k) rads(4,k)
rads(4,k) rads(4,k) rads(4,k) rads(4,k)]';
                    [~, ~, ~, ~, ~, ~, ~, ~, ~, ~, ~, epsz, ~, ~,
~]=analycomp(Lpres_tan,Lrad_tan,Lpos_tan,mods_CCRM); %tandem axle
                    ind_num = num_load_app(m,k);
                    if ind_num>0
                        gathered_strain_CCRM(:,count:(count+ind_num)) =
ones(11,size(count:(count+ind_num),2)).*epsz;
                        count = count+ind_num+1;
                    end
                elseif m==15
                    %Class 10 Single Axles
                    Lrad_S = [rads(1,k) rads(1,k)]';
                    Lrad_tan = [rads(2,k) rads(2,k) rads(2,k) rads(2,k)]';
                    Lrad_tri = [rads(3,k) rads(3,k) rads(3,k) rads(3,k)
rads(3,k) rads(3,k)]';
                    Lrad_quad = [rads(4,k) rads(4,k) rads(4,k) rads(4,k)
rads(4,k) rads(4,k) rads(4,k) rads(4,k)]';
                    [~, ~, ~, ~, ~, ~, ~, ~, ~, ~, ~, epsz, ~, ~,
~]=analycomp(Lpres_S,Lrad_S,Lpos_S,mods_CCRM); %single axle
                    ind_num = num_load_app(m,k);
                    if ind_num>0
                        gathered_strain_CCRM(:,count:(count+ind_num)) =
ones(11,size(count:(count+ind_num),2)).*epsz;
                        count = count+ind_num+1;
                    end
                elseif m==16
                    %Class 10 Quad Axles
                    Lrad_S = [rads(1,k) rads(1,k)]';
                    Lrad_tan = [rads(2,k) rads(2,k) rads(2,k) rads(2,k)]';
                    Lrad_tri = [rads(3,k) rads(3,k) rads(3,k) rads(3,k)
rads(3,k) rads(3,k)]';
                    Lrad_quad = [rads(4,k) rads(4,k) rads(4,k) rads(4,k)
rads(4,k) rads(4,k) rads(4,k) rads(4,k)]';
                    [~, ~, ~, ~, ~, ~, ~, ~, ~, ~, ~, epsz, ~, ~,
~]=analycomp(Lpres_quad,Lrad_quad,Lpos_quad,mods_CCRM); %quad axle
                    ind_num = num_load_app(m,k);
                    if ind_num>0
                        gathered_strain_CCRM(:,count:(count+ind_num)) =
ones(11,size(count:(count+ind_num),2)).*epsz;
                        count = count+ind_num+1;
                    end
                elseif m==17
                    %Class 10 Tandem Axles
                    Lrad_S = [rads(1,k) rads(1,k)]';
```

```
                    Lrad_tan = [rads(2,k) rads(2,k) rads(2,k) rads(2,k)]';
                    Lrad_tri = [rads(3,k) rads(3,k) rads(3,k) rads(3,k)
rads(3,k) rads(3,k)]';
                    Lrad_quad = [rads(4,k) rads(4,k) rads(4,k) rads(4,k)
rads(4,k) rads(4,k) rads(4,k) rads(4,k)]';
                    [~, ~, ~, ~, ~, ~, ~, ~, ~, ~, ~, epsz, ~, ~,
~]=analycomp(Lpres_tan,Lrad_tan,Lpos_tan,mods_CCRM); %tandem axle
                    ind_num = num_load_app(m,k);
                    if ind_num>0
                        gathered_strain_CCRM(:,count:(count+ind_num)) =
ones(11,size(count:(count+ind_num),2)).*epsz;
                        count = count+ind_num+1;
                    end
                elseif m==18
                    %Class 10 Tridem Axles
                    Lrad_S = [rads(1,k) rads(1,k)]';
                    Lrad_tan = [rads(2,k) rads(2,k) rads(2,k) rads(2,k)]';
                    Lrad_tri = [rads(3,k) rads(3,k) rads(3,k) rads(3,k)
rads(3,k) rads(3,k)]';
                    Lrad_quad = [rads(4,k) rads(4,k) rads(4,k) rads(4,k)
rads(4,k) rads(4,k) rads(4,k) rads(4,k)]';
                    [~, ~, ~, ~, ~, ~, ~, ~, ~, ~, ~, epsz, ~, ~,
~]=analycomp(Lpres_tri,Lrad_tri,Lpos_tri,mods_CCRM); %tridem axle
                    ind_num = num_load_app(m,k);
                    if ind_num>0
                        gathered_strain_CCRM(:,count:(count+ind_num)) =
ones(11,size(count:(count+ind_num),2)).*epsz;
                        count = count+ind_num+1;
                    end
                elseif m==19
                    %Class 11 Single Axles
                    Lrad_S = [rads(1,k) rads(1,k)]';
                    Lrad_tan = [rads(2,k) rads(2,k) rads(2,k) rads(2,k)]';
                    Lrad_tri = [rads(3,k) rads(3,k) rads(3,k) rads(3,k)
rads(3,k) rads(3,k)]';
                    Lrad_quad = [rads(4,k) rads(4,k) rads(4,k) rads(4,k)
rads(4,k) rads(4,k) rads(4,k) rads(4,k)]';
                    [~, ~, ~, ~, ~, ~, ~, ~, ~, ~, ~, epsz, ~, ~,
~]=analycomp(Lpres_S,Lrad_S,Lpos_S,mods_CCRM); %single axle
                    ind_num = num_load_app(m,k);
                    if ind_num>0
                        gathered_strain_CCRM(:,count:(count+ind_num)) =
ones(11,size(count:(count+ind_num),2)).*epsz;
                        count = count+ind_num+1;
                    end
                elseif m==20
                    %Class 12 Tandem Axles
                    Lrad_S = [rads(1,k) rads(1,k)]';
                    Lrad_tan = [rads(2,k) rads(2,k) rads(2,k) rads(2,k)]';
                    Lrad_tri = [rads(3,k) rads(3,k) rads(3,k) rads(3,k)
rads(3,k) rads(3,k)]';
                    Lrad_quad = [rads(4,k) rads(4,k) rads(4,k) rads(4,k)
rads(4,k) rads(4,k) rads(4,k) rads(4,k)]';
                    [~, ~, ~, ~, ~, ~, ~, ~, ~, ~, ~, epsz, ~, ~,
~]=analycomp(Lpres_tan,Lrad_tan,Lpos_tan,mods_CCRM); %tandem axle
                    ind_num = num_load_app(m,k);
                    if ind_num>0
```

```
                        gathered_strain_CCRM(:,count:(count+ind_num)) =
ones(11,size(count:(count+ind_num),2)).*epsz;
                        count = count+ind_num+1;
                    end
                elseif m==21
                    %Class 12 Single Axles
                    Lrad_S = [rads(1,k) rads(1,k)]';
                    Lrad_tan = [rads(2,k) rads(2,k) rads(2,k) rads(2,k)]';
                    Lrad_tri = [rads(3,k) rads(3,k) rads(3,k) rads(3,k)
rads(3,k) rads(3,k)]';
                    Lrad_quad = [rads(4,k) rads(4,k) rads(4,k) rads(4,k)
rads(4,k) rads(4,k) rads(4,k) rads(4,k)]';
                    [~, ~, ~, ~, ~, ~, ~, ~, ~, ~, ~, epsz, ~, ~,
~]=analycomp(Lpres_S,Lrad_S,Lpos_S,mods_CCRM); %single axle
                    ind_num = num_load_app(m,k);
                    if ind_num>0
                        gathered_strain_CCRM(:,count:(count+ind_num)) =
ones(11,size(count:(count+ind_num),2)).*epsz;
                        count = count+ind_num+1;
                    end
                elseif m==22
                    %Class 13 Single Axles
                    Lrad_S = [rads(1,k) rads(1,k)]';
                    Lrad_tan = [rads(2,k) rads(2,k) rads(2,k) rads(2,k)]';
                    Lrad_tri = [rads(3,k) rads(3,k) rads(3,k) rads(3,k)
rads(3,k) rads(3,k)]';
                    Lrad_quad = [rads(4,k) rads(4,k) rads(4,k) rads(4,k)
rads(4,k) rads(4,k) rads(4,k) rads(4,k)]';
                    [~, ~, ~, ~, ~, ~, ~, ~, ~, ~, ~, epsz, ~, ~,
~]=analycomp(Lpres_S,Lrad_S,Lpos_S,mods_CCRM); %single axle
                    ind_num = num_load_app(m,k);
                    if ind_num>0
                        gathered_strain_CCRM(:,count:(count+ind_num)) =
ones(11,size(count:(count+ind_num),2)).*epsz;
                        count = count+ind_num+1;
                    end
                elseif m==23
                    %Class 13 Tandem Axles
                    Lrad_S = [rads(1,k) rads(1,k)]';
                    Lrad_tan = [rads(2,k) rads(2,k) rads(2,k) rads(2,k)]';
                    Lrad_tri = [rads(3,k) rads(3,k) rads(3,k) rads(3,k)
rads(3,k) rads(3,k)]';
                    Lrad_quad = [rads(4,k) rads(4,k) rads(4,k) rads(4,k)
rads(4,k) rads(4,k) rads(4,k) rads(4,k)]';
                    [~, ~, ~, ~, ~, ~, ~, ~, ~, ~, ~, epsz, ~, ~,
~]=analycomp(Lpres_tan,Lrad_tan,Lpos_tan,mods_CCRM); %tandem axle
                    ind_num = num_load_app(m,k);
                    if ind_num>0
                        gathered_strain_CCRM(:,count:(count+ind_num)) =
ones(11,size(count:(count+ind_num),2)).*epsz;
                        count = count+ind_num+1;
                    end
                elseif m==24
                    %Class 13 Tridem Axles
                    Lrad_S = [rads(1,k) rads(1,k)]';
                    Lrad_tan = [rads(2,k) rads(2,k) rads(2,k) rads(2,k)]';
```

```
                    Lrad_tri = [rads(3,k) rads(3,k) rads(3,k) rads(3,k)
rads(3,k) rads(3,k)]';
                    Lrad_quad = [rads(4,k) rads(4,k) rads(4,k) rads(4,k)
rads(4,k) rads(4,k) rads(4,k) rads(4,k)]';
                    [~, ~, ~, ~, ~, ~, ~, ~, ~, ~, ~, epsz, ~, ~,
~]=analycomp(Lpres_tri,Lrad_tri,Lpos_tri,mods_CCRM); %tridem axle
                    ind_num = num_load_app(m,k);
                    if ind_num>0
                        gathered_strain_CCRM(:,count:(count+ind_num)) =
ones(11,size(count:(count+ind_num),2)).*epsz;
                        count = count+ind_num+1;
                    end
                end
            end
        end
    end
end

%% Future Climate Revised Model

count = 1;
for i = 1:12
    for j=1:5
        num_load_app = round(mths(:,:,i)./5);
        %define moduli
        l=find(mod_mat_FCRM(10,:)==i);

        if j==1
            mods_FCRM = prctile(mod_mat_FCRM(1:9,l)',10);
        elseif j==2
            mods_FCRM = prctile(mod_mat_FCRM(1:9,l)',30);
        elseif j==3
            mods_FCRM = prctile(mod_mat_FCRM(1:9,l)',50);
        elseif j==4
            mods_FCRM = prctile(mod_mat_FCRM(1:9,l)',70);
        elseif j==5
            mods_FCRM = prctile(mod_mat_FCRM(1:9,l)',90);
        end


        for k = 1:39 %k represents loading group

            for m = 1:24
                if m==1 %m represents truck classes, divided based on axle
type per LTPP data
                    %Class 4 Tandem Axles
                    Lrad_S = [rads(1,k) rads(1,k)]';
                    Lrad_tan = [rads(2,k) rads(2,k) rads(2,k) rads(2,k)]';
                    Lrad_tri = [rads(3,k) rads(3,k) rads(3,k) rads(3,k)
rads(3,k) rads(3,k)]';
                    Lrad_quad = [rads(4,k) rads(4,k) rads(4,k) rads(4,k)
rads(4,k) rads(4,k) rads(4,k) rads(4,k)]';
                    [~, ~, ~, ~, ~, ~, ~, ~, ~, ~, ~, epsz, ~, ~,
~]=analycomp(Lpres_tan,Lrad_tan,Lpos_tan,mods_FCRM); %tandem axle
                    ind_num = num_load_app(m,k);
                    if ind_num>0
```

```
                        gathered_strain_FCRM(:,count:(count+ind_num)) =
ones(11,size(count:(count+ind_num),2)).*epsz;
                        count = count+ind_num+1;
                    end
                elseif m==2
                    %Class 4 Single Axles
                    Lrad_S = [rads(1,k) rads(1,k)]';
                    Lrad_tan = [rads(2,k) rads(2,k) rads(2,k) rads(2,k)]';
                    Lrad_tri = [rads(3,k) rads(3,k) rads(3,k) rads(3,k)
rads(3,k) rads(3,k)]';
                    Lrad_quad = [rads(4,k) rads(4,k) rads(4,k) rads(4,k)
rads(4,k) rads(4,k) rads(4,k) rads(4,k)]';
                    [~, ~, ~, ~, ~, ~, ~, ~, ~, ~, ~, epsz, ~, ~,
~]=analycomp(Lpres_S,Lrad_S,Lpos_S,mods_FCRM); %single axle
                    ind_num = num_load_app(m,k);
                    if ind_num>0
                        gathered_strain_FCRM(:,count:(count+ind_num)) =
ones(11,size(count:(count+ind_num),2)).*epsz;
                        count = count+ind_num+1;
                    end
                elseif m==3
                    %Class 5 Tandem Axles
                    Lrad_S = [rads(1,k) rads(1,k)];
                    Lrad_tan = [rads(2,k) rads(2,k) rads(2,k) rads(2,k)]';
                    Lrad_tri = [rads(3,k) rads(3,k) rads(3,k) rads(3,k)
rads(3,k) rads(3,k)]';
                    Lrad_quad = [rads(4,k) rads(4,k) rads(4,k) rads(4,k)
rads(4,k) rads(4,k) rads(4,k) rads(4,k)]';
                    [~, ~, ~, ~, ~, ~, ~, ~, ~, ~, ~, epsz, ~, ~,
~]=analycomp(Lpres_tan,Lrad_tan,Lpos_tan,mods_FCRM); %tandem axle
                    ind_num = num_load_app(m,k);
                    if ind_num>0
                        gathered_strain_FCRM(:,count:(count+ind_num)) =
ones(11,size(count:(count+ind_num),2)).*epsz;
                        count = count+ind_num+1;
                    end
                elseif m==4
                    %Class 5 Single Axles
                    Lrad_S = [rads(1,k) rads(1,k)]';
                    Lrad_tan = [rads(2,k) rads(2,k) rads(2,k) rads(2,k)]';
                    Lrad_tri = [rads(3,k) rads(3,k) rads(3,k) rads(3,k)
rads(3,k) rads(3,k)]';
                    Lrad_quad = [rads(4,k) rads(4,k) rads(4,k) rads(4,k)
rads(4,k) rads(4,k) rads(4,k) rads(4,k)]';
                    [~, ~, ~, ~, ~, ~, ~, ~, ~, ~, ~, epsz, ~, ~,
~]=analycomp(Lpres_S,Lrad_S,Lpos_S,mods_FCRM); %single axle
                    ind_num = num_load_app(m,k);
                    if ind_num>0
                        gathered_strain_FCRM(:,count:(count+ind_num)) =
ones(11,size(count:(count+ind_num),2)).*epsz;
                        count = count+ind_num+1;
                    end
                elseif m==5
                    %Class 6 Tandem Axles
                    Lrad_S = [rads(1,k) rads(1,k)]';
                    Lrad_tan = [rads(2,k) rads(2,k) rads(2,k) rads(2,k)]';
```

```
                    Lrad_tri = [rads(3,k) rads(3,k) rads(3,k) rads(3,k)
rads(3,k) rads(3,k)]';
                    Lrad_quad = [rads(4,k) rads(4,k) rads(4,k) rads(4,k)
rads(4,k) rads(4,k) rads(4,k) rads(4,k)]';
                    [~, ~, ~, ~, ~, ~, ~, ~, ~, ~, ~, epsz, ~, ~,
~]=analycomp(Lpres_tan,Lrad_tan,Lpos_tan,mods_FCRM); %tandem axle
                    ind_num = num_load_app(m,k);
                    if ind_num>0
                        gathered_strain_FCRM(:,count:(count+ind_num)) =
ones(11,size(count:(count+ind_num),2)).*epsz;
                        count = count+ind_num+1;
                    end
                elseif m==6
                    %Class 6 Single Axles
                    Lrad_S = [rads(1,k) rads(1,k)]';
                    Lrad_tan = [rads(2,k) rads(2,k) rads(2,k) rads(2,k)]';
                    Lrad_tri = [rads(3,k) rads(3,k) rads(3,k) rads(3,k)
rads(3,k) rads(3,k)]';
                    Lrad_quad = [rads(4,k) rads(4,k) rads(4,k) rads(4,k)
rads(4,k) rads(4,k) rads(4,k) rads(4,k)]';
                    [~, ~, ~, ~, ~, ~, ~, ~, ~, ~, ~, epsz, ~, ~,
~]=analycomp(Lpres_S,Lrad_S,Lpos_S,mods_FCRM); %single axle
                    ind_num = num_load_app(m,k);
                    if ind_num>0
                        gathered_strain_FCRM(:,count:(count+ind_num)) =
ones(11,size(count:(count+ind_num),2)).*epsz;
                        count = count+ind_num+1;
                    end
                elseif m==7
                    %Class 7 Quad Axles
                    Lrad_S = [rads(1,k) rads(1,k)]';
                    Lrad_tan = [rads(2,k) rads(2,k) rads(2,k) rads(2,k)]';
                    Lrad_tri = [rads(3,k) rads(3,k) rads(3,k) rads(3,k)
rads(3,k) rads(3,k)]';
                    Lrad_quad = [rads(4,k) rads(4,k) rads(4,k) rads(4,k)
rads(4,k) rads(4,k) rads(4,k) rads(4,k)]';
                    [~, ~, ~, ~, ~, ~, ~, ~, ~, ~, ~, epsz, ~, ~,
~]=analycomp(Lpres_quad,Lrad_quad,Lpos_quad,mods_FCRM); %quad axle
                    ind_num = num_load_app(m,k);
                    if ind_num>0
                        gathered_strain_FCRM(:,count:(count+ind_num)) =
ones(11,size(count:(count+ind_num),2)).*epsz;
                        count = count+ind_num+1;
                    end
                elseif m==8
                    %Class 7 Tridem Axles
                    Lrad_S = [rads(1,k) rads(1,k)]';
                    Lrad_tan = [rads(2,k) rads(2,k) rads(2,k) rads(2,k)]';
                    Lrad_tri = [rads(3,k) rads(3,k) rads(3,k) rads(3,k)
rads(3,k) rads(3,k)]';
                    Lrad_quad = [rads(4,k) rads(4,k) rads(4,k) rads(4,k)
rads(4,k) rads(4,k) rads(4,k) rads(4,k)]';
                    [~, ~, ~, ~, ~, ~, ~, ~, ~, ~, ~, epsz, ~, ~,
~]=analycomp(Lpres_tri,Lrad_tri,Lpos_tri,mods_FCRM); %tridem axle
                    ind_num = num_load_app(m,k);
                    if ind_num>0
```

```
                        gathered_strain_FCRM(:,count:(count+ind_num)) =
ones(11,size(count:(count+ind_num),2)).*epsz;
                        count = count+ind_num+1;
                    end
                elseif m==9
                    %Class 7 Single Axles
                    Lrad_S = [rads(1,k) rads(1,k)]';
                    Lrad_tan = [rads(2,k) rads(2,k) rads(2,k) rads(2,k)]';
                    Lrad_tri = [rads(3,k) rads(3,k) rads(3,k) rads(3,k)
rads(3,k) rads(3,k)]';
                    Lrad_quad = [rads(4,k) rads(4,k) rads(4,k) rads(4,k)
rads(4,k) rads(4,k) rads(4,k) rads(4,k)]';
                    [~, ~, ~, ~, ~, ~, ~, ~, ~, ~, ~, epsz, ~, ~,
~]=analycomp(Lpres_S,Lrad_S,Lpos_S,mods_FCRM); %single axle
                    ind_num = num_load_app(m,k);
                    if ind_num>0
                        gathered_strain_FCRM(:,count:(count+ind_num)) =
ones(11,size(count:(count+ind_num),2)).*epsz;
                        count = count+ind_num+1;
                    end
                elseif m==10
                    %Class 7 Tandem Axles
                    Lrad_S = [rads(1,k) rads(1,k)]';
                    Lrad_tan = [rads(2,k) rads(2,k) rads(2,k) rads(2,k)]';
                    Lrad_tri = [rads(3,k) rads(3,k) rads(3,k) rads(3,k)
rads(3,k) rads(3,k)]';
                    Lrad_quad = [rads(4,k) rads(4,k) rads(4,k) rads(4,k)
rads(4,k) rads(4,k) rads(4,k) rads(4,k)]';
                    [~, ~, ~, ~, ~, ~, ~, ~, ~, ~, ~, epsz, ~, ~,
~]=analycomp(Lpres_tan,Lrad_tan,Lpos_tan,mods_FCRM); %tandem axle
                    ind_num = num_load_app(m,k);
                    if ind_num>0
                        gathered_strain_FCRM(:,count:(count+ind_num)) =
ones(11,size(count:(count+ind_num),2)).*epsz;
                        count = count+ind_num+1;
                    end
                elseif m==11
                    %Class 8 Single Axles
                    Lrad_S = [rads(1,k) rads(1,k)]';
                    Lrad_tan = [rads(2,k) rads(2,k) rads(2,k) rads(2,k)]';
                    Lrad_tri = [rads(3,k) rads(3,k) rads(3,k) rads(3,k)
rads(3,k) rads(3,k)]';
                    Lrad_quad = [rads(4,k) rads(4,k) rads(4,k) rads(4,k)
rads(4,k) rads(4,k) rads(4,k) rads(4,k)]';
                    [~, ~, ~, ~, ~, ~, ~, ~, ~, ~, ~, epsz, ~, ~,
~]=analycomp(Lpres_S,Lrad_S,Lpos_S,mods_FCRM); %single axle
                    ind_num = num_load_app(m,k);
                    if ind_num>0
                        gathered_strain_FCRM(:,count:(count+ind_num)) =
ones(11,size(count:(count+ind_num),2)).*epsz;
                        count = count+ind_num+1;
                    end
                elseif m==12
                    %Class 8 Tandem Axles
                    Lrad_S = [rads(1,k) rads(1,k)]';
                    Lrad_tan = [rads(2,k) rads(2,k) rads(2,k) rads(2,k)]';
```

```
                    Lrad_tri = [rads(3,k) rads(3,k) rads(3,k) rads(3,k)
rads(3,k) rads(3,k)]';
                    Lrad_quad = [rads(4,k) rads(4,k) rads(4,k) rads(4,k)
rads(4,k) rads(4,k) rads(4,k) rads(4,k)]';
                    [~, ~, ~, ~, ~, ~, ~, ~, ~, ~, ~, epsz, ~, ~,
~]=analycomp(Lpres_tan,Lrad_tan,Lpos_tan,mods_FCRM); %tandem axle
                    ind_num = num_load_app(m,k);
                    if ind_num>0
                        gathered_strain_FCRM(:,count:(count+ind_num)) =
ones(11,size(count:(count+ind_num),2)).*epsz;
                        count = count+ind_num+1;
                    end
                elseif m==13
                    %Class 9 Single Axles
                    Lrad_S = [rads(1,k) rads(1,k)]';
                    Lrad_tan = [rads(2,k) rads(2,k) rads(2,k) rads(2,k)]';
                    Lrad_tri = [rads(3,k) rads(3,k) rads(3,k) rads(3,k)
rads(3,k) rads(3,k)]';
                    Lrad_quad = [rads(4,k) rads(4,k) rads(4,k) rads(4,k)
rads(4,k) rads(4,k) rads(4,k) rads(4,k)]';
                    [~, ~, ~, ~, ~, ~, ~, ~, ~, ~, ~, epsz, ~, ~,
~]=analycomp(Lpres_S,Lrad_S,Lpos_S,mods_FCRM); %single axle
                    ind_num = num_load_app(m,k);
                    if ind_num>0
                        gathered_strain_FCRM(:,count:(count+ind_num)) =
ones(11,size(count:(count+ind_num),2)).*epsz;
                        count = count+ind_num+1;
                    end
                elseif m==14
                    %Class 9 Tandem Axles
                    Lrad_S = [rads(1,k) rads(1,k)]';
                    Lrad_tan = [rads(2,k) rads(2,k) rads(2,k) rads(2,k)]';
                    Lrad_tri = [rads(3,k) rads(3,k) rads(3,k) rads(3,k)
rads(3,k) rads(3,k)]';
                    Lrad_quad = [rads(4,k) rads(4,k) rads(4,k) rads(4,k)
rads(4,k) rads(4,k) rads(4,k) rads(4,k)]';
                    [~, ~, ~, ~, ~, ~, ~, ~, ~, ~, ~, epsz, ~, ~,
~]=analycomp(Lpres_tan,Lrad_tan,Lpos_tan,mods_FCRM); %tandem axle
                    ind_num = num_load_app(m,k);
                    if ind_num>0
                        gathered_strain_FCRM(:,count:(count+ind_num)) =
ones(11,size(count:(count+ind_num),2)).*epsz;
                        count = count+ind_num+1;
                    end
                elseif m==15
                    %Class 10 Single Axles
                    Lrad_S = [rads(1,k) rads(1,k)]';
                    Lrad_tan = [rads(2,k) rads(2,k) rads(2,k) rads(2,k)]';
                    Lrad_tri = [rads(3,k) rads(3,k) rads(3,k) rads(3,k)
rads(3,k) rads(3,k)]';
                    Lrad_quad = [rads(4,k) rads(4,k) rads(4,k) rads(4,k)
rads(4,k) rads(4,k) rads(4,k) rads(4,k)]';
                    [~, ~, ~, ~, ~, ~, ~, ~, ~, ~, ~, epsz, ~, ~,
~]=analycomp(Lpres_S,Lrad_S,Lpos_S,mods_FCRM); %single axle
                    ind_num = num_load_app(m,k);
                    if ind_num>0
```

```
                        gathered_strain_FCRM(:,count:(count+ind_num)) =
ones(11,size(count:(count+ind_num),2)).*epsz;
                        count = count+ind_num+1;
                    end
                elseif m==16
                    %Class 10 Quad Axles
                    Lrad_S = [rads(1,k) rads(1,k)]';
                    Lrad_tan = [rads(2,k) rads(2,k) rads(2,k) rads(2,k)]';
                    Lrad_tri = [rads(3,k) rads(3,k) rads(3,k) rads(3,k)
rads(3,k) rads(3,k)]';
                    Lrad_quad = [rads(4,k) rads(4,k) rads(4,k) rads(4,k)
rads(4,k) rads(4,k) rads(4,k) rads(4,k)]';
                    [~, ~, ~, ~, ~, ~, ~, ~, ~, ~, ~, epsz, ~, ~,
~]=analycomp(Lpres_quad,Lrad_quad,Lpos_quad,mods_FCRM); %quad axle
                    ind_num = num_load_app(m,k);
                    if ind_num>0
                        gathered_strain_FCRM(:,count:(count+ind_num)) =
ones(11,size(count:(count+ind_num),2)).*epsz;
                        count = count+ind_num+1;
                    end
                elseif m==17
                    %Class 10 Tandem Axles
                    Lrad_S = [rads(1,k) rads(1,k)]';
                    Lrad_tan = [rads(2,k) rads(2,k) rads(2,k) rads(2,k)]';
                    Lrad_tri = [rads(3,k) rads(3,k) rads(3,k) rads(3,k)
rads(3,k) rads(3,k)]';
                    Lrad_quad = [rads(4,k) rads(4,k) rads(4,k) rads(4,k)
rads(4,k) rads(4,k) rads(4,k) rads(4,k)]';
                    [~, ~, ~, ~, ~, ~, ~, ~, ~, ~, ~, epsz, ~, ~,
~]=analycomp(Lpres_tan,Lrad_tan,Lpos_tan,mods_FCRM); %tandem axle
                    ind_num = num_load_app(m,k);
                    if ind_num>0
                        gathered_strain_FCRM(:,count:(count+ind_num)) =
ones(11,size(count:(count+ind_num),2)).*epsz;
                        count = count+ind_num+1;
                    end
                elseif m==18
                    %Class 10 Tridem Axles
                    Lrad_S = [rads(1,k) rads(1,k)]';
                    Lrad_tan = [rads(2,k) rads(2,k) rads(2,k) rads(2,k)]';
                    Lrad_tri = [rads(3,k) rads(3,k) rads(3,k) rads(3,k)
rads(3,k) rads(3,k)]';
                    Lrad_quad = [rads(4,k) rads(4,k) rads(4,k) rads(4,k)
rads(4,k) rads(4,k) rads(4,k) rads(4,k)]';
                    [~, ~, ~, ~, ~, ~, ~, ~, ~, ~, ~, epsz, ~, ~,
~]=analycomp(Lpres_tri,Lrad_tri,Lpos_tri,mods_FCRM); %tridem axle
                    ind_num = num_load_app(m,k);
                    if ind_num>0
                        gathered_strain_FCRM(:,count:(count+ind_num)) =
ones(11,size(count:(count+ind_num),2)).*epsz;
                        count = count+ind_num+1;
                    end
                elseif m==19
                    %Class 11 Single Axles
                    Lrad_S = [rads(1,k) rads(1,k)]';
                    Lrad_tan = [rads(2,k) rads(2,k) rads(2,k) rads(2,k)]';
```

```
                    Lrad_tri = [rads(3,k) rads(3,k) rads(3,k) rads(3,k)
rads(3,k) rads(3,k)]';
                    Lrad_quad = [rads(4,k) rads(4,k) rads(4,k) rads(4,k)
rads(4,k) rads(4,k) rads(4,k) rads(4,k)]';
                    [~, ~, ~, ~, ~, ~, ~, ~, ~, ~, ~, epsz, ~, ~,
~]=analycomp(Lpres_S,Lrad_S,Lpos_S,mods_FCRM); %single axle
                    ind_num = num_load_app(m,k);
                    if ind_num>0
                        gathered_strain_FCRM(:,count:(count+ind_num)) =
ones(11,size(count:(count+ind_num),2)).*epsz;
                        count = count+ind_num+1;
                    end
                elseif m==20
                    %Class 12 Tandem Axles
                    Lrad_S = [rads(1,k) rads(1,k)]';
                    Lrad_tan = [rads(2,k) rads(2,k) rads(2,k) rads(2,k)]';
                    Lrad_tri = [rads(3,k) rads(3,k) rads(3,k) rads(3,k)
rads(3,k) rads(3,k)]';
                    Lrad_quad = [rads(4,k) rads(4,k) rads(4,k) rads(4,k)
rads(4,k) rads(4,k) rads(4,k) rads(4,k)]';
                    [~, ~, ~, ~, ~, ~, ~, ~, ~, ~, ~, epsz, ~, ~,
~]=analycomp(Lpres_tan,Lrad_tan,Lpos_tan,mods_FCRM); %tandem axle
                    ind_num = num_load_app(m,k);
                    if ind_num>0
                        gathered_strain_FCRM(:,count:(count+ind_num)) =
ones(11,size(count:(count+ind_num),2)).*epsz;
                        count = count+ind_num+1;
                    end
                elseif m==21
                    %Class 12 Single Axles
                    Lrad_S = [rads(1,k) rads(1,k)]';
                    Lrad_tan = [rads(2,k) rads(2,k) rads(2,k) rads(2,k)]';
                    Lrad_tri = [rads(3,k) rads(3,k) rads(3,k) rads(3,k)
rads(3,k) rads(3,k)]';
                    Lrad_quad = [rads(4,k) rads(4,k) rads(4,k) rads(4,k)
rads(4,k) rads(4,k) rads(4,k) rads(4,k)]';
                    [~, ~, ~, ~, ~, ~, ~, ~, ~, ~, ~, epsz, ~, ~,
~]=analycomp(Lpres_S,Lrad_S,Lpos_S,mods_FCRM); %single axle
                    ind_num = num_load_app(m,k);
                    if ind_num>0
                        gathered_strain_FCRM(:,count:(count+ind_num)) =
ones(11,size(count:(count+ind_num),2)).*epsz;
                        count = count+ind_num+1;
                    end
                elseif m==22
                    %Class 13 Single Axles
                    Lrad_S = [rads(1,k) rads(1,k)]';
                    Lrad_tan = [rads(2,k) rads(2,k) rads(2,k) rads(2,k)]';
                    Lrad_tri = [rads(3,k) rads(3,k) rads(3,k) rads(3,k)
rads(3,k) rads(3,k)]';
                    Lrad_quad = [rads(4,k) rads(4,k) rads(4,k) rads(4,k)
rads(4,k) rads(4,k) rads(4,k) rads(4,k)]';
                    [~, ~, ~, ~, ~, ~, ~, ~, ~, ~, ~, epsz, ~, ~,
~]=analycomp(Lpres_S,Lrad_S,Lpos_S,mods_FCRM); %single axle
                    ind_num = num_load_app(m,k);
                    if ind_num>0
```

```
                        gathered_strain_FCRM(:,count:(count+ind_num)) =
ones(11,size(count:(count+ind_num),2)).*epsz;
                        count = count+ind_num+1;
                    end
                elseif m==23
                    %Class 13 Tandem Axles
                    Lrad_S = [rads(1,k) rads(1,k)]';
                    Lrad_tan = [rads(2,k) rads(2,k) rads(2,k) rads(2,k)]';
                    Lrad_tri = [rads(3,k) rads(3,k) rads(3,k) rads(3,k)
rads(3,k) rads(3,k)]';
                    Lrad_quad = [rads(4,k) rads(4,k) rads(4,k) rads(4,k)
rads(4,k) rads(4,k) rads(4,k) rads(4,k)]';
                    [~, ~, ~, ~, ~, ~, ~, ~, ~, ~, ~, epsz, ~, ~,
~]=analycomp(Lpres_tan,Lrad_tan,Lpos_tan,mods_FCRM); %tandem axle
                    ind_num = num_load_app(m,k);
                    if ind_num>0
                        gathered_strain_FCRM(:,count:(count+ind_num)) =
ones(11,size(count:(count+ind_num),2)).*epsz;
                        count = count+ind_num+1;
                    end
                elseif m==24
                    %Class 13 Tridem Axles
                    Lrad_S = [rads(1,k) rads(1,k)]';
                    Lrad_tan = [rads(2,k) rads(2,k) rads(2,k) rads(2,k)]';
                    Lrad_tri = [rads(3,k) rads(3,k) rads(3,k) rads(3,k)
rads(3,k) rads(3,k)]';
                    Lrad_quad = [rads(4,k) rads(4,k) rads(4,k) rads(4,k)
rads(4,k) rads(4,k) rads(4,k) rads(4,k)]';
                    [~, ~, ~, ~, ~, ~, ~, ~, ~, ~, ~, epsz, ~, ~,
~]=analycomp(Lpres_tri,Lrad_tri,Lpos_tri,mods_FCRM); %tridem axle
                    ind_num = num_load_app(m,k);
                    if ind_num>0
                        gathered_strain_FCRM(:,count:(count+ind_num)) =
ones(11,size(count:(count+ind_num),2)).*epsz;
                        count = count+ind_num+1;
                    end
                end
            end
        end
    end
end
```

APPENDIX I: EXCEL SUPPLEMENT - YEAR1TRAFFIC

Base Year Traffic

Axle Configuration	VEHICLE_CLASS	VEHICLE_CLASS_DESCRIP	MEPDG_LGD1	MEPDG_LGD2	MEPDG_LG03	MEPDG_LG04	MEPDG_LG05	MEPDG_LG06	MEPDG_LG07	MEPDG_LG08	MEPDG_LG09	MEPDG_LG10	MEPDG_LG11	MEPDG_LG12	MEPDG_LG13	MEPDG_LG14	MEPDG_LG15	MEPDG_LG16	MEPDG_LG17	MEPDG_LG18	MEPDG_LG19	MEPDG_LG20	MEPDG_LG21	MEPDG_LG22	MEPDG_LG23	MEPDG_LG24	MEPDG_LG25	MEPDG_LG26	MEPDG_LG27	MEPDG_LG28	MEPDG_LG29	MEPDG_LG30	MEPDG_LG31	MEPDG_LG32	MEPDG_LG33	MEPDG_LG34	MEPDG_LG35	MEPDG_LG36	MEPDG_LG37	MEPDG_LG38	MEPDG_LG39
Tandem axle	4	FHWA Class 4 (Buses)	0.00	1.22	9.06	48.08	129.55	163.43	137.47	205.72	417.56	499.20	587.36	828.18	1301.50	1516.04	850.88	284.58	193.47	131.35	36.49	4.25	0.41	0.49	0.82	0.00	0.00	0.00	0.00	0.00	0.00	0.00	0.00	0.00	0.00	0.00	0.00	0.00	0.00	0.00	0.00	0.00
Single axle	4	FHWA Class 4 (Buses)	0.00	0.00	0.00	20.78	73.89	549.77	905.48	1297.61	835.05	922.17	752.35	915.03	397.79	151.88	156.39	106.01	127.84	86.70	33.27	7.45	3.67	0.00	0.00	0.00	0.00	3.99	0.00	0.00	0.00	0.00	0.00	0.00	0.00	0.00	0.00	0.00	0.00	0.00	0.00	0.00
Tandem axle	5	FHWA Class 5 (Two axle, 6-Tire, Single-unit truck)	20348.65	12878.99	3630.63	561.15	18.30	0.00	0.00	0.00	0.00	0.00	0.00	0.00	0.00	0.00	0.00	0.00	0.00	0.00	0.00	0.00	0.00	0.00	0.00	0.00	0.00	0.00	0.00	0.00	0.00	0.00	0.00	0.00	0.00	0.00	0.00	0.00	0.00	0.00	0.00	0.00
Single axle	5	FHWA Class 5 (Two axle, 6-Tire, Single-unit truck)	401.12	6937.21	9829.54	6662.84	2314.72	2993.41	2072.98	1930.72	1074.46	969.64	533.75	500.60	337.47	184.51	178.63	147.61	115.52	65.25	64.18	36.37	33.16	31.55	18.18	3.21	0.53	0.53	0.00	0.00	0.00	0.00	0.00	0.00	0.00	0.00	0.00	0.00	0.00	0.00	0.00	0.00	0.00
Tandem axle	6	FHWA Class 6 (Three axle Single-unit truck)	2.76	20.21	33.08	33.08	42.27	222.67	932.31	3606.75	4859.12	4890.67	3185.00	2186.22	581.01	128.02	219.30	195.41	183.16	73.81	21.13	2.76	0.00	0.00	3.68	3.37	0.00	2.45	0.00	3.37	2.76	0.00	0.00	0.00	0.00	2.76	0.00	2.45	0.00	0.00	0.00	0.00
Single axle	6	FHWA Class 6 (Three axle Single-unit truck)	38.90	486.37	3949.78	2168.76	3083.01	2561.72	1153.14	1106.59	1247.17	1128.64	865.55	864.32	695.56	610.41	475.04	429.40	220.83	169.99	111.49	41.65	18.38	10.41	2.45	0.00	0.00	0.00	0.00	0.00	0.00	0.00	0.00	0.00	0.00	0.00	0.00	0.00	0.00	0.00	0.00	0.00	0.00
Quad axle and	7	FHWA Class 7 (Four or more axle Single-unit truck)	1.29	1.23	1.67	4.24	4.63	11.69	13.26	23.04	39.86	106.20	122.53	148.98	137.06	86.55	100.75	57.20	63.35	34.18	13.97	4.01	1.54	0.21	0.38	0.05	0.00	0.00	0.00	0.00	0.00	0.00	0.00	0.07	0.00	0.00	0.00	0.00	0.00	0.00	0.00	0.00
Tridem axle	7	FHWA Class 7 (Four or more axle Single-unit truck)	0.00	0.00	0.00	0.86	1.83	1.71	2.97	12.20	36.48	68.46	96.60	64.53	64.03	176.98	211.40	107.82	67.70	39.45	14.81	3.31	3.55	0.17	1.58	1.51	0.00	0.00	0.00	0.00	0.00	0.00	0.00	NaN	NaN	NaN	NaN	NaN	NaN	NaN	NaN	NaN
Single axle	7	FHWA Class 7 (Four or more axle Single-unit truck)	0.00	0.00	41.85	39.23	61.82	49.65	19.70	26.73	11.67	48.19	36.13	52.68	65.70	44.87	17.51	56.53	34.29	92.43	95.04	63.06	67.82	16.34	21.36	5.82	0.67	2.16	2.24	0.00	0.00	0.00	0.00	4.45	0.00	0.00	0.00	0.00	0.00	0.00	0.00	0.00
Tandem axle	7	FHWA Class 7 (Four or more axle Single-unit truck)	0.00	1.98	5.51	16.33	7.57	62.88	54.88	47.22	70.35	83.03	110.49	154.22	155.02	91.35	53.69	29.54	15.23	7.64	6.24	3.15	1.36	0.52	0.14	0.00	0.00	0.00	0.00	0.00	0.00	0.00	0.00	NaN	NaN	NaN	NaN	NaN	NaN	NaN	NaN	NaN
Single axle	8	FHWA Class 8 (Four or less axle, one trailer truck)	581.80	125.44	395.67	574.64	645.60	1178.42	1655.57	4196.15	2198.91	954.30	663.28	758.14	671.88	493.40	584.43	417.18	331.40	130.22	87.21	39.42	19.83	9.08	6.21	4.06	0.72	2.39	0.00	0.00	0.00	0.00	0.00	0.00	0.00	0.00	0.00	0.00	0.00	0.00	0.00	0.00	0.00
Tandem axle	8	FHWA Class 8 (Four or less axle, one trailer truck)	71.20	152.44	479.54	3495.84	3283.67	1868.94	1570.27	1689.74	1573.38	1118.69	720.86	457.56	99.64	60.21	22.22	28.19	15.53	9.56	3.11	0.00	0.00	0.00	2.39	0.00	0.00	2.39	0.00	0.00	0.00	0.00	0.00	0.00	0.00	0.00	0.00	0.00	0.00	0.00	0.00	0.00	0.00
Single axle	9	FHWA Class 9 (Five axle, one trailer truck)	300.56	2088.31	3907.24	2266.42	1585.16	2731.73	4497.22	22995.93	43044.18	50248.63	6886.09	1487.20	1680.89	2420.04	3829.32	2531.36	1803.34	710.20	451.95	198.14	97.96	28.94	20.04	13.36	6.68	8.91	2.23	2.23	0.00	0.00	0.00	0.00	0.00	0.00	0.00	0.00	0.00	0.00	0.00	0.00
Tandem axle	9	FHWA Class 9 (Five axle, one trailer truck)	100.19	1400.37	7024.12	19525.06	20787.39	14117.26	10283.49	7736.55	6999.63	5229.69	4695.36	5784.05	10285.72	17614.85	15508.73	5817.44	1936.92	685.71	209.28	80.15	15.58	4.45	2.23	0.00	0.00	0.00	0.00	0.00	0.00	0.00	0.00	0.00	0.00	0.00	0.00	0.00	0.00	0.00	0.00	0.00
Single axle	10	FHWA Class 10 (Six or more axle, one trailer truck)	9.26	3.42	5.19	14.06	31.88	43.92	113.71	551.79	492.21	520.98	222.33	115.99	30.91	9.31	5.67	3.30	2.69	1.31	1.72	1.45	0.29	0.10	0.00	0.10	0.00	0.00	0.00	0.00	0.00	0.00	0.00	0.00	0.00	0.00	0.00	0.00	0.00	0.00	0.00	0.00
Quad axle and	10	FHWA Class 10 (Six or more axle, one trailer truck)	6.11	8.85	20.51	61.28	150.67	162.16	256.67	266.30	162.31	123.67	138.82	181.19	171.20	142.48	96.21	65.71	47.41	35.44	24.85	17.60	11.76	9.82	5.43	4.29	3.56	2.98	1.89	0.85	0.99	0.44	0.00	0.12	0.00	0.00	0.00	0.00	0.00	0.00	0.00	0.00
Tandem axle	10	FHWA Class 10 (Six or more axle, one trailer truck)	6.71	54.88	266.44	247.24	95.43	77.88	79.97	94.29	105.61	143.57	200.10	185.41	154.43	118.63	90.78	88.60	77.69	52.48	22.54	8.31	5.36	2.96	1.12	0.48	0.00	0.34	0.32	0.00	0.00	0.00	0.00	NaN	NaN	NaN	NaN	NaN	NaN	NaN	NaN	NaN
Tridem axle	10	FHWA Class 10 (Six or more axle, one trailer truck)	5.52	12.06	50.23	78.88	67.53	63.85	38.51	22.47	37.76	51.31	100.75	207.69	289.62	362.55	299.78	133.68	83.43	81.27	73.75	51.04	18.04	9.57	7.66	10.10	11.61	5.40	6.09	1.41	0.00	0.00	0.00	NaN	NaN	NaN	NaN	NaN	NaN	NaN	NaN	NaN
Single axle	11	FHWA Class 11 (Five or less axle, multi trailer truck)	3.30	11.66	27.93	340.26	474.32	287.25	466.95	1304.73	986.03	813.37	580.77	700.20	547.67	357.64	338.94	195.42	158.91	64.88	28.37	6.05	2.53	0.66	0.00	0.33	0.00	0.00	0.00	0.00	0.00	0.00	0.00	0.00	0.00	0.00	0.00	0.00	0.00	0.00	0.00	0.00
Tandem axle	12	FHWA Class 12 (Six axle, multi trailer truck)	0.00	1.17	5.09	62.98	147.46	81.00	150.73	193.38	197.51	148.89	68.76	18.14	2.54	0.37	0.23	0.00	0.00	0.00	0.00	0.00	0.00	0.00	0.00	0.00	0.00	0.00	0.00	0.00	0.00	0.00	0.00	0.00	0.00	0.00	0.00	0.00	0.00	0.00	0.00	0.00
Single axle	12	FHWA Class 12 (Six axle, multi trailer truck)	1.08	2.11	4.39	48.10	104.54	80.74	150.69	171.16	113.61	115.01	70.11	81.59	58.81	34.53	29.11	6.67	4.36	0.77	0.86	0.00	0.00	0.00	0.00	0.00	0.00	0.00	0.00	0.00	0.00	0.00	0.00	0.00	0.00	0.00	0.00	0.00	0.00	0.00	0.00	0.00
Single axle	13	FHWA Class 13 (Seven or more axle, multi trailer truck)	0.00	0.00	0.00	0.00	0.00	0.00	0.00	0.00	0.00	0.00	0.00	0.00	0.00	0.00	0.00	0.00	0.00	0.00	0.00	0.00	0.00	0.00	0.00	0.00	0.00	0.00	0.00	0.00	0.00	0.00	0.00	0.00	0.00	0.00	0.00	0.00	0.00	0.00	0.00	0.00
Tandem axle	13	FHWA Class 13 (Seven or more axle, multi trailer truck)	0.00	0.00	0.00	0.00	0.00	0.00	0.00	0.00	0.00	0.00	0.00	0.00	0.00	0.00	0.00	0.00	0.00	0.00	0.00	0.00	0.00	0.00	0.00	0.00	0.00	0.00	0.00	0.00	0.00	0.00	0.00	0.00	0.00	0.00	0.00	0.00	0.00	0.00	0.00	0.00
Tridem axle	13	FHWA Class 13 (Seven or more axle, multi trailer truck)	0.00	0.00	0.00	0.00	0.00	0.00	0.00	0.00	0.00	0.00	0.00	0.00	0.00	0.00	0.00	0.00	0.00	0.00	0.00	0.00	0.00	0.00	0.00	0.00	0.00	0.00	0.00	0.00	0.00	0.00	0.00	NaN	NaN	NaN	NaN	NaN	NaN	NaN	NaN	NaN

Modified to be integers:

Axle Configuration	VEHICLE_CLASS	VEHICLE_CLASS_DESCRIP	MEPDG_LG01	MEPDG_LG02	MEPDG_LG03	MEPDG_LG04	MEPDG_LG05	MEPDG_LG06	MEPDG_LG07	MEPDG_LG08	MEPDG_LG09	MEPDG_LG10	MEPDG_LG11	MEPDG_LG12	MEPDG_LG13	MEPDG_LG14	MEPDG_LG15	MEPDG_LG16	MEPDG_LG17	MEPDG_LG18	MEPDG_LG19	MEPDG_LG20	MEPDG_LG21	MEPDG_LG22	MEPDG_LG23	MEPDG_LG24	MEPDG_LG25	MEPDG_LG26	MEPDG_LG27	MEPDG_LG28	MEPDG_LG29	MEPDG_LG30	MEPDG_LG31	MEPDG_LG32	MEPDG_LG33	MEPDG_LG34	MEPDG_LG35	MEPDG_LG36	MEPDG_LG37	MEPDG_LG38	MEPDG_LG39
Tandem axle	4	FHWA Class 4 (Buses)	0	1	9	48	129	163	137	205	417	499	587	828	1301	1516	850	284	193	131	36	4	0	0	0	0	0	0	0	0	0	0	0	0	0	0	0	0	0	0	0
Single axle	4	FHWA Class 4 (Buses)	0	0	0	20	73	549	905	1297	835	922	752	915	397	151	156	106	127	86	33	7	3	0	0	0	0	3	0	0	0	0	0	0	0	0	0	0	0	0	0
Tandem axle	5	FHWA Class 5 (Two axle, 6-Tire, Single-unit truck)	20348	12878	3630	561	18	0	0	0	0	0	0	0	0	0	0	0	0	0	0	0	0	0	0	0	0	0	0	0	0	0	0	0	0	0	0	0	0	0	0
Single axle	5	FHWA Class 5 (Two axle, 6-Tire, Single-unit truck)	401	6937	9829	6662	2334	2933	2072	1930	1074	969	533	500	337	184	178	147	115	65	64	36	33	31	18	3	0	0	0	0	0	0	0	0	0	0	0	0	0	0	0
Tandem axle	6	FHWA Class 6 (Three axle Single-unit truck)	2	20	33	33	42	222	932	3606	4859	4890	3184	2186	581	128	219	195	183	73	21	2	0	0	3	3	0	2	0	3	2	0	0	0	2	0	2	0	0	0
Single axle	6	FHWA Class 6 (Three axle Single-unit truck)	38	486	3949	2168	3083	2561	1153	1106	1247	1128	865	864	695	610	475	429	220	169	111	41	18	10	2	0	0	0	0	0	0	0	0	0	0	0	0	0	0	0	0
Quad axle and 5+ axle groups	7	FHWA Class 7 (Four or more axle Single-unit truck)	1	1	1	4	4	11	13	23	39	106	122	148	137	86	100	57	63	34	13	4	1	0	0	0	0	0	0	0	0	0	0	0	0	0	0	0	0	0	0
Tridem axle	7	FHWA Class 7 (Four or more axle Single-unit truck)	0	0	0	0	1	1	2	12	36	68	96	64	64	176	211	107	67	39	14	3	3	0	1	1	0	0	0	0	0	0	0	0	0	0	0	0	0	0	0
Single axle	7	FHWA Class 7 (Four or more axle Single-unit truck)	0	0	41	39	61	49	19	26	11	48	36	52	65	44	17	56	34	92	95	63	67	16	21	5	0	2	2	0	0	0	0	4	0	0	0	0	0	0	0
Tandem axle	7	FHWA Class 7 (Four or more axle Single-unit truck)	0	1	5	16	7	62	54	47	70	83	110	154	155	91	53	29	15	7	6	3	1	0	0	0	0	0	0	0	0	0	0	0	0	0	0	0	0	0	0
Single axle	8	FHWA Class 8 (Four or less axle, one trailer truck)	581	125	395	574	645	1178	1655	4196	2198	954	663	758	671	493	584	417	331	130	87	39	19	9	6	4	0	2	0	0	0	0	0	0	0	0	0	0	0	0	0
Tandem axle	8	FHWA Class 8 (Four or less axle, one trailer truck)	71	152	479	3495	3283	1868	1570	1689	1573	1118	720	457	99	60	22	28	15	9	3	0	0	0	2	0	0	2	0	0	0	0	0	0	0	0	0	0	0	0	0
Single axle	9	FHWA Class 9 (Five axle, one trailer truck)	300	2088	3907	2266	1585	2731	4497	22995	43044	50248	6886	1487	1680	2420	3829	2531	1803	710	451	198	97	28	20	13	6	8	2	2	0	0	0	0	0	0	0	0	0	0	0
Tandem axle	9	FHWA Class 9 (Five axle, one trailer truck)	100	1400	7024	19525	20787	14117	10283	7736	6999	5229	4695	5784	10285	17614	15508	5817	1936	685	209	80	15	4	2	0	0	0	0	0	0	0	0	0	0	0	0	0	0	0	0
Single axle	10	FHWA Class 10 (Six or more axle, one trailer truck)	9	3	5	14	31	43	113	551	492	520	222	115	30	9	5	3	2	1	1	1	0	0	0	0	0	0	0	0	0	0	0	0	0	0	0	0	0	0	0
Quad axle and 5+ axle groups	10	FHWA Class 10 (Six or more axle, one trailer truck)	6	8	20	61	150	162	256	266	162	123	138	181	171	142	96	65	47	35	24	17	11	9	5	4	3	2	1	0	0	0	0	0	0	0	0	0	0	0	0
Tandem axle	10	FHWA Class 10 (Six or more axle, one trailer truck)	6	54	266	247	95	77	79	94	105	143	200	185	154	118	90	88	77	52	22	8	5	2	1	0	0	0	0	0	0	0	0	0	0	0	0	0	0	0	0
Tridem axle	10	FHWA Class 10 (Six or more axle, one trailer truck)	5	12	50	78	67	63	38	22	37	51	100	207	289	362	299	133	83	81	73	51	18	9	7	10	11	5	6	1	0	0	0	0	0	0	0	0	0	0	0
Single axle	11	FHWA Class 11 (Five or less axle, multi trailer truck)	3	11	27	340	474	287	466	1304	986	813	580	700	547	357	338	195	158	64	28	6	2	0	0	0	0	0	0	0	0	0	0	0	0	0	0	0	0	0	0
Tandem axle	12	FHWA Class 12 (Six axle, multi trailer truck)	0	1	5	62	147	81	150	193	197	148	68	18	2	0	0	0	0	0	0	0	0	0	0	0	0	0	0	0	0	0	0	0	0	0	0	0	0	0	0
Single axle	12	FHWA Class 12 (Six axle, multi trailer truck)	1	2	4	48	104	80	150	171	113	115	70	81	58	34	29	6	4	0	0	0	0	0	0	0	0	0	0	0	0	0	0	0	0	0	0	0	0	0	0
Single axle	13	FHWA Class 13 (Seven or more axle, multi trailer truck)	0	0	0	0	0	0	0	0	0	0	0	0	0	0	0	0	0	0	0	0	0	0	0	0	0	0	0	0	0	0	0	0	0	0	0	0	0	0	0
Tandem axle	13	FHWA Class 13 (Seven or more axle, multi trailer truck)	0	0	0	0	0	0	0	0	0	0	0	0	0	0	0	0	0	0	0	0	0	0	0	0	0	0	0	0	0	0	0	0	0	0	0	0	0	0	0
Tridem axle	13	FHWA Class 13 (Seven or more axle, multi trailer truck)	0	0	0	0	0	0	0	0	0	0	0	0	0	0	0	0	0	0	0	0	0	0	0	0	0	0	0	0	0	0	0	0	0	0	0	0	0	0	0

Bins	Loads according to the Load Bins								
	Single Axle [lb]			Tandem Axle [lb]			Tridem & Quad Axles [lb]		
1	0	1499.5	2999	0	2999.5	5999	0	5999.5	11999
2	3000	3499.5	3999	6000	6999.5	7999	12000	13499.5	14999
3	4000	4499.5	4999	8000	8999.5	9999	15000	16499.5	17999
4	5000	5499.5	5999	10000	10999.5	11999	18000	19499.5	20999
5	6000	6499.5	6999	12000	12999.5	13999	21000	22499.5	23999
6	7000	7499.5	7999	14000	14999.5	15999	24000	25499.5	26999
7	8000	8499.5	8999	16000	16999.5	17999	27000	28499.5	29999
8	9000	9499.5	9999	18000	18999.5	19999	30000	31499.5	32999
9	10000	10499.5	10999	20000	20999.5	21999	33000	34499.5	35999
10	11000	11499.5	11999	22000	22999.5	23999	36000	37499.5	38999
11	12000	12499.5	12999	24000	24999.5	25999	39000	40499.5	41999
12	13000	13499.5	13999	26000	26999.5	27999	42000	43499.5	44999
13	14000	14499.5	14999	28000	28999.5	29999	45000	46499.5	47999
14	15000	15499.5	15999	30000	30999.5	31999	48000	49499.5	50999
15	16000	16499.5	16999	32000	32999.5	33999	51000	52499.5	53999
16	17000	17499.5	17999	34000	34999.5	35999	54000	55499.5	56999
17	18000	18499.5	18999	36000	36999.5	37999	57000	58499.5	59999
18	19000	19499.5	19999	38000	38999.5	39999	60000	61499.5	62999
19	20000	20499.5	20999	40000	40999.5	41999	63000	64499.5	65999
20	21000	21499.5	21999	42000	42999.5	43999	66000	68999.5	71999
21	22000	22499.5	22999	44000	44999.5	45999	72000	73499.5	74999
22	23000	23499.5	23999	46000	46999.5	47999	75000	76499.5	77999
23	24000	24499.5	24999	48000	48999.5	49999	78000	79499.5	80999
24	25000	25499.5	25999	50000	50999.5	51999	81000	82499.5	83999
25	26000	26499.5	26999	52000	52999.5	53999	84000	85499.5	86999
26	27000	27499.5	27999	54000	54999.5	55999	87000	88499.5	89999
27	28000	28499.5	28999	56000	56999.5	57999	90000	91499.5	92999
28	29000	29499.5	29999	58000	58999.5	59999	93000	94499.5	95999
29	30000	30499.5	30999	60000	60999.5	61999	96000	97499.5	98999
30	31000	31499.5	31999	62000	62999.5	63999	99000	100499.5	101999
31	32000	32499.5	32999	64000	64999.5	65999	0	0	0
32	33000	33499.5	33999	66000	66999.5	67999	0	0	0
33	34000	34499.5	34999	68000	68999.5	69999	0	0	0
34	35000	35499.5	35999	70000	70999.5	71999	0	0	0
35	36000	36499.5	36999	72000	72999.5	73999	0	0	0
36	37000	37499.5	37999	74000	74999.5	75999	0	0	0
37	38000	38499.5	38999	76000	76999.5	77999	0	0	0
38	39000	39499.5	39999	78000	78999.5	79999	0	0	0
39	40000	40499.5	40999	80000	80999.5	81999	0	0	0

P for single tires across loading categories (not accounting for multiple axles)

VEHICLE_CLASS	VEHICLE_CLASS EXP	Axle Configuration	MEPDG_LG01	MEPDG_LG02	MEPDG_LG03	MEPDG_LG04	MEPDG_LG05	MEPDG_LG06	MEPDG_LG07	MEPDG_LG08	MEPDG_LG09	MEPDG_LG10	MEPDG_LG11	MEPDG_LG12	MEPDG_LG13	MEPDG_LG14	MEPDG_LG15	MEPDG_LG16	MEPDG_LG17	MEPDG_LG18	MEPDG_LG19	MEPDG_LG20	MEPDG_LG21	MEPDG_LG22	MEPDG_LG23	MEPDG_LG24	MEPDG_LG25	MEPDG_LG26	MEPDG_LG27	MEPDG_LG28	MEPDG_LG29	MEPDG_LG30	MEPDG_LG31	MEPDG_LG32	MEPDG_LG33	MEPDG_LG34	MEPDG_LG35	MEPDG_LG36	MEPDG_LG37	MEPDG_LG38	MEPDG_LG39
4	FHWA Class 4 (Buses)	Single Axle	1500	3500	4500	5500	6500	7500	8500	9500	10500	11500	12500	13500	14500	15500	16500	17500	18500	19500	20500	21500	22500	23500	24500	25500	26500	27500	28500	29500	30500	31500	32500	33500	34500	35500	36500	37500	38500	39500	40500	
		Tandem Axle	3000	7000	9000	11000	13000	15000	17000	19000	21000	23000	25000	27000	29000	31000	33000	35000	37000	39000	41000	43000	45000	47000	49000	51000	53000	55000	57000	59000	61000	63000	65000	67000	69000	71000	73000	75000	77000	79000	81000	
		Tridem Axle	6000	13500	16500	19500	22500	25500	28500	31500	34500	37500	40500	43500	46500	49500	52500	55500	58500	61500	64500	69000	73500	76500	79500	82500	85500	88500	91500	94500	97500	100500	0	0	0	0	0	0	0	0	0	
		Quad Axle	6000	13500	16500	19500	22500	25500	28500	31500	34500	37500	40500	43500	46500	49500	52500	55500	58500	61500	64500	69000	73500	76500	79500	82500	85500	88500	91500	94500	97500	100500	0	0	0	0	0	0	0	0	0	
		Single Axle P [lbs]	750	1750	2250	2750	3250	3750	4250	4750	5250	5750	6250	6750	7250	7750	8250	8750	9250	9750	10250	10750	11250	11750	12250	12750	13250	13750	14250	14750	15250	15750	16250	16750	17250	17750	18250	18750	19250	19750	20250	
		Tandem Axle P [lbs]	750	1750	2250	2750	3250	3750	4250	4750	5250	5750	6250	6750	7250	7750	8250	8750	9250	9750	10250	10750	11250	11750	12250	12750	13250	13750	14250	14750	15250	15750	16250	16750	17250	17750	18250	18750	19250	19750	20250	
		Tridem Axle P [lbs]	1000	2250	2750	3250	3750	4250	4750	5250	5750	6250	6750	7250	7750	8250	8750	9250	9750	10250	10750	11500	12250	12750	13250	13750	14250	14750	15250	15750	16250	16750	0	0	0	0	0	0	0	0	0	
		Quad Axle P [lbs]	750	1687	2062	2437	2812	3187	3562	3937	4312	4687	5062	5437	5812	6187	6562	6937	7312	7687	8062	8625	9187	9562	9937	10312	10687	11062	11437	11812	12187	12562	0	0	0	0	0	0	0	0	0	

P [lbs]

Axle Configuration	MEPDG_LG0 1	MEPDG_LG0 2	MEPDG_LG03	MEPDG_LG04	MEPDG_LG05	MEPDG_LG06	MEPDG_LG07	MEPDG_LG08	MEPDG_LG09	MEPDG_LG10	MEPDG_LG11	MEPDG_LG12	MEPDG_LG13	MEPDG_LG14	MEPDG_LG15	MEPDG_LG16	MEPDG_LG17	MEPDG_LG18	MEPDG_LG19	MEPDG_LG20	MEPDG_LG21	MEPDG_LG22	MEPDG_LG23	MEPDG_LG24	MEPDG_LG25	MEPDG_LG26	MEPDG_LG27	MEPDG_LG28	MEPDG_LG29	MEPDG_LG30	MEPDG_LG31	MEPDG_LG32	MEPDG_LG33	MEPDG_LG34	MEPDG_LG35	MEPDG_LG36	MEPDG_LG37	MEPDG_LG38	MEPDG_LG39
Single	750	1750	2250	2750	3250	3750	4250	4750	5250	5750	6250	6750	7250	7750	8250	8750	9250	9750	10250	10750	11250	11750	12250	12750	13250	13750	14250	14750	15250	15750	16250	16750	17250	17750	18250	18750	19250	19750	20250
Tandem	750	1750	2250	2750	3250	3750	4250	4750	5250	5750	6250	6750	7250	7750	8250	8750	9250	9750	10250	10750	11250	11750	12250	12750	13250	13750	14250	14750	15250	15750	16250	16750	17250	17750	18250	18750	19250	19750	20250
Tridem	1000	2250	2750	3250	3750	4250	4750	5250	5750	6250	6750	7250	7750	8250	8750	9250	9750	10250	10750	11500	12250	12750	13250	13750	14250	14750	15250	15750	16250	16750	0	0	0	0	0	0	0	0	0	0
Quad	750	1687	2062	2437	2812	3187	3562	3937	4312	4687	5062	5437	5812	6187	6562	6937	7312	7687	8062	8625	9187	9562	9937	10312	10687	11062	11437	11812	12187	12562	0	0	0	0	0	0	0	0	0	0

P [Newtons]

Axle Configuration	MEPDG_LG0 1	MEPDG_LG0 2	MEPDG_LG03	MEPDG_LG04	MEPDG_LG05	MEPDG_LG06	MEPDG_LG07	MEPDG_LG08	MEPDG_LG09	MEPDG_LG10	MEPDG_LG11	MEPDG_LG12	MEPDG_LG13	MEPDG_LG14	MEPDG_LG15	MEPDG_LG16	MEPDG_LG17	MEPDG_LG18	MEPDG_LG19	MEPDG_LG20	MEPDG_LG21	MEPDG_LG22	MEPDG_LG23	MEPDG_LG24	MEPDG_LG25	MEPDG_LG26	MEPDG_LG27	MEPDG_LG28	MEPDG_LG29	MEPDG_LG30	MEPDG_LG31	MEPDG_LG32	MEPDG_LG33	MEPDG_LG34	MEPDG_LG35	MEPDG_LG36	MEPDG_LG37	MEPDG_LG38	MEPDG_LG39
Single	3335	7783	10007	12231	14455	16679	18903	21127	23351	25575	27799	30023	32247	34471	36695	38919	41143	43367	45591	47815	50039	52263	54487	56711	58935	61159	63383	65607	67831	70055	72279	74503	76727	78951	81175	83399	85623	87847	90071
Tandem	3335	7783	10007	12231	14455	16679	18903	21127	23351	25575	27799	30023	32247	34471	36695	38919	41143	43367	45591	47815	50039	52263	54487	56711	58935	61159	63383	65607	67831	70055	72279	74503	76727	78951	81175	83399	85623	87847	90071
Tridem	4448	10008	12232	14456	16680	18904	21128	23352	25576	27800	30024	32248	34472	36696	38920	41144	43368	45592	47816	51152	54488	56712	58936	61160	63384	65608	67832	70056	72280	74504	0	0	0	0	0	0	0	0	0	0
Quad	3336	7506	9174	10842	12510	14178	15846	17514	19182	20850	22518	24186	25854	27522	29190	30858	32526	34194	35862	38364	40866	42534	44202	45870	47538	49206	50874	52542	54210	55878	0	0	0	0	0	0	0	0	0	0

Contact Radii [cm]

Axle Configuration	MEPDG_LG0 1	MEPDG_LG0 2	MEPDG_LG03	MEPDG_LG04	MEPDG_LG05	MEPDG_LG06	MEPDG_LG07	MEPDG_LG08	MEPDG_LG09	MEPDG_LG10	MEPDG_LG11	MEPDG_LG12	MEPDG_LG13	MEPDG_LG14	MEPDG_LG15	MEPDG_LG16	MEPDG_LG17	MEPDG_LG18	MEPDG_LG19	MEPDG_LG20	MEPDG_LG21	MEPDG_LG22	MEPDG_LG23	MEPDG_LG24	MEPDG_LG25	MEPDG_LG26	MEPDG_LG27	MEPDG_LG28	MEPDG_LG29	MEPDG_LG30	MEPDG_LG31	MEPDG_LG32	MEPDG_LG33	MEPDG_LG34	MEPDG_LG35	MEPDG_LG36	MEPDG_LG37	MEPDG_LG38	MEPDG_LG39
Single	3.6	5.6	6.3	7.0	7.6	8.1	8.7	9.2	9.6	10.1	10.5	10.9	11.3	11.7	12.1	12.4	12.8	13.1	13.5	13.8	14.1	14.4	14.7	15.0	15.3	15.6	15.9	16.2	16.4	16.7	17.0	17.2	17.5	17.7	18.0	18.2	18.5	18.7	18.9
Tandem	3.6	5.6	6.3	7.0	7.6	8.1	8.7	9.2	9.6	10.1	10.5	10.9	11.3	11.7	12.1	12.4	12.8	13.1	13.5	13.8	14.1	14.4	14.7	15.0	15.3	15.6	15.9	16.2	16.4	16.7	17.0	17.2	17.5	17.7	18.0	18.2	18.5	18.7	18.9
Tridem	4.2	6.3	7.0	7.6	8.1	8.7	9.2	9.6	10.1	10.5	10.9	11.3	11.7	12.1	12.4	12.8	13.1	13.5	13.8	14.3	14.7	15.0	15.3	15.6	15.9	16.2	16.4	16.7	17.0	17.2	0.0	0.0	0.0	0.0	0.0	0.0	0.0	0.0	0.0
Quad	3.6	5.5	6.0	6.6	7.1	7.5	7.9	8.3	8.7	9.1	9.5	9.8	10.1	10.5	10.8	11.1	11.4	11.7	11.9	12.4	12.8	13.0	13.3	13.5	13.8	14.0	14.2	14.5	14.7	14.9	0.0	0.0	0.0	0.0	0.0	0.0	0.0	0.0	0.0

Contact Radii [mm]

Axle Configuration	MEPDG_LG0 1	MEPDG_LG0 2	MEPDG_LG03	MEPDG_LG04	MEPDG_LG05	MEPDG_LG06	MEPDG_LG07	MEPDG_LG08	MEPDG_LG09	MEPDG_LG10	MEPDG_LG11	MEPDG_LG12	MEPDG_LG13	MEPDG_LG14	MEPDG_LG15	MEPDG_LG16	MEPDG_LG17	MEPDG_LG18	MEPDG_LG19	MEPDG_LG20	MEPDG_LG21	MEPDG_LG22	MEPDG_LG23	MEPDG_LG24	MEPDG_LG25	MEPDG_LG26	MEPDG_LG27	MEPDG_LG28	MEPDG_LG29	MEPDG_LG30	tMEPDG_LG31	tMEPDG_LG32	tMEPDG_LG33	tMEPDG_LG34	tMEPDG_LG35	dMEPDG_LG36	tMEPDG_LG37	MEPDG_LG38	tMEPDG_LG39
Single	36.4	55.6	63.1	69.8	75.8	81.5	86.7	91.7	96.4	100.9	105.2	109.3	113.3	117.1	120.8	124.4	127.9	131.4	134.7	137.9	141.1	144.2	147.2	150.2	153.1	156.0	158.8	161.6	164.3	167.0	169.6	172.2	174.7	177.2	179.7	182.2	184.6	187.0	189.3
Tandem	36.4	55.7	63.1	69.8	75.8	81.5	86.7	91.7	96.4	100.9	105.2	109.3	113.3	117.1	120.8	124.4	127.9	131.4	134.7	137.9	141.1	144.2	147.2	150.2	153.1	156.0	158.8	161.6	164.3	167.0	169.6	172.2	174.7	177.2	179.7	182.2	184.6	187.0	189.3
Tridem	42.1	63.1	69.8	75.8	81.5	86.7	91.7	96.4	100.9	105.2	109.3	113.3	117.1	120.8	124.4	127.9	131.4	134.7	137.9	142.7	147.2	150.2	153.1	156.0	158.8	161.6	164.3	167.0	169.6	172.2	0.0	0.0	0.0	0.0	0.0	0.0	0.0	0.0	0.0
Quad	36.4	54.6	60.4	65.7	70.6	75.1	79.4	83.5	87.4	91.1	94.7	98.1	101.4	104.6	107.8	110.8	113.8	116.6	119.5	123.5	127.5	130.1	132.6	135.1	137.5	139.9	142.3	144.6	146.9	149.1	0.0	0.0	0.0	0.0	0.0	0.0	0.0	0.0	0.0

Contact Radii [in]

Axle Configuration	MEPDG_LG0 1	MEPDG_LG0 2	MEPDG_LG03	MEPDG_LG04	MEPDG_LG05	MEPDG_LG06	MEPDG_LG07	MEPDG_LG08	MEPDG_LG09	MEPDG_LG10	MEPDG_LG11	MEPDG_LG12	MEPDG_LG13	MEPDG_LG14	MEPDG_LG15	MEPDG_LG16	MEPDG_LG17	MEPDG_LG18	MEPDG_LG19	MEPDG_LG20	MEPDG_LG21	tMEPDG_LG22	tMEPDG_LG23	dEPDG_LG24	tMEPDG_LG25	dEPDG_LG26	dMEPDG_LG27	dEPDG_LG28	tEPDG_LG29	dEPDG_LG30	tEPDG_LG31	tEPDG_LG32	tEPDG_LG33	EPDG_LG34	EPDG_LG35	EPDG_LG36	EPDG_LG37	EPDG_LG38	EPDG_LG39
Single	1.4	2.2	2.5	2.7	3.0	3.21	3.41	3.61	3.79	3.97	4.14	4.30	4.46	4.61	4.76	4.90	5.04	5.17	5.30	5.43	5.56	5.68	5.80	5.91	6.03	6.14	6.25	6.36	6.47	6.57	6.68	6.78	6.88	6.98	7.08	7.17	7.27	7.36	7.45
Tandem	1.4	2.2	2.5	2.7	3.0	3.21	3.41	3.61	3.79	3.97	4.14	4.30	4.46	4.61	4.76	4.90	5.04	5.17	5.30	5.43	5.56	5.68	5.80	5.91	6.03	6.14	6.25	6.36	6.47	6.57	6.68	6.78	6.88	6.98	7.08	7.17	7.27	7.36	7.45
Tridem	1.7	2.5	2.7	3.0	3.2	3.41	3.61	3.79	3.97	4.14	4.30	4.46	4.61	4.76	4.90	5.04	5.17	5.30	5.43	5.62	5.80	5.91	6.03	6.14	6.25	6.36	6.47	6.57	6.68	6.78	0.00	0.00	0.00	0.00	0.00	0.00	0.00	0.00	0.00
Quad	1.4	2.2	2.4	2.6	2.8	2.96	3.13	3.29	3.44	3.59	3.73	3.86	3.99	4.12	4.24	4.36	4.48	4.59	4.70	4.86	5.02	5.12	5.22	5.32	5.41	5.51	5.60	5.69	5.78	5.87	0.00	0.00	0.00	0.00	0.00	0.00	0.00	0.00	0.00

APPENDIX J: EXCEL SUPPLEMENT - DANVILLEVADATABUCKET.V2

STATE_CODE	STATE_CODE_EXP	SHRP_ID	TRAFFIC_OPEN_YEAR_EXP_NO	VEHICLE_CLASS	VEHICLE_CLASS_EXP	VEH_CLASS_GROWTH_RATE
51	Virginia	0113	1996	4	FHWA Class 4 (Buses)	-5.405999847
51	Virginia	0113	1996	5	FHWA Class 5 (Two axle, 6-Tire, Single-unit truck)	6
51	Virginia	0113	1996	6	FHWA Class 6 (Three axle Single-unit truck)	-1.009999999
51	Virginia	0113	1996	7	FHWA Class 7 (Four or more axle Single-unit truck)	3.259999999
51	Virginia	0113	1996	8	FHWA Class 8 (Four or less axle, one trailer truck)	0.800000012
51	Virginia	0113	1996	9	FHWA Class 9 (Five axle, one trailer truck)	1.460000038
51	Virginia	0113	1996	10	FHWA Class 10 (Six or more axle, one trailer truck)	0.209999993
51	Virginia	0113	1996	11	FHWA Class 11 (Five or less axle, multi trailer truck)	2.230000019
51	Virginia	0113	1996	12	FHWA Class 12 (Six axle, multi trailer truck)	4.320000172
51	Virginia	0113	1996	13	FHWA Class 13 (Seven or more axle, multi trailer truck)	-26.40999985

VEHICLE_CLASS_EXP	VEH_CLASS_DIST	VEH_CLA	AADTT_PER_VEHICLE_CLASS	MADTT (Jan)	AAMT (Feb)	MADTT (Mar)	MADTT (Apr)	MADTT (May)	MADTT (Jun)	MADTT (Jul)	MADTT (Aug)	AAMT (Sep)	MADTT (Oct)	MADTT (Nov)	MADTT (Dec)
FHWA Class 4 (Buses)	2.930000067	0.0293	20	624	584	624	604	624	604	624	624	604	624	604	624
FHWA Class 5 (Two axle, 6-Tire, Single-unit truck)	14.99999931	0.1493	103	3180	2975	3180	3077	3180	3077	3180	3180	3077	3180	3077	3180
FHWA Class 6 (Three axle Single-unit truck)	8.550000191	0.0855	59	1821	1703	1821	1762	1821	1762	1821	1821	1762	1821	1762	1821
FHWA Class 7 (Four or more axle Single-unit truck)	0.389999986	0.0039	3	83	78	83	80	83	80	83	83	80	83	80	83
FHWA Class 8 (Four or less axle, one trailer truck)	6.670000076	0.0667	46	1421	1329	1421	1375	1421	1375	1421	1421	1375	1421	1375	1421
FHWA Class 9 (Five axle, one trailer truck)	62.15000153	0.6215	427	13236	12382	13236	12809	13236	12809	13236	13236	12809	13236	12809	13236
FHWA Class 10 (Six or more axle, one trailer truck)	0.870000005	0.0087	6	185	173	185	179	185	179	185	185	179	185	179	185
FHWA Class 11 (Five or less axle, multi trailer truck)	3.069999933	0.0307	21	654	612	654	633	654	633	654	654	633	654	633	654
FHWA Class 12 (Six axle, multi trailer truck)	0.430000007	0.0043	3	92	86	92	89	92	89	92	92	89	92	89	92
FHWA Class 13 (Seven or more axle, multi trailer truc	0	0	0	0	0	0	0	0	0	0	0	0	0	0	0

The days per month multiplication is for the days per month in the base

0.084699454	0.079234973	0.084699454	0.081967213	0.084699454	0.081967213	0.084699454	0.084699454	0.081967213	0.084699454	0.081967213	0.084699454
0.084699454	0.079234973	0.084699454	0.081967213	0.084699454	0.081967213	0.084699454	0.084699454	0.081967213	0.084699454	0.081967213	0.084699454
0.084699454	0.079234973	0.084699454	0.081967213	0.084699454	0.081967213	0.084699454	0.084699454	0.081967213	0.084699454	0.081967213	0.084699454
0.084699454	0.079234973	0.084699454	0.081967213	0.084699454	0.081967213	0.084699454	0.084699454	0.081967213	0.084699454	0.081967213	0.084699454
0.084699454	0.079234973	0.084699454	0.081967213	0.084699454	0.081967213	0.084699454	0.084699454	0.081967213	0.084699454	0.081967213	0.084699454
0.084699454	0.079234973	0.084699454	0.081967213	0.084699454	0.081967213	0.084699454	0.084699454	0.081967213	0.084699454	0.081967213	0.084699454
0.084699454	0.079234973	0.084699454	0.081967213	0.084699454	0.081967213	0.084699454	0.084699454	0.081967213	0.084699454	0.081967213	0.084699454
0.084699454	0.079234973	0.084699454	0.081967213	0.084699454	0.081967213	0.084699454	0.084699454	0.081967213	0.084699454	0.081967213	0.084699454

APPENDIX K: EXCEL SUPPLEMENT - DANVILLEVAMODULIDATA

Units:					(PSI)	(PSI)	(PSI)	(PSI)	Celcius	Celcius	Celcius					
SHRP_ID	LAYER_NO	STATE_CODE	STATE_CODE_EXP	ESTAR_LINK	SIGMOIDAL_COEFF_1	SIGMOIDAL_COEFF_2	SIGMOIDAL_COEFF_3	SIGMOIDAL_COEFF_4	SHIFT_FACTOR_COEFF_1	SHIFT_FACTOR_COEFF_2	SHIFT_FACTOR_COEFF_3	PREDICTIVE_MODEL	PREDICTIVE_MODEL_EXP		SAMPLE_TYPE_ESTAR	SAMPLE_TYPE_ESTAR_EXP
0113	4	51	Virginia	1114	3.752000093	2.875	-1.356999993	0.493000001	0.001	-0.216999993	4.05	2	Viscosity ANN		1	Original Binder
0113	5	51	Virginia	1117	3.798000097	2.822000027	-1.06099999	0.500999987	0.002	-0.244000003	4.375	2	Viscosity ANN		1	Original Binder
0113	4	51	Virginia	1115	3.746000051	2.894000053	-1.282999992	0.488999993	0.001	-0.229000002	4.204	5	Viscosity ANN with viscosity from binder grade		2	RTFO/TFO Aged Binder
0113	5	51	Virginia	1118	3.778000116	2.851000071	-1.296000004	0.495999992	0.001	-0.224000007	4.145	5	Viscosity ANN with viscosity from binder grade		2	RTFO/TFO Aged Binder
0113	4	51	Virginia	1113	3.813999891	2.792000055	-0.638000011	0.488000005	0.001	-0.165000007	3.161	1	Resilient modulus ANN		4	Field Aged Binder
0113	5	51	Virginia	1116	3.880000114	2.704999924	-0.497000009	0.493999988	0.001	-0.165000007	3.161	1	Resilient modulus ANN		4	Field Aged Binder

Data with Proper Unit Conversions:

Units:					(PSI)	(PSI)	(PSI)	(PSI)	Celcius	Celcius	Celcius					
SHRP_ID	LAYER_NO	STATE_CODE	STATE_CODE_EXP	ESTAR_LINK	SIGMOIDAL_COEFF_1	SIGMOIDAL_COEFF_2	SIGMOIDAL_COEFF_3	SIGMOIDAL_COEFF_4	SHIFT_FACTOR_COEFF_1	SHIFT_FACTOR_COEFF_2	SHIFT_FACTOR_COEFF_3	PREDICTIVE_MODEL	PREDICTIVE_MODEL_EXP		SAMPLE_TYPE_ESTAR	SAMPLE_TYPE_ESTAR_EXP
RUN A 0113		4	51	Virginia	1113	3.813999891	2.792000055	-0.638000011	0.488000005	0.001	-0.165000007	3.161	1	Resilient modulus ANN	4	Field Aged Binder

f (hz) = 25

LINKED_SHRP_ID	LINKED_LAYER_NO	SHRP_ID	STATE_CODE	STATE_CODE_EXP	LAYER_NO	TEST_NO	TEST_NO_EXP		FIELD_SET	LOC_NO	SAMPLE_NO	CON_PRESSURE	NOM_MAX_AXIAL_STRESS	CONSTRUCTION_NO	LAYER_TYPE	LAYER_TYPE_EXP	RES_STRAIN_AVG	RES_MOD_AVG	TEST_DATE			
0113	3	0117		51 Virginia	3		2 Material sample obtained from area adjacent to leave end of test section.		2 BAX03	BGX03		20.70000076	19.79999924	2		2 Base/subbase	0.0005	37	07/29/2008			
0113	3	0117		51 Virginia	3		2 Material sample obtained from area adjacent to leave end of test section.		2 BAX03	BGX03		20.70000076	40.40000153	2		2 Base/subbase	0.00082	45	07/29/2008			
0113	3	0117		51 Virginia	3		2 Material sample obtained from area adjacent to leave end of test section.		2 BAX03	BGX03		20.70000076	61.20000076	2		2 Base/subbase	0.00104	54	07/29/2008			
0113	3	0117		51 Virginia	3		2 Material sample obtained from area adjacent to leave end of test section.		2 BAX03	BGX03		34.5	34.5	2		2 Base/subbase	0.00055	57	07/29/2008			
0113	3	0117		51 Virginia	3		2 Material sample obtained from area adjacent to leave end of test section.		2 BAX03	BGX03		34.5	69	2		2 Base/subbase	0.0009	69	07/29/2008			
0113	3	0117		51 Virginia	3		2 Material sample obtained from area adjacent to leave end of test section.		2 BAX03	BGX03		34.5	103.1999969	2		2 Base/subbase	0.0012	78	07/29/2008			
0113	3	0117		51 Virginia	3		2 Material sample obtained from area adjacent to leave end of test section.		2 BAX03	BGX03		69	71	2		2 Base/subbase	0.00065	95	07/29/2008			
0113	3	0117		51 Virginia	3		2 Material sample obtained from area adjacent to leave end of test section.		2 BAX03	BGX03		103.5	211	2		2 Base/subbase	0.00133	140	07/29/2008			
0113	3	0119		51 Virginia	3		2 Material sample obtained from area adjacent to leave end of test section.		2 BAX02	BGX02		20.70000076	40.59999847	2		2 Base/subbase	0.00068	55	06/25/2008			
0113	3	0119		51 Virginia	3		2 Material sample obtained from area adjacent to leave end of test section.		2 BAX02	BGX02		69.19999695	209	2		2 Base/subbase	0.00137	136	06/25/2008			
0113	3	0119		51 Virginia	3		2 Material sample obtained from area adjacent to leave end of test section.		2 BAX02	BGX02		103.5	73.19999695	2		2 Base/subbase	0.00054	115	06/25/2008			
0113	3	0119		51 Virginia	3		2 Material sample obtained from area adjacent to leave end of test section.		2 BAX02	BGX02		103.5999985	210.8000031	2		2 Base/subbase	0.00121	154	06/25/2008			
0113	3	0119		51 Virginia	3		2 Material sample obtained from area adjacent to leave end of test section.		2 BAX02	BGX02		137.8999939	144.5	2		2 Base/subbase	0.00083	149	06/25/2008			
0113	3	0119		51 Virginia	3		2 Material sample obtained from area adjacent to leave end of test section.		2 BAX02	BGX02		138	109.6999969	2		2 Base/subbase	0.00068	138	06/25/2008			
0113	3	0121		51 Virginia	3		2 Material sample obtained from area adjacent to leave end of test section.		2 BAX01	BGX01		103.1999969	107.5999985	2		2 Base/subbase	0.001	93	06/25/2008			
0113	3	0121		51 Virginia	3		2 Material sample obtained from area adjacent to leave end of test section.		2 BAX01	BGX01		103.3000031	73.19999695	2		2 Base/subbase	0.00072	86	06/25/2008			
0113	3	0121		51 Virginia	3		2 Material sample obtained from area adjacent to leave end of test section.		2 BAX01	BGX01		69.69999695	140.1000061	2		2 Base/subbase	0.00129	97	06/25/2008			
0113	3	0117		51 Virginia	3		2 Material sample obtained from area adjacent to leave end of test section.		2 BAX03	BGX03		69.09999847	139.8000031	2		2 Base/subbase	0.00112	110	07/29/2008			
0113	3	0117		51 Virginia	3		2 Material sample obtained from area adjacent to leave end of test section.		2 BAX03	BGX03		138	144.1999969	2		2 Base/subbase	0.0009	138	07/29/2008			
0113	3	0119		51 Virginia	3		2 Material sample obtained from area adjacent to leave end of test section.		2 BAX02	BGX02		138.3000031	282.2000122	2		2 Base/subbase	0.00137	181	06/25/2008			
0113	3	0117		51 Virginia	3		2 Material sample obtained from area adjacent to leave end of test section.		2 BAX03	BGX03		69.30000305	208.6000061	2		2 Base/subbase	0.0016	116	07/29/2008			
0113	3	0117		51 Virginia	3		2 Material sample obtained from area adjacent to leave end of test section.		2 BAX03	BGX03		103.5	73.30000305	2		2 Base/subbase	0.00058	107	07/29/2008			
0113	3	0117		51 Virginia	3		2 Material sample obtained from area adjacent to leave end of test section.		2 BAX03	BGX03		103.4000015	107.5	2		2 Base/subbase	0.00082	114	07/29/2008			
0113	3	0117		51 Virginia	3		2 Material sample obtained from area adjacent to leave end of test section.		2 BAX03	BGX03		137.8000031	281.7999878	2		2 Base/subbase	0.00148	168	07/29/2008			
0113	3	0117		51 Virginia	3		2 Material sample obtained from area adjacent to leave end of test section.		2 BAX03	BGX03		138	109.6999969	2		2 Base/subbase	0.00071	131	07/29/2008			
0113	3	0119		51 Virginia	3		2 Material sample obtained from area adjacent to leave end of test section.		2 BAX02	BGX02		20.79999924	19.79999924	2		2 Base/subbase	0.0004	46	06/25/2008			
0113	3	0121		51 Virginia	3		2 Material sample obtained from area adjacent to leave end of test section.		2 BAX01	BGX01		34.5	34.40000153	2		2 Base/subbase	0.00058	54	06/25/2008			
0113	3	0121		51 Virginia	3		2 Material sample obtained from area adjacent to leave end of test section.		2 BAX01	BGX01		69.5	71.19999695	2		2 Base/subbase	0.00075	83	06/25/2008			
0113	3	0121		51 Virginia	3		2 Material sample obtained from area adjacent to leave end of test section.		2 BAX01	BGX01		103.6999969	211.1000061	2		2 Base/subbase	0.00152	122	06/25/2008			
0113	3	0121		51 Virginia	3		2 Material sample obtained from area adjacent to leave end of test section.		2 BAX01	BGX01		137.8999939	281.7000122	2		2 Base/subbase	0.0018	138	06/25/2008			
0113	3	0119		51 Virginia	3		2 Material sample obtained from area adjacent to leave end of test section.		2 BAX02	BGX02		20.79999924	61.29999924	2		2 Base/subbase	0.00087	65	06/25/2008			
0113	3	0119		51 Virginia	3		2 Material sample obtained from area adjacent to leave end of test section.		2 BAX02	BGX02		34.5	34.5	2		2 Base/subbase	0.00047	66	06/25/2008			
0113	3	0119		51 Virginia	3		2 Material sample obtained from area adjacent to leave end of test section.		2 BAX02	BGX02		34.59999847	68.90000153	2		2 Base/subbase	0.00077	81	06/25/2008			
0113	3	0121		51 Virginia	3		2 Material sample obtained from area adjacent to leave end of test section.		2 BAX01	BGX01		20.70000076	40.5	2		2 Base/subbase	0.00082	46	06/25/2008			
0113	3	0119		51 Virginia	3		2 Material sample obtained from area adjacent to leave end of test section.		2 BAX02	BGX02		34.70000076	103.5	2		2 Base/subbase	0.00103	91	06/25/2008			
0113	3	0119		51 Virginia	3		2 Material sample obtained from area adjacent to leave end of test section.		2 BAX02	BGX02		69	71.09999847	2		2 Base/subbase	0.0006	104	06/25/2008			
0113	3	0119		51 Virginia	3		2 Material sample obtained from area adjacent to leave end of test section.		2 BAX02	BGX02		69	139.8999939	2		2 Base/subbase	0.00101	123	06/25/2008			
0113	3	0121		51 Virginia	3		2 Material sample obtained from area adjacent to leave end of test section.		2 BAX01	BGX01		138	143.6999969	2		2 Base/subbase	0.00111	112	06/25/2008			
0113	3	0119		51 Virginia	3		2 Material sample obtained from area adjacent to leave end of test section.		2 BAX02	BGX02		103.5	107.5999985	2		2 Base/subbase	0.00075	124	06/25/2008			
0113	3	0121		51 Virginia	3		2 Material sample obtained from area adjacent to leave end of test section.		2 BAX01	BGX01		20.70000076	19.60000038	2		2 Base/subbase	0.0005	37	06/25/2008			
0113	3	0121		51 Virginia	3		2 Material sample obtained from area adjacent to leave end of test section.		2 BAX01	BGX01		20.70000076	61.20000076	2		2 Base/subbase	0.00105	53	06/25/2008			
0113	3	0121		51 Virginia	3		2 Material sample obtained from area adjacent to leave end of test section.		2 BAX01	BGX01		137.8999939	110	2		2 Base/subbase	0.00091	102	06/25/2008			
0113	3	0121		51 Virginia	3		2 Material sample obtained from area adjacent to leave end of test section.		2 BAX01	BGX01		34.5	68.90000153	2		2 Base/subbase	0.00095	65	06/25/2008			
0113	3	0121		51 Virginia	3		2 Material sample obtained from area adjacent to leave end of test section.		2 BAX01	BGX01		69.19999695	209.1000061	2		2 Base/subbase	0.00172	108	06/25/2008			
0113	3	0121		51 Virginia	3		2 Material sample obtained from area adjacent to leave end of test section.		2 BAX01	BGX01		34.5	103.4000015	2		2 Base/subbase	0.00127	73	06/25/2008			
																	Average:		96.8			

APPENDIX L: EXCEL SUPPLEMENT - DANVILLEVASUBGRADEMODULIDATA

LINKED_SHRP_ID	LINKED_LAYER_NO	SHRP_ID	STATE_CODE	STATE_CODE_EXP	LAYER_NO	TEST_NO	TEST_NO_EXP			FIELD_SE	LOC_NO	SAMPLE_NO	CON_PRE	NOM_MA	CONSTRUCTION_NO	LAYER_TYPE	LAYER_TYPE_EXP	RES_STRAIN_AVG	RES_MOD_AVG	TEST_DATE
2004	1	2004	51	Virginia	1	1	Material sample obtained from area adjacent to approach end of test section.			1	BA*	BS**	13.8	13.8	1	1	Subgrade	0.000319	40	11/11/1992
2004	1	2004	51	Virginia	1	1	Material sample obtained from area adjacent to approach end of test section.			1	BA*	BS**	13.8	27.6	1	1	Subgrade	0.000796	31	11/11/1992
2004	1	2004	51	Virginia	1	1	Material sample obtained from area adjacent to approach end of test section.			1	BA*	BS**	27.6	55.2	1	1	Subgrade	0.001694	29	11/11/1992
2004	1	2004	51	Virginia	1	1	Material sample obtained from area adjacent to approach end of test section.			1	BA*	BS**	41.4	68.9	1	1	Subgrade	0.001923	32	11/11/1992
2004	1	2004	51	Virginia	1	1	Material sample obtained from area adjacent to approach end of test section.			1	BA*	BS**	41.4	55.2	1	1	Subgrade	0.001452	34	11/11/1992
2004	1	2004	51	Virginia	1	1	Material sample obtained from area adjacent to approach end of test section.			1	BA*	BS**	13.8	41.4	1	1	Subgrade	0.001395	26	11/11/1992
2004	1	2004	51	Virginia	1	1	Material sample obtained from area adjacent to approach end of test section.			1	BA*	BS**	13.8	55.2	1	1	Subgrade	0.002016	24	11/11/1992
2004	1	2004	51	Virginia	1	1	Material sample obtained from area adjacent to approach end of test section.			1	BA*	BS**	13.8	68.9	1	1	Subgrade	0.002624	23	11/11/1992
2004	1	2004	51	Virginia	1	1	Material sample obtained from area adjacent to approach end of test section.			1	BA*	BS**	27.6	27.6	1	1	Subgrade	0.000651	38	11/11/1992
2004	1	2004	51	Virginia	1	1	Material sample obtained from area adjacent to approach end of test section.			1	BA*	BS**	41.4	13.8	1	1	Subgrade	0.000249	51	11/11/1992
2004	1	2004	51	Virginia	1	1	Material sample obtained from area adjacent to approach end of test section.			1	BA*	BS**	27.6	13.8	1	1	Subgrade	0.000261	48	11/11/1992
2004	1	2004	51	Virginia	1	1	Material sample obtained from area adjacent to approach end of test section.			1	BA*	BS**	27.6	41.4	1	1	Subgrade	0.001154	32	11/11/1992
2004	1	2004	51	Virginia	1	1	Material sample obtained from area adjacent to approach end of test section.			1	BA*	BS**	27.6	68.9	1	1	Subgrade	0.002214	28	11/11/1992
2004	1	2004	51	Virginia	1	1	Material sample obtained from area adjacent to approach end of test section.			1	BA*	BS**	41.4	27.6	1	1	Subgrade	0.000589	43	11/11/1992
2004	1	2004	51	Virginia	1	1	Material sample obtained from area adjacent to approach end of test section.			1	BA*	BS**	41.4	41.4	1	1	Subgrade	0.001012	37	11/11/1992
																		Average:	34.4	